Tasmania Department of Resources and Energy

Division of Mines and Mineral Resources
Report 1991/32

The origin of the gold mineralisation at the Henty Prospect

By J. Taheri and G. R. Green

September 1991

CONTENTS

TABLES

FIGURES

ACKNOWLEDGMENTS

We would like to thank RGC Exploration Pty Ltd, particularly Phillip Uttley, and Little River (Resources) Pty Ltd for allowing us to undertake this project and for financial support to cover some of the analytical and lapidary expenses. Special thanks to RGC geologists Ray Roberts, Scott Halley and Mark Fleming who provided us with all the available data, for generous support during sampling, and stimulating discussions. We are grateful for the full support and co-operative assistance of colleagues in the Division of Mines and Mineral Resources; Janine Triffett and Jane Mackey (lapidary), Richie Woolley (sulphur isotope determinations and XRD analyses), Michael Power (oxygen isotope determinations), Tim Bishop and Les Hay (XRF analyses); Andrew McGuiness and John Ladaniwskyj (drafting).

We would like to thank Nick Turner and Emyr Williams, and especially Ralph Bottrill, for their assistance in the petrographical studies and valuable discussions. We would also thank Michael Dix for editing and preparing the manuscript. Finally we are particularly grateful to Rod Hargreaves and David Duncan who appreciated the significance of this study and allowed the research to be undertaken as a part of the MRV Project. Their support throughout the project is appreciated.

INTRODUCTION

The Henty Prospect is located by the Henty River in a valley between Gooseneck Hill and Mt Read, about 30 km north of Queenstown, within the former Exploration Licence 9/66 initially granted to the Mount Lyell Mining and Railway Co. Ltd in 1966. The area is currently held under Mining Lease 16M/89 by a joint venture between RGC (Tasmania) Ltd and Little River Resources Pty Ltd but operated by RGC Exploration Ltd.

Exploration in the Henty Prospect area began in 1968, as the area was considered to be prospective for Mt Lyell-type mineralisation. Between 1968 and 1969 preliminary geophysical and geological studies and soil sampling were undertaken but the results were not considered worthy of follow up.

In 1971 minor old workings were discovered in the north of the area. Costeaning of these workings revealed a copper-rich zone assaying 1.22% Cu over 12 m in "py-chalcopyrite-bearing chloritic schists" (McKibben, 1972). This resulted in more detailed mapping, geophysics (including IP) and soil sampling. Eight IP anomalies were found, some of which coincided with geophysical anomalies. These areas were subsequently costeaned or drilled (Wells, 1974). A 2.5 m wide massive sulphide (pyrite, chalcopyrite, galena, sphalerite) body was exposed in one of the costeans. Sampling of the body yielded average values of 1.8% Cu, 1.8% Pb, 0.2% Zn and 37.9% FeS_2 (Wells, 1974). However the overall results were considered to be discouraging, mainly due to the absence of massive sulphide bodies of economic significance, the close proximity of the Henty Fault, and the occurrence of the unfavourable Tyndall Group as the host rocks.

Consequently the exploration was downgraded until 1983, when further holes were drilled and some of the core from the pre-existing holes was re-assayed for Au contents. The results from the re-assaying were very encouraging, and revealed the association of gold mineralisation with silicified volcanic rocks. This led to continuous intense exploration activities in the area to the present time. To date more than 180 holes have been drilled. Further information regarding the geology, structure and gold distribution was obtained from a 900 m decline and a 200 m drive along the mineralisation at about 130 m beneath the surface.

The mineralisation at the Henty Prospect is of particular interest and importance, as it is the only known mineralisation of economic significance that is hosted by the Tyndall Group of the Mount Read Volcanics in western Tasmania. Therefore understanding of the genesis of the mineralisation (i.e. syngenetic vs epigenetic) can have great impact on the possible further ore discoveries in rocks of the Tyndall Group. The objects of this study are to determine:

(i) the original rock type(s) for different hydrothermally altered rocks,

(ii) the significance of the Henty Fault in the formation, deformation or remobilisation of the ore body,

(iii) the importance of the Devonian and Cambrian ore fluid processes, and

(iv) the origin of the mineralisation (e.g. mesothermal vs VMS).

CHAPTER 1

Geology

The geology of western Tasmania has been reviewed by Williams (1978), Solomon (1981), Corbett (1981), Corbett and Lees (1987), Corbett and Solomon (1989) and Green (1990), from which a brief outline is presented here. In the Cambrian, two blocks of Precambrian rocks, the Tyennan Nucleus and Rocky Cape Region, formed the eastern and western margins of a relatively narrow basin, the Dundas Trough (fig. 1.1) which is mainly filled with fossiliferous Middle to Late Cambrian sedimentary sequences overlying sheets of possibly allochthonous ultramafic and mafic rocks (Berry and Crawford,1988). The Mt Read Volcanics, a belt of felsic to intermediate volcanic rocks, occupies the eastern margin of the Dundas Trough and appears to be coeval with the fossiliferous sedimentary sequence. The Mt Read Volcanics has been divided into three lithological groups (fig. 1.1):

(1) Central volcanic complex, mainly consisting of rhyolitic and andesitic lavas, pyroclastic rocks, shale, and siltstone, with minor granitic intrusions. The rocks in the northern portion of the Mt Read Volcanics (Que–Hellyer Volcanics) are more mafic and may represent younger volcanic rocks (Corbett and Komyshan, 1989). The Central Volcanic Complex and the Que–Hellyer Volcanics host the main Pb-Zn-Cu-Ag-Au massive and disseminated sulphide deposits in western Tasmania (e.g. Rosebery, Que River, Hellyer, Mt Lyell; fig. 1.1).

(2) The Tyndall Group, comprising mainly quartz-phyric felsic and intermediate lavas and tuffs with interbedded sandstone, shale and volcaniclastic conglomerate. It hosts the mineralisation at the Henty Prospect.

(3) A western volcano-sedimentary succession of tuff, shale, felsic porphyry intrusive rocks and minor quartzose and volcaniclastic turbidites.

A major NNE-trending fault system (the Henty Fault) divides the Mt Read Volcanics into two parts. The fault extends from north of Tullah to south of Mt Read (fig. 1.1). The Farrell Slates, consisting mainly of slate and tuffaceous sandstone, occur along the eastern side of the Henty Fault Zone, and host Pb, Zn, Ag, Au, and Sn mineralisation in the Tullah area.

The Cambrian and younger (to early Middle Devonian) rocks in western Tasmania have been affected by a widespread Devonian folding (Tabberabberan Orogeny). This was followed by the emplacement of high-level granitoid plutons such as the Granite Tor Granite, Heemskirk Granite and Meredith Granite; fig. 1.1). Tin, tungsten and silver-lead-zinc mineralisation and remobilisation of some Cambrian sulphides are related to emplacement of these granites, which are broadly related to later orogenic faulting (Berry, 1989).

MINERALISATION ALONGSIDE THE HENTY FAULT

Several vein-type Pb-Ag deposits occur adjacent to the Henty Fault and are hosted by the Farrell Slates and by the massive volcanics of the CVC (fig. 1.2). The deposits were discovered in 1897 (Hall *et al*., 1953) and have been described by Brooks (1962) and Hall and Solomon (1962). The recent discovery of the polymetallic Sn-Au mineralisation at the Lakeside and Sterling Valley Tin Prospects, and also gold mineralisation at the Henty Prospect, indicate that the Henty Fault may have played a major role in the formation and remobilisation of the deposits (e.g. Taheri and Green, 1990).

The mineralisation along the Henty Fault Zone (fig. 1.2) may be divided into three broad categories:

(1) Pb-Ag dominated deposits which are hosted by the Farrell Slates in the Tullah area. They occur as sub-parallel lenticular fissure lodes and veins in shears striking NNW to NNE. The common minerals include galena, sphalerite, chalcopyrite, arsenopyrite, tetrahedrite and siderite.

(2) Polymetallic Sn-Au mineralisation hosted by the Farrell Slates (e.g. Lakeside Prospect) or the Mt Black Volcanics (Sterling Valley Tin Prospect). They mainly occur as vein and fissure-fillings, and the common minerals are pyrite, arsenopyrite, pyrrhotite, stannite, quartz, carbonate, tourmaline, cassiterite, and fluorite.

(3) Massive to disseminated pyrite, sphalerite and galena in sericite-quartz schist and veinlets of sulphides-gold-tellurides, dominantly in strongly silicified rocks of the Tyndall Group (Henty Prospect).

LOCAL GEOLOGY

The geology in the vicinity of the Henty Prospect is dominated by the Henty Fault and has been described by Arnold (1988, 1989), Yeats (1989), Carrasco *et al*., (1990) and Berry (1990). The fault strikes NNE (020° AMG) and dips 70° west. A complex history of movement for the Henty Fault has been reported by Berry (1989). The fault appears to have been active from the early Palaeozoic to the Tertiary. The earliest movement is east-directed thrusting, pre-dating the Devonian folding, and may correlate with the early Ordovician movement on the Great Lyell Fault. Brittle-ductile deformation is indicated for this phase of movement. Devonian movements include high-angle reverse faulting,

post-dating Devonian folding, but synchronous with the Granite Tor intrusion and vein mineralisation in the Tullah area. Later Devonian sinistral wrench faults involved displacements of less than five kilometres. These are generally exposed as brittle deformation overprinting the earlier brittle-ductile fabric. There are also late phases of reactivation of the Henty Fault, including possibly Jurassic sinistral wrench movement, and Tertiary normal faulting (Berry, 1989).

The Central Volcanic Complex to the west of the Henty Fault mainly consist of fine-grained pink rhyolitic to dacitic feldspar-phyric lava and volcaniclastic rocks which are intruded by fine-grained mafic dykes. The Henty Fault zone in the vicinity of the Henty Prospect area consists of a mylonite zone with some broken puggy sections, varying in thickness from 10 to 20 m (Carrasco *et al*., 1990).

The Tyndall Group to the east of the fault has been subdivided into upper and lower units by Arnold (1988). The lower Tyndall unit hosts the mineralisation at the Henty Prospect and consists mainly of fragmental felsic pyroclastic rocks with minor epiclastic and fine-grained felsic volcanic rocks. It is considered to be a correlate of the Comstock Tuff (Carrasco, *et al*., 1990).The rocks have further been subdivided by RGC geologists based on grain size and crystal content. The upper Tyndall unit consists mainly of epiclastic rocks and quartz-feldspar phyric crystal tuff showing a wide range in grain size from siltstone to conglomerate. It is overlain conformably by siliciclastic conglomerate, sandstone and green to black slates of turbidite origin of the Newton Creek Sandstone (Corbett, 1975).

Based on our petrographical studies, the sheared and moderately hydrothermally-altered host rocks (i.e. MA, RGC classifications) are mainly polymict epiclastic rocks (see next chapter for more detail). However systematic petrochemical studies are needed to establish the rock types in the upper and lower units. The significance of this work will be discussed later in this text.

The rocks have been strongly affected by a strong regional foliation striking NNW (340° AMG). However according to Arnold (1988) the foliation direction in the hanging wall (i.e. Central Volcanic Complex) is not parallel to that of the footwall, and broadly follows the direction of the Henty Fault. The footwall at the Henty prospect (i.e. Tyndall Group) dips steeply west and appears to have been overturned, and is repeated parallel to the Henty Fault by faulting (Arnold, 1988, fig. 1.3). The lower Tyndall unit occurs to the west of the upper Tyndall unit and is in contact with the Henty Fault Zone. The repetition is marked by a fault (CF2, fig. 1.3) across which the footwall sequence, including the upper Tyndall unit and Newton Creek Sandstone, passes eastward into the lower Tyndall unit. There are also two more faults characterised by major lithological changes; CF1 and CF3. CF1 marks the contact between the upper and the lower Tyndall units and may be simply a conformable contact. CF3 marks the contact between the footwall unit and a quartz porphyry body at depth to the east of the deposit (fig. 1.3; Arnold, 1988; Carrasco *et al*., 1990).

The rocks within the area have also been affected by numerous small faults ranging in movements from less than one to 30 metres. The fault zones are normally puggy and characterised by extensively broken rocks. The small faults exposed in the sill have been divided into three different groups by Arnold (1989). Group A faults strike sub-parallel to the foliation but are shallower and dip at about 45° to the east. Reverse displacements of up to two metres have been measured on these faults. Group B faults strike NW and dip steeply to the northeast and exhibit both dextral and sinistral movements. Group C faults strike ENE and dip steeply (~65°) to the northwest and commonly truncate group A faults. They commonly exhibit dextral displacement of up to three metres. The small faults in general appear to be related to late movements on the Henty Fault. They cut and displace the mineralised and altered rocks at the Henty Prospect area and are probably of Devonian or younger age (Berry, 1990; Carrasco *et al.*, 1990). According to Arnold (1989), most of the post-cleavage movements on the Henty Fault may have been strike-slip faults (i.e. Group B and C).

The lithological units at the Henty Prospect strike NNW and dip vertically. However in a gross sense, they are parallel to the Henty Fault over the length of the prospect. The parallelism has been interpreted to be due to drag or systematic displacements on the faults within the area (Berry, 1990; Carrasco *et al*., 1990).

Our preliminary studies on some oriented samples from the sill indicate that during cleavage development faulting was mainly dip slip and that most shearing indicators are consistent with reverse movement.

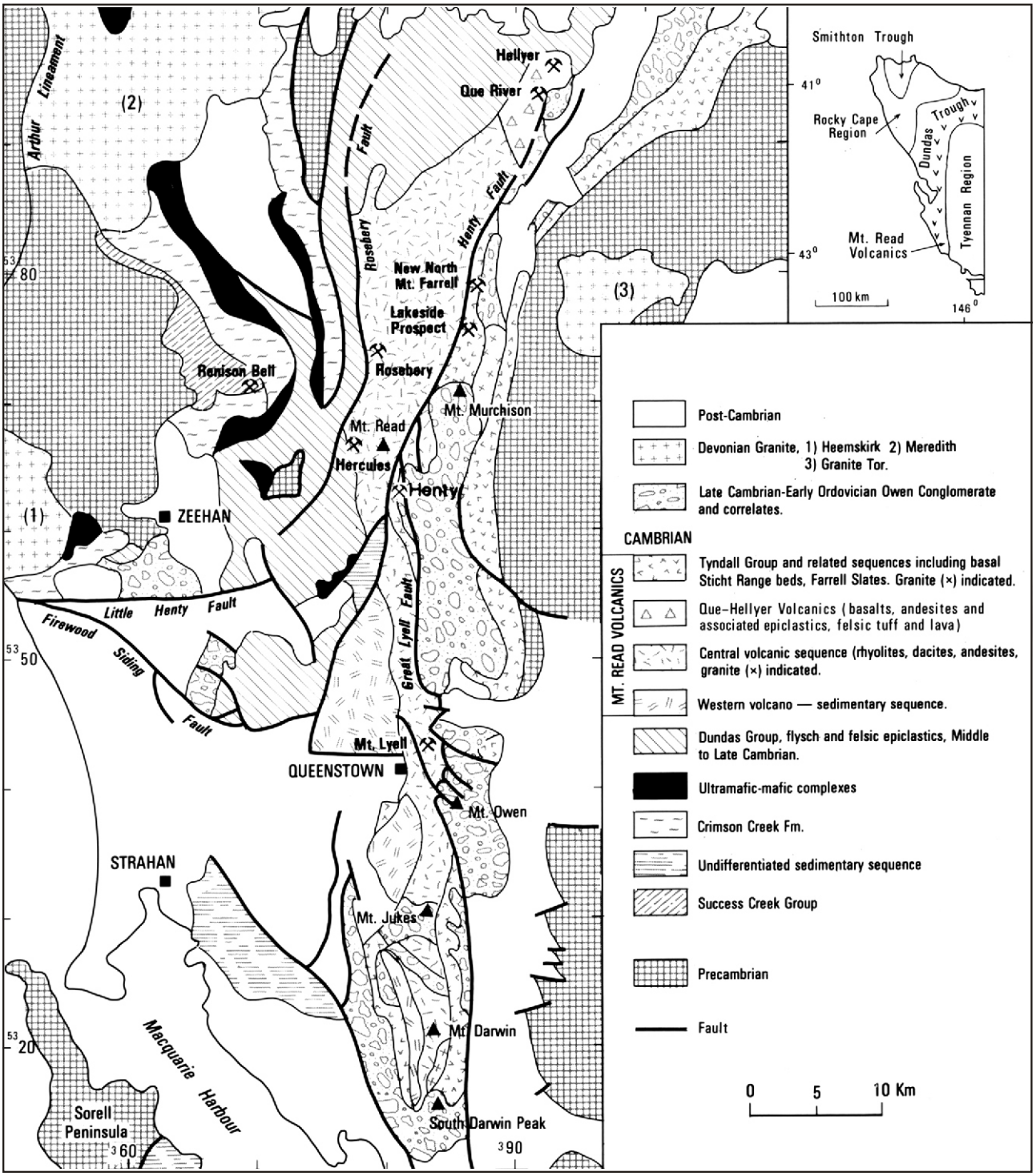

Figure 1.1

Simplified geology of western Tasmania showing the Mt Read Volcanics between Hellyer and South Darwin Peak. Inset shows the major palaeogeographic elements in western Tasmania (after Corbett and McNeill, 1987; Corbett and Komyshan, 1989).

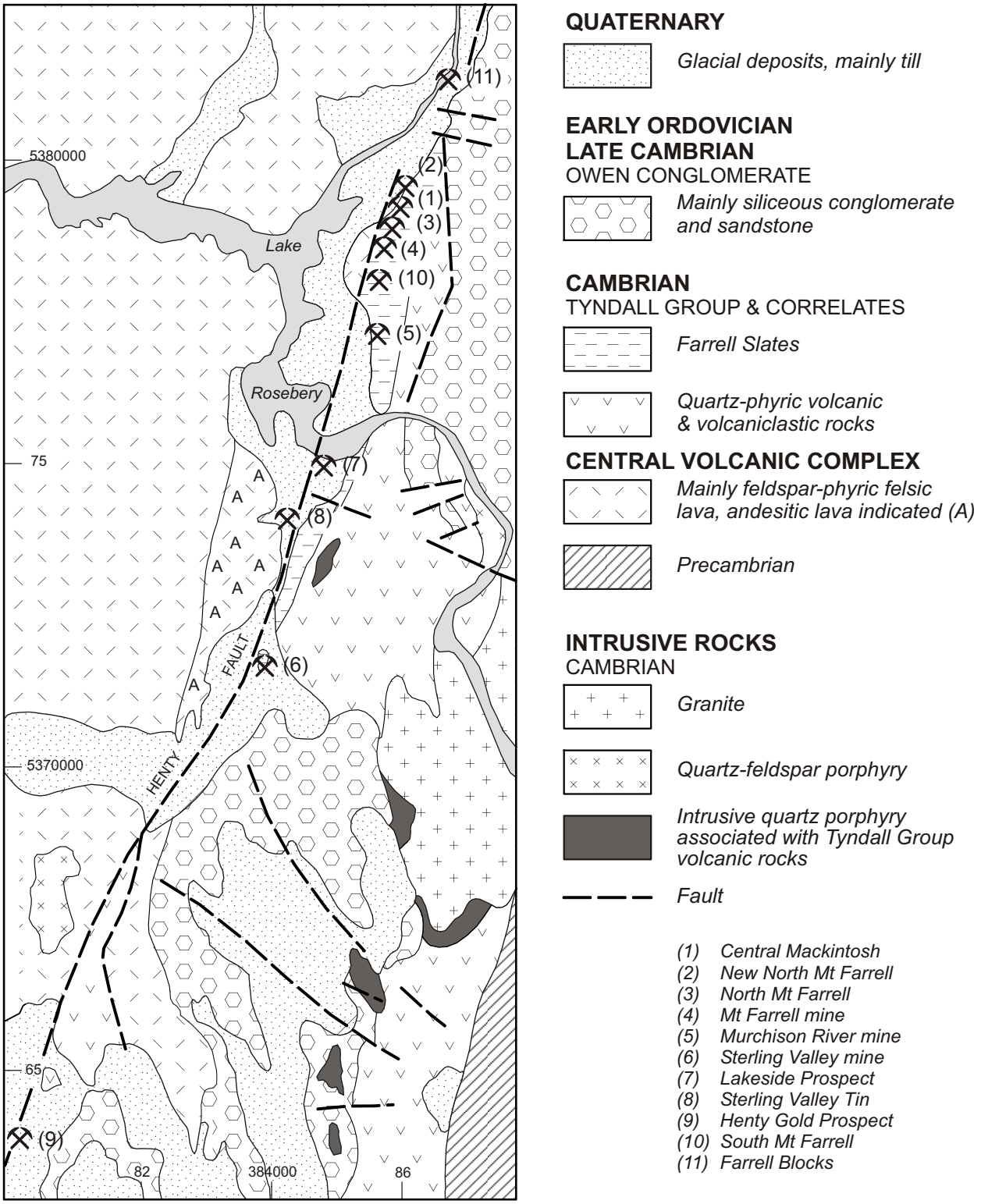

Figure 1.2

Geology of the Henty Fault Zone area with locations of the main deposits from the Farrell Blocks to the Henty Prospects (after Corbett and McNeill, 1987; Corbett and Komyshan, 1989)

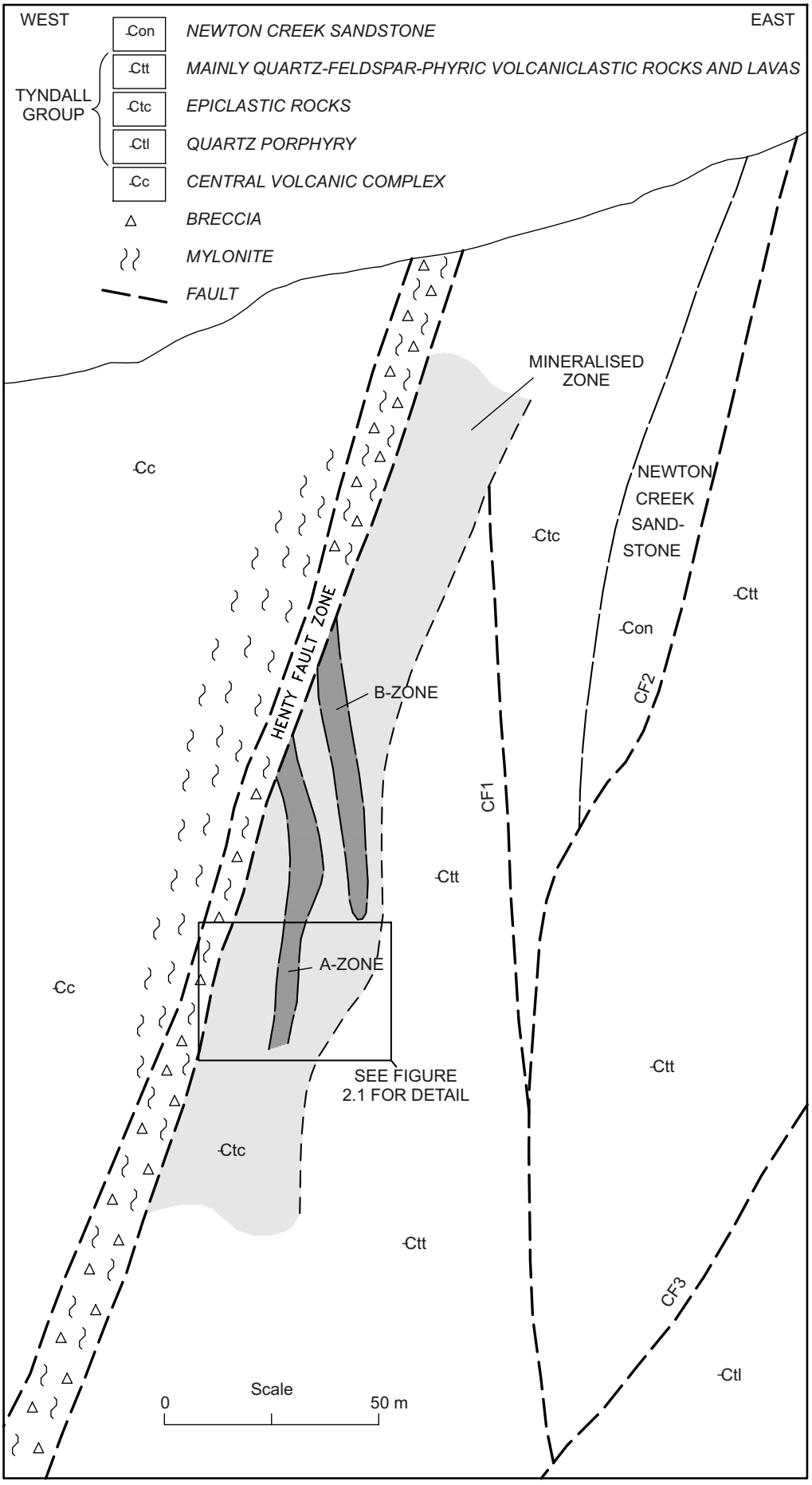

Figure 1.3

Generalised cross section showing the main mineralised zone and the major faults (after Carrasco et al., 1990)

CHAPTER 2

Hydrothermal alteration and associated mineralisation

The mineralisation occurs over a strike length of one kilometre and is up to 650 m deep at the south end of the prospect (R. H. Roberts, pers. comm.). The ore lies in a mineralised zone up to 35 m thick, which shows a systematic stratigraphic order (fig. 2.1).

The mineralised rocks at the Henty Prospect have been affected by shearing, fracturing and brecciation. Based on drill core and underground observations by RGC geologists, and also petrochemical studies, the alteration may be divided into six broad categories:

(1) Quartz-feldspar-sericite pyrite carbonate (MA)

(2) Main Mineralised Zone including:

  (a) Quartz-sericite-sulphides (MZ)

  (b) Quartz-sericite (MV)

  (c) Massive quartz-sulphides gold tellurides (MQ)

  (d) Massive pyrite quartz carbonate (MP)

(3) Quartz-carbonate-sericite-feldspar pyrite (SC)

(4) Massive carbonate hematite (LL)

(5) Minor alteration or mineral assemblages including:

  (a) Chlorite alteration

  (b) Massive to semi-massive sulphides-quartz-carbonate (MS)

  (c) Fuchsite-sericite alteration

  (d) Quartz gash-sulphides gold tellurides

(6) Quartz + albite (AS)

The mineral assemblages are simply the observed hydrothermally altered rocks or alteration types without considering the paragenetic stage of individual minerals in each mineral assemblage.

Apart from quartz-albite (AS) alteration, these mineral assemblages do not appear to reflect primary lithological differences, but reflect different degrees of alteration of epiclastic rocks. With increase in depth the strongly silicified and sericitised lithologies of the main mineralised zone grade into chlorite-carbonate and quartz-feldspar-sericite-pyrite-carbonate (MA) alteration types (e.g. HP 138A).

The thickness of the main mineralised zone (MZ-MV-MQ) varies widely, ranging from few metres to over 35 metres. However based on present drilling, the mineralised zone appears to thin both to the north and south, and is truncated by the Henty Fault in the upper southern part of the deposit. In a broad sense, the mineralisation parallels the Henty Fault, i.e. striking 020°. In a detailed sense the mineralised zone appears to be at a similar attitude to the sediments. The alteration assemblages within the main mineralised zone occur as elongated bodies along the strike of the mineralisation. Thicker sections of the main mineralised zone display complementary thickening of all the mineral assemblages within the zone. Alteration assemblages may also be repeated within the zone. The MZ zone is the thickest, followed progressively by the MV, MQ and MP zones. The mineralisation has been divided into zones A and B (RGC geologists, fig. 1.3). The B zone is restricted to the upper part of the deposit and is located to the east of the A zone. The rocks of the B zone mainly consist of quartz, sericite and pyrite with zones enriched in chalcopyrite and quartz and are generally very low in gold contents. However rare patches with high gold content have been intersected by drilling. General features of the mineralisation are shown in Figure 1.3. The A zone is continuous along the strike of the deposit and includes all of the alteration styles within the Henty Prospect.

Deposits such as the Henty Prospect, which have been affected by metamorphism and deformation, may exhibit extensive dissolution of material in "source region" and precipitation of such species in pore surfaces, veins and microcracks during deformation. Therefore, the establishment of paragenetic stages for different minerals, as it is normally carried out for undeformed hydrothermal deposits, can be misleading.

One of the common phenomena in describing the processes of mobilisation or remobilisation is 'pressure solution', which indicates the dissolution of minerals under non-hydrostatic stress. It is responsible for the formation of stylolites, pressure shadows, and truncation of minerals or fossils (see Durney, 1972 and Paterson, 1973 for details).

In this chapter, the paragenetic stages of minerals are considered relative to deformation (e.g. pre-, syn- or post-tectonic). Paragenesis of the hydrothermally-formed minerals is shown in Table 2.1.

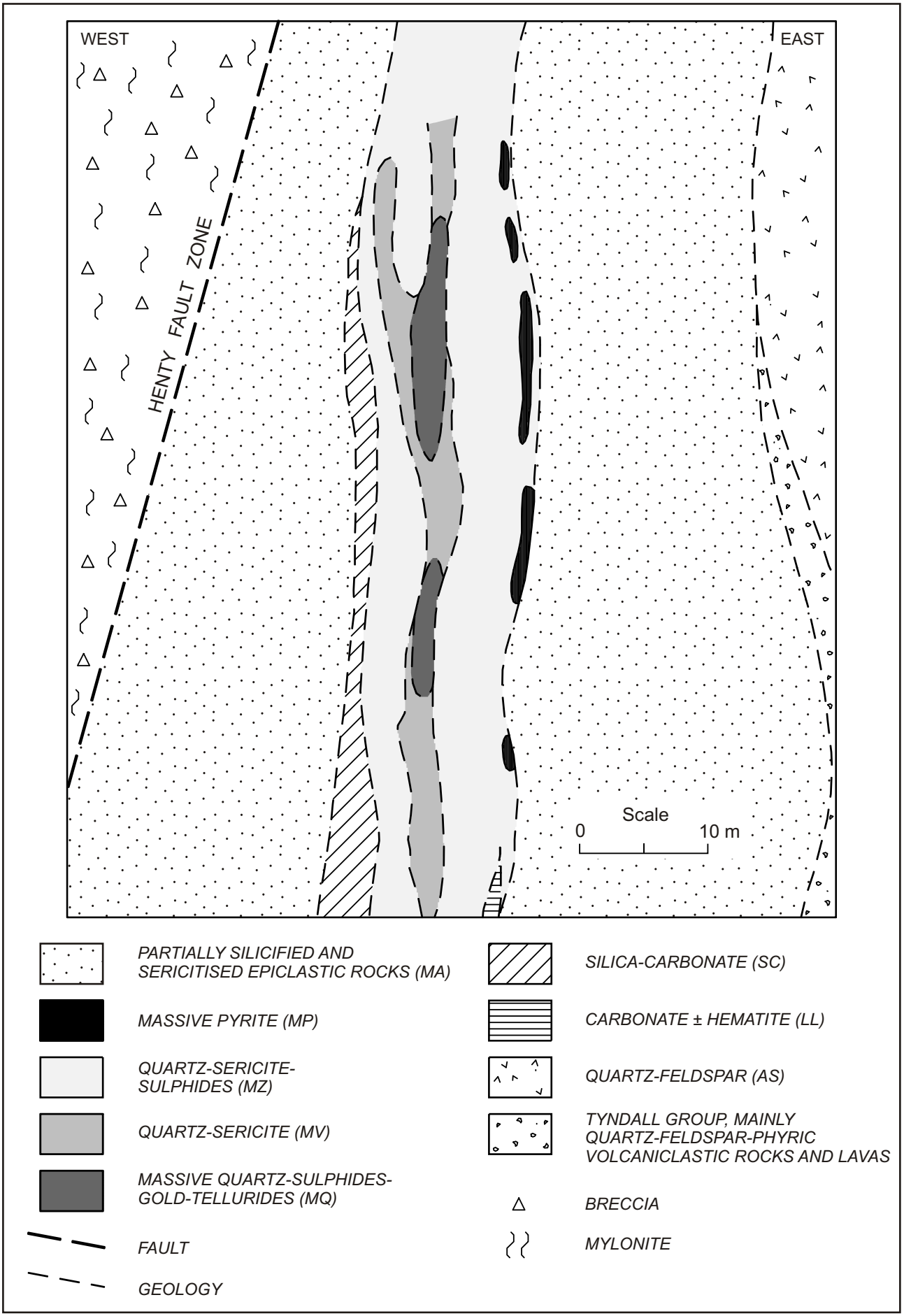

Figure 2.1

Schematic cross section showing the main mineralised zone

Table 2.1

Paragenesis of hydrothermally formed minerals at the Henty Prospect

Mineral	*Deformation*		
	Pre	*Syn*	*Post*
Massive pyrite	———		
Recrystallised pyrite		———	------
Carbonate		———	------
Musvovite	———	———	
Sericite		———	
Fuchsite		———	
Chalcopyrite		———	
Galena		———	------
Electrum		———	------
Tellurides		———	------
Quartz	cherty ———	———	------
Chlorite		———	
Hematite		———	
Bismuthinite		———	

------ Restricted to quartz gashes or veins

(1) QUARTZ-FELDSPAR-SERICITE PYRITE CARBONATE (MA)

This mineral assemblage represents hydrothermally altered rocks enveloping the main mineralisation (MA), and ranges in thickness from 15 to 60 metres. The rocks appear to be predominantly epiclastic sandstone and conglomerate with minor siltstone and shale. The most common rock type is an open framework conglomerate to sandstone consisting of poorly-sorted, rounded clasts varying in size from less than one millimetre to a few centimetres in a sericite-muscovite matrix. Most clasts are silicified. The rocks are mainly derived from a felsic volcanic terrain, and remnants of varieties of clast types including snow flake, perlitic, granophyre, quartz-feldspar porphyry and pumice have been recorded, although pumice is rare. Other clasts include andesite which is typically fuchsite-altered, pyrite, sandstone and siltstone, the latter commonly altered to chert. Two or three clasts with different textures may be observed in the same field of view under the microscope.

Rocks with similar features are also observed in the mineralised zones but textural preservation is poorer. Figures 2.2 to 2.10 illustrate some of the common features of these rocks. The observed features are consistent with deposition from debris flows. The clasts are commonly elongated parallel to sub-parallel to the foliation. Sulphide clasts in one sample located stratigraphically below the mineralised zone from DDH 140 were characterised by the occurrence of quartz pressure shadows inside the clast, grown normal to the foliation direction. This may indicate the rotation of the clasts or the change in the direction of the stress field. The latter is more likely, as another sample with similar clasts from the mineralised zone (103776) indicated that this phenomenon is related to an earlier phase of deformation which resulted in the development of cleavages broadly normal to the late cleavages.

The above descriptions are based on samples taken from the sill and randomly selected drill core, and may not represent the whole spectrum of the host rock types at the Henty Prospect. More work is also required to place the host rocks in their regional context.

(2) MAIN MINERALISED ZONE

(a) QUARTZ-SERICITE-SULPHIDE (MZ)

Volumetrically this is the main and most continuous mineralogical association at the Henty Prospect. It varies in thickness from a few metres to over 30 metres. In a broad sense the quartz-sericite (MV) and the massive quartz sulphides-gold-tellurides (MQ) assemblages occur as discontinuous, lenticular bodies within the MZ zone. However in detail, the relationships and the positions of MQ and MV may vary locally.

Hydrothermal alteration, including intense sericitisation, silicification and sulphidisation along with the shearing and brecciation, have largely obliterated the original rock textures. The rocks are grey-green in colour and exhibit similar features as those observed in the surrounding rocks (MA). The ratios of the clasts to the matrix, the sizes and types of the clasts and also the grain sizes of the sericite may vary over the length of a thin section. The rocks have been more intensely affected by hydrothermal alteration than those in the MA zone and consequently exhibit fewer relict primary textures. Most of the clasts have been subject to intense silicification. There are basically three different types of silicified clasts:

(1) fine-grained cherty silicified clasts characterised by randomly oriented, disseminated fine-grained mica,

(2) fine-grained cherty clasts free of mica, and

(3) clasts showing a coarse, granular texture, some of which may show sutured subgrain boundaries. The latter were probably quartz phenocrysts which have been recrystallised during deformation. There are also some pyrite clasts varying from massive to disseminated with minor carbonate, quartz and chlorite. The pyrite clasts are clearly wrapped by thin sericite layers along the cleavages.

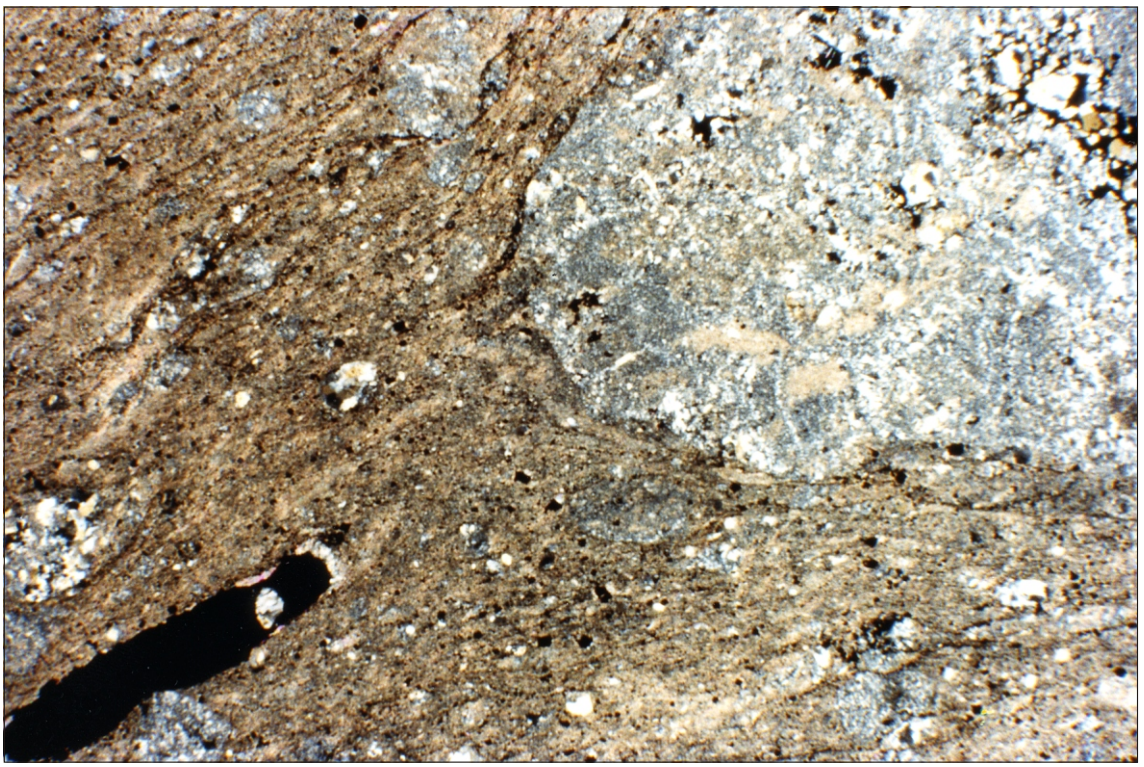

Figure 2.2

Epiclastic rock, characterised by poorly-sorted silicified clasts. Different quartz grain sizes may reflect the original textures of the clasts or later secondary silicification. Note the relatively coarsely crystallised quartz associated with chalcopyrite in the large last. Also note disseminated euhedral pyrite crystals in the sericite matrix and the concentration of opaque minerals along the late S_2 cleavages. Quartz pressure shadows associated with pyrite clast are parallel to the general foliations. Photomicrograph also illustrates the open framework (matrix supported) nature of the rocks. Sample 103969, FOV 11.7 mm 7.8 mm.

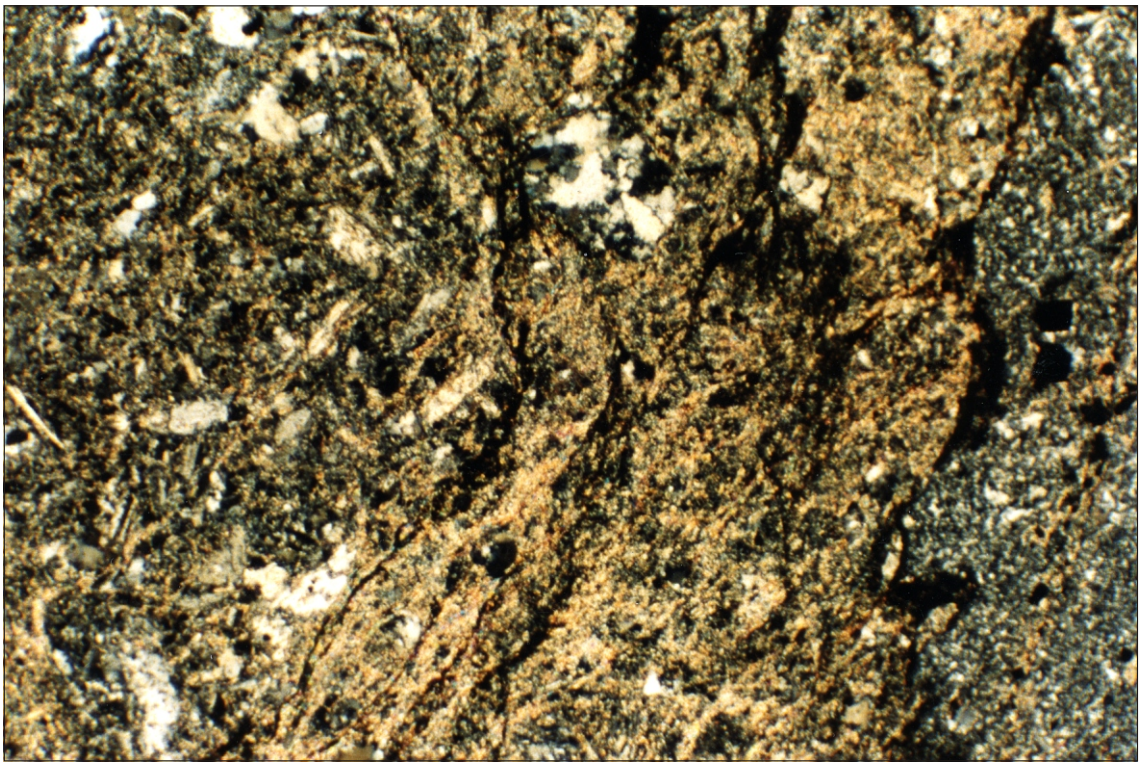

Figure 2.3

Occurrence of fine, silicified clast (right) and quartz-feldspar-porphyry clast (left) in a sericite matrix. Note the anastomosing nature of the later S_2 cleavages. The cleavage planes are filled with Ti oxides or disseminated fine grains of pyrite. Sample 104905, FOV 4.6 3.1 mm.

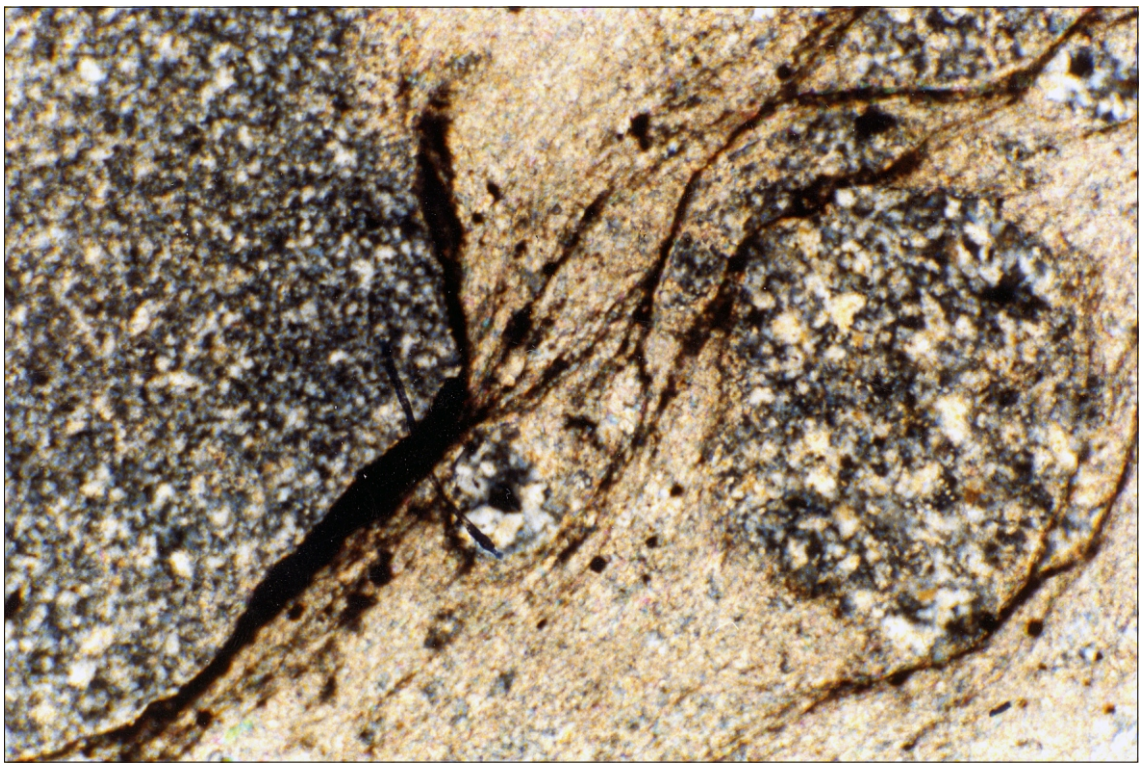

Figure 2.4

Two silicified clasts showing distinctly different textures in a sericite matrix. Note partial dissolution of lower part of the silicified clast on the right. Minor disseminated euhedral pyrite crystals occur in the matrix. Photo also illustrates the anastomosing and discontinuous nature of S_2 cleavages. Sample 103963, FOV 4.6 3.1 mm.

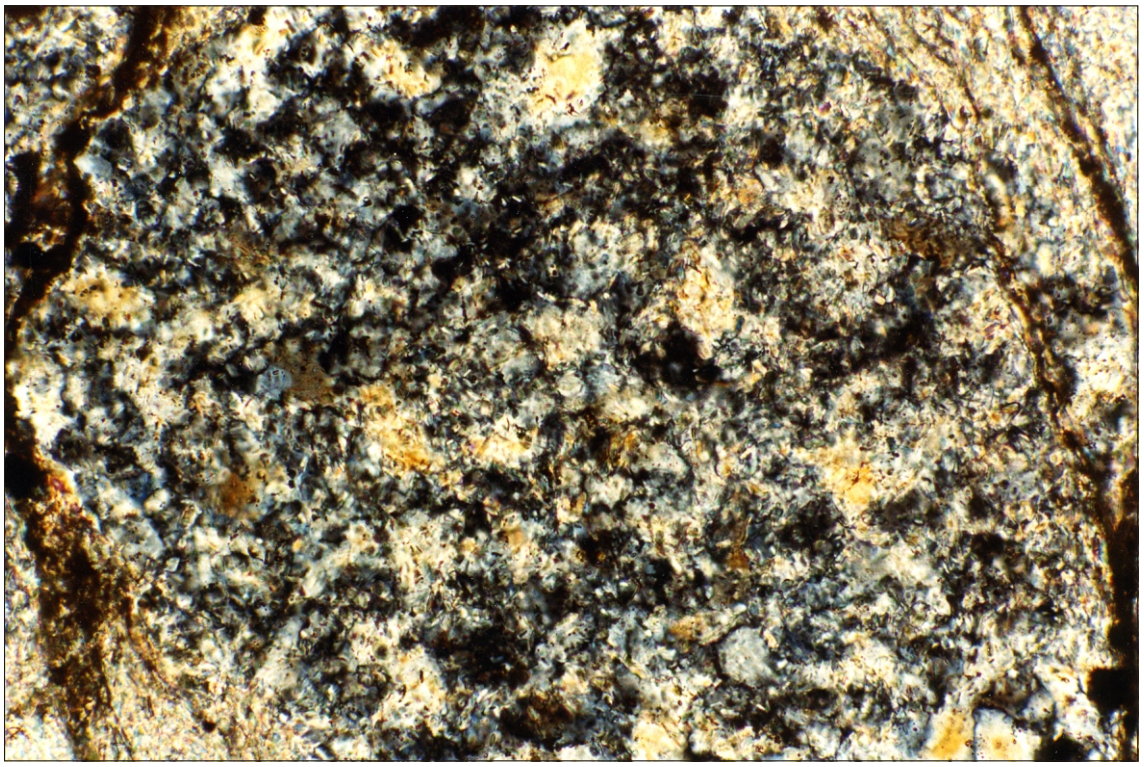

Figure 2.5

A clast showing snowflake texture. Note the remnants of randomly oriented fine mica flakes in the clast and also the concentration of opaque minerals along the cleavages. Sample 104931, FOV 710 475 m.

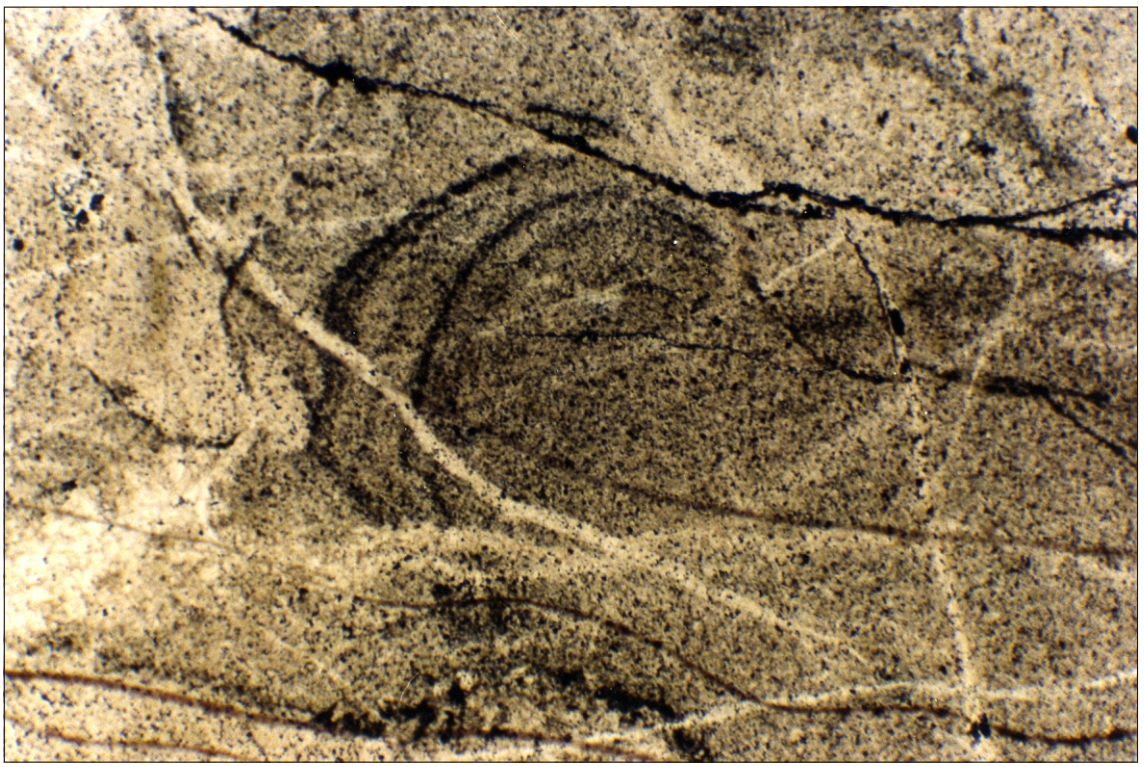

Figure 2.6

Remnants of perlitic structure in a silicified matrix. Devitrified perlite has been affected by brecciation and quartz veining. Sample 103979, FOV 4.6 3.1 mm.

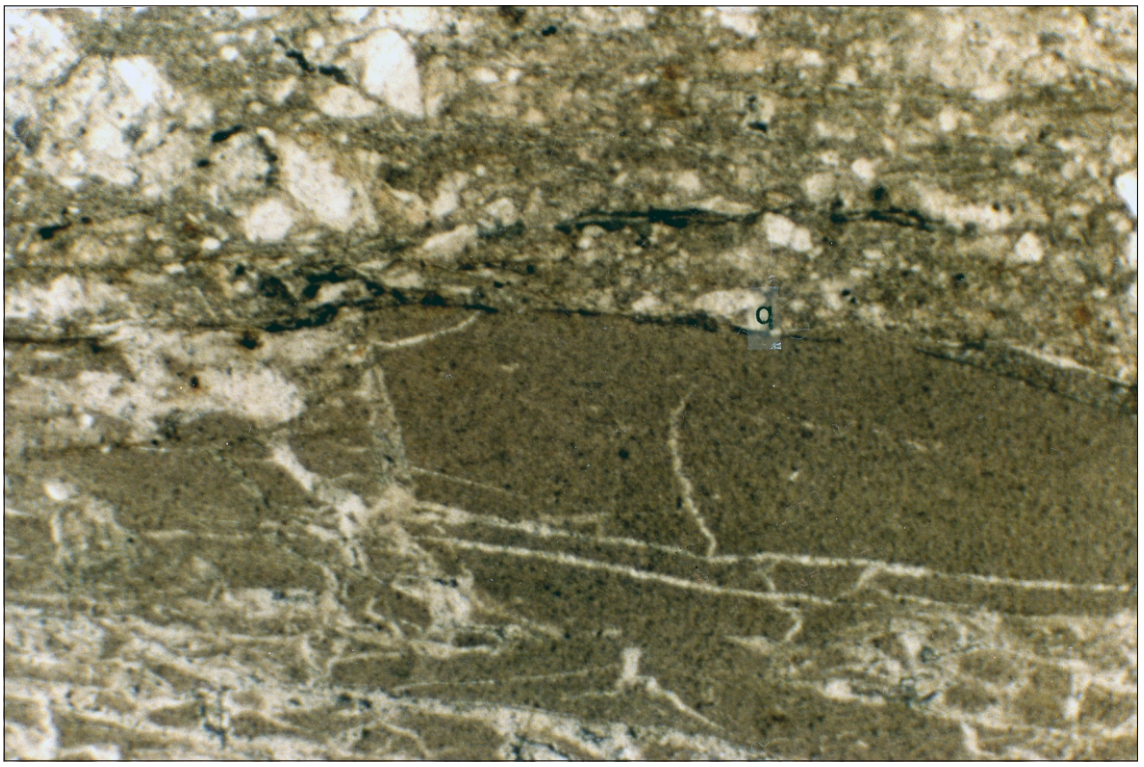

Figure 2.7

Occurrence of sedimentary rocks (greywacke and siltstone) in MA. Note the truncation of quartz grain (q) along the sheared contact. Also note the competency contrast between the two rock types (i.e. formation of cleavages in the sericitic matrix in the greywacke and fracturing in the finer silicified rock). Sample 3032, FOV 4.6 3.1 mm.

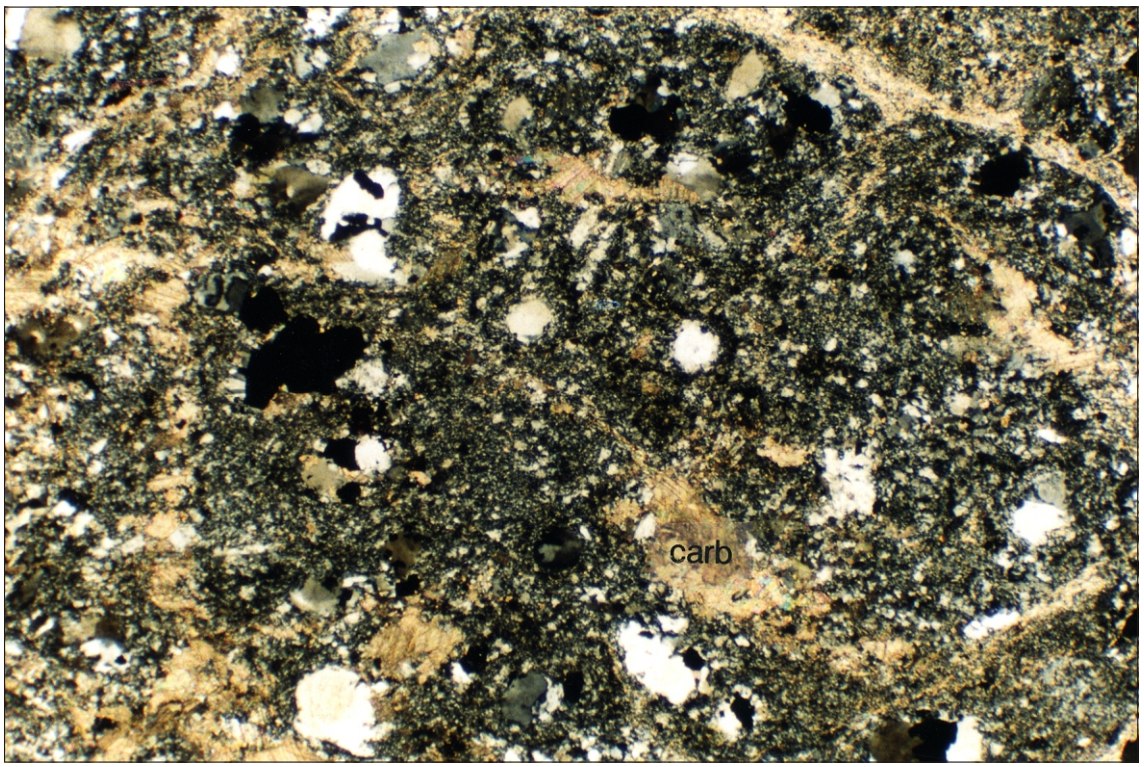

Figure 2.8

Hydrothermally-altered pumiceous clast in sericite-quartz matrix. The clast has been particularly affected by carbonate alteration (carb.). Sample 003033, FOV 1.8 1.2 mm.

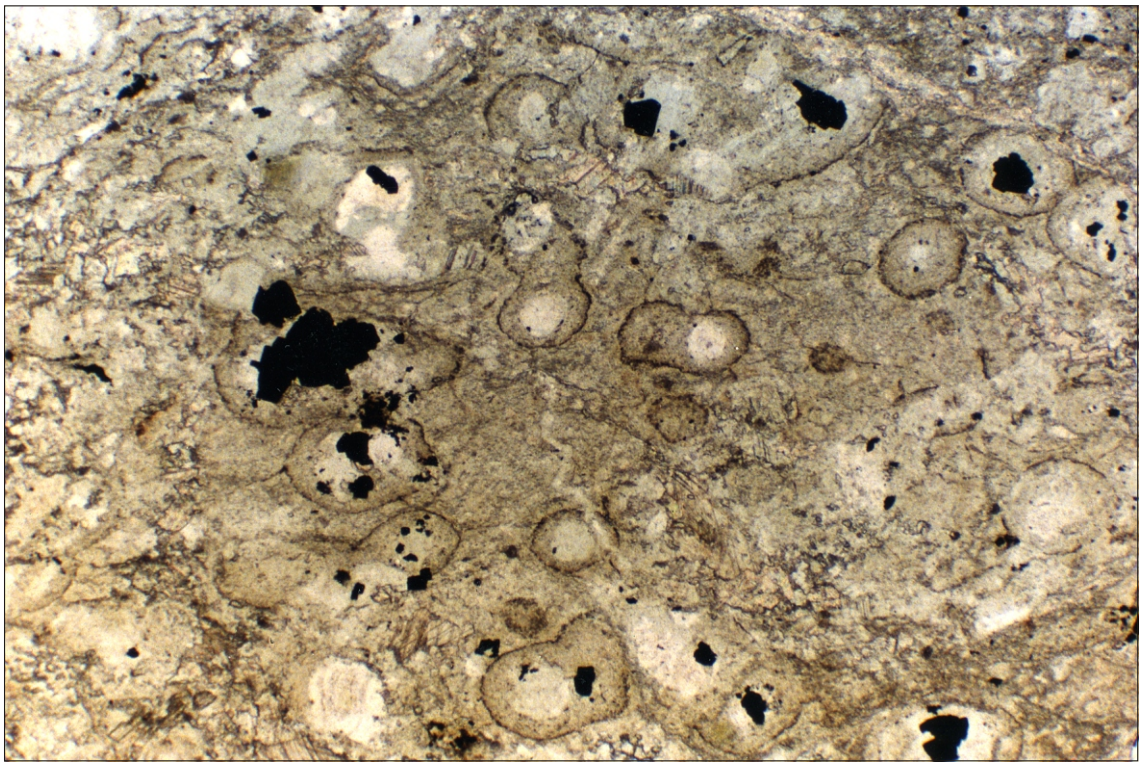

Figure 2.9

As Figure 2.8, showing the selective replacement of centre of pumice by pyrite or coarse-grained quartz. Pyrite grains have probably formed by replacement of earlier-formed minerals (e.g. carbonate) in the centre of the pumice voids. Plain polarised light.

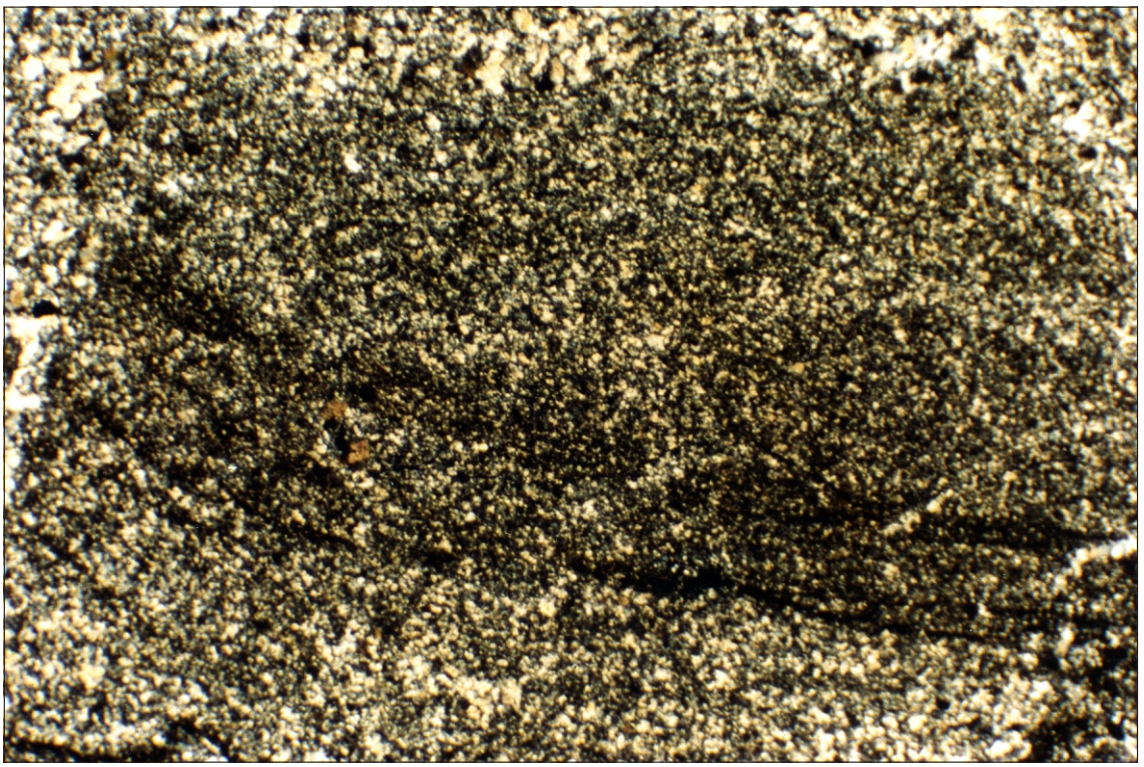

Figure 2.10

Occurrence of silicified sedimentary clast showing remnants of bedding. The silicified matrix is characterised by coarser-grained quartz. Sample 103979, FOV 4.6 3.1 mm.

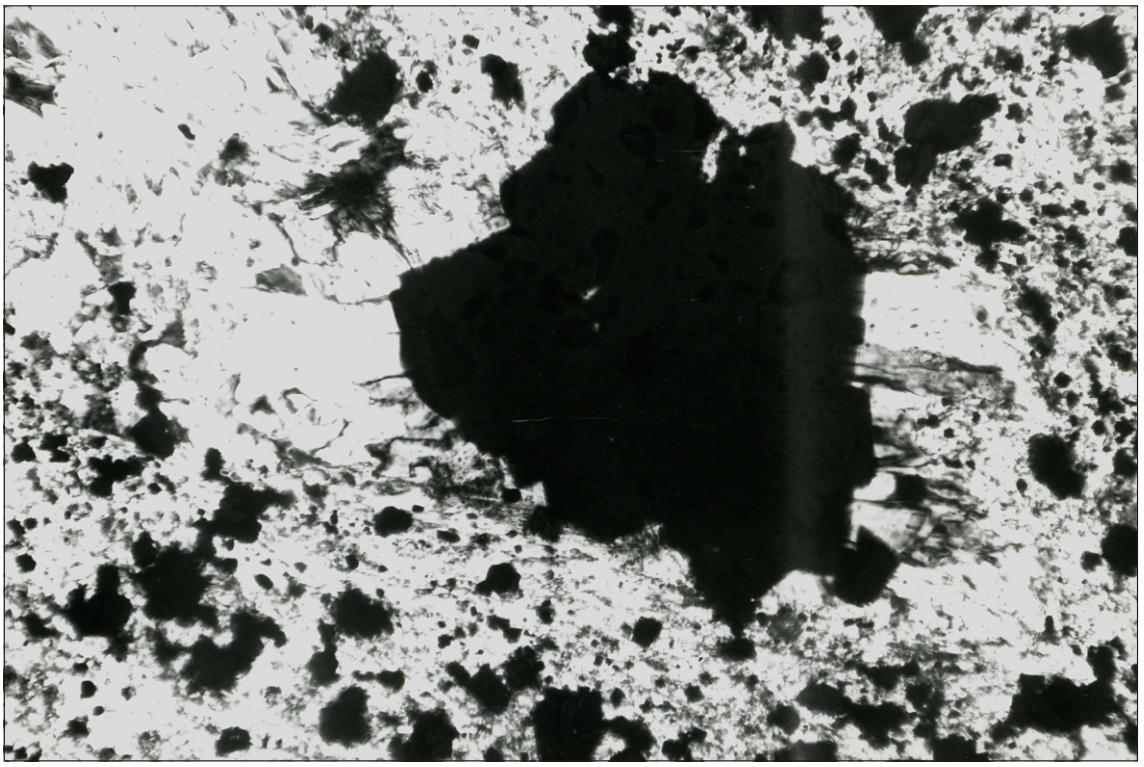

Figure 2.11

Disseminated pyrite grains in MZ showing quartz pressure shadows adjacent to the large pyrite crystal. Note there are two generations of quartz pressure shadows: (1) parallel to the general foliation (horizontal in photo), and; (2) grown from different surface of pyrite and are in the same direction as the early formed cleavages (S_1). See text for detail. Sample 103776. FOV 710 475 m.

The matrix consists of sericite of varying grain sizes, and less commonly muscovite with rare phenocrysts and minor partially sericitised feldspar and quartz phenocrysts. Fine-grained chert in close association with sericite may also form the matrix of the rocks.

Mineralogically, the rocks consist of quartz, sericite, pyrite with local carbonate and minor chlorite, feldspar, chalcopyrite, sphalerite, galena and traces of rutile-leucoxene and sphene which are probably the alteration products of pre-existing titaniferous oxides, apatite and zircon. Detailed mineralogical studies revealed that the rocks appear to have been affected by two generations of cleavage (S_1 and S_2). S_1 cleavages are rare and have mostly been overprinted by the later S_2 cleavages, and in places been bent and dragged by S_2 cleavages. They are marked by the growth of sericite with no sulphides, and were only positively identified in sample 103776. In places where S_1 cleavages have been preserved the elongation of the silicified clasts are parallel to sub-parallel to the cleavages.

S_2 cleavages are dominant in all the mineralised rocks. They are characteristically filled with fine, disseminated pyrite, sphalerite and some rutile-leucoxene. In general the clasts are mostly elongated sub-parallel to the S_2 foliation. Some of the clasts have also been cut by the late S_2 cleavages.

The occurrence of the fine-grained cherty clasts wrapped by the S_1 cleavages indicate that the early silicification is pre-tectonic at the Henty Prospect. This is also supported by the occurrence of randomly-oriented fine mica flakes in some of the silicified clasts.

Quartz pressure shadows adjacent to some of the disseminated pyrite are mostly parallel to S_2. However the quartz pressure shadows on a few pyrite grains exhibit two distinct directions, each of which has grown from different surfaces of the grains with one set being elongated parallel to the S_1 cleavage and the other parallel to S_2 (fig. 2.11). There is also evidence of rotation of some of the pyrite grains (i.e. bent quartz pressure shadows).

Another important observation from sample 103776 was the occurrence of a few semi-massive pyrite clasts (defined morphologically) elongated parallel to the general foliation. The pyrite grains within the clasts are mostly characterised by quartz pressure shadows grown parallel to the S_1 orientation (i.e. oblique to S_2 cleavages) with few pressure shadows elongated parallel to S_2 cleavages. This relationship demonstrates that the early (original) mineralisation must have been formed before or during the early cleavage development, and it pre-dates the late Devonian cleavage formation.

The concentrations of disseminated sulphides and oxides along the late cleavage planes is indicative of the remobilisation and reprecipitation of the earlier-formed minerals during a later (Devonian) phase of deformation.

The etching of the pyrite clasts in sample 103776 revealed that the pyrite has been affected by brecciation and is characterised by the broken, fine grains of early-formed zoned pyrite which have been healed by later pyrite. There are also some irregularly shaped, disseminated pyrite grains which have probably formed by the early brecciation of these clasts. These features are similar to those observed in the massive pyrite. Sample 103776 occurs to the west of the MQ horizon. This may indicate the occurrence of a pre-existing massive pyrite horizon below the horizon of the Henty Prospect mineralisation, which was subsequently eroded, transported and redeposited at the same or a higher level. This will be discussed further in the last chapter.

The rounded shape or the parallelism between the elongated clasts and the foliation direction is due to dissolution of silicified clasts at interfaces abutting the phyllosilicate layers, which consist of thin (10 to 100 m) muscovite grains commonly oriented parallel or sub-parallel to the foliation. Sericite and muscovite appear to have been extensively remobilised during deformation and may occur as:

(a) beard microstructure (mostly asymmetric) on surface parallel to the elongation,

(b) in shear zones truncating the silicified clasts, and

(c) partial replacement of the silicified clasts.

All of these features indicate that substantial dissolution and mass transport have occurred during deformation at the Henty Prospect.

Microfabrics preserved in the interlayered silicate domain in the MZ zone are only phenocrysts of quartz (up to 1 mm) and sericitised feldspar phenocrysts.

Carbonates are commonly deformed and show deformation twinning and kinked or bent cleavages, and in places are finely recrystallised. They occur as veinlets of millimetric thickness, partially replaced patches, or as late undeformed veinlets cross-cutting the rocks.

Disseminated euhedral pyrite is mainly concentrated along the foliation planes, sheared zones, and also as small (5–10 m) grains disseminated in the matrix (fig. 2.2). Larger crystals of pyrite (>100 m) may exhibit quartz, muscovite, chlorite and rarely sphalerite pressure shadows, some of which show up to three different directions of elongations. This may be due to different stress fields or rotation of clasts in a single stress field. The latter is more likely, as this phenomenon is not commonly observed and the elongation directions may vary within the same field of view under a microscope.

Etching of a polished thin section (103760) revealed that the disseminated euhedral pyrite is morphologically uniform and lacks zoning and

colloform or framboidal textures, and has not been affected by brecciation. This may indicate that the majority of pyrite has been recrystallised during deformation.

Chlorite is a minor mineral and is blue to green in colour. It mainly occurs along the sheared zones or as pressure shadows adjacent to pyrite grains.

In terms of veining, there are at least four styles of quartz veining within the MZ zone including:

(1) fibrous barren quartz,

(2) barren micro-veins,

(3) mineralised veins, and

(4) late, undeformed veins.

Fibrous barren quartz veinlets are relatively common and are up to 2 mm thick. The elongation of quartz fibres is commonly sub-parallel to the direction of elongation. However quartz fibres in different fractures may show two or more different directions of elongation in the same thin section. Some of the quartz fibres have been partially recrystallised.

Micro-veins have a planar to irregular shape and are up to 1 mm wide. They are commonly confined to the silicified clasts and form as network veining, although some cross-cut the clasts. Quartz micro-veins have been recrystallised and are often indistinguishable from the silicified cherty clasts and the silicified matrix. These micro-veins appear to have been formed early in the stage of alteration (i.e. pre-tectonic). This was shown in sample 103776, in which a 400 m thick micro-vein was clearly bent parallel to the S_1 orientation.

Mineralised quartz veins are common in MZ and MV, and mainly occur along the foliation planes. They range up to about 30 cm in width and have commonly been affected by shearing. The quartz is strained and is partially recrystallised in places. The common sulphides are pyrite, chalcopyrite, galena and sphalerite. Deformed carbonate may also be associated with the sulphides. It is not clear if the quartz-sulphide veins were formed during S_2 cleavage formation or whether they represent pre-Devonian mineralisation which has been dragged into the Devonian cleavages, a feature which is clearly shown in sample 103776.

Unstrained to moderately strained granular quartz may occur in low-strain zones (pores, voids) and is commonly associated with irregular patches of chalcopyrite and galena.

(b) QUARTZ-SERICITE (MV)

These rocks occurs as lenticular bodies ranging from less than one metre to about 15 m in thickness. The MV zone is volumetrically smaller than MZ zone. In general the MV rocks are enclosed by the MZ zone. The rocks are mineralogically similar to the MZ. However MV is distinguished from MZ by:

(a) pale green to cream colour,

(b) more intense silicification of the matrix and the clasts,

(c) lower pyrite contents, and

(d) occasional occurrence of fluorite.

The rocks appear to be the silicified versions of quartz-sericite-sulphides rocks (MZ) in which most of the primary microfabrics have been overprinted. However there are enough silicified clasts and different relict textures in some of the clasts to indicate similar original rock types to those observed in MZ. Silicification occurs as fine-grained cherty quartz or as small patches of coarse, granular quartz associated with chalcopyrite, galena and sphalerite.

MV zones are also characterised by more sheared quartz-pyrite-chalcopyrite-galena sphalerite veins (i.e. the equivalents of mineralised quartz veins in MZ) ranging in thickness from less than 1 mm to several centimetres. These sheared veins mostly occur along the cleavage planes, and in places exhibit thinning at both ends (fig. 2.12). Fibrous quartz veins are also more common and are perpendicular to the foliation (i.e. parallel to the extension direction), and may also exhibit crack and seal structures.

Fluorite is not common and mainly occurs in fractures, most of which are normal to the cleavage (extensional fractures, fig. 2.13). Lenticular, fractured patches of fluorite (up to 300 mm long) were also observed in an extensively fractured quartz-sericite rock at the north end of the sill. Quartz-sericite rocks associated with fluorite appear to be richer in gold than typical MV alteration (R. H. Roberts, pers. comm.).

Detailed mineralogical studies showed that gold has been formed during a late stage of deformation. This is demonstrated by the occurrence of gold as pressure shadows adjacent to euhedral recrystallised pyrite and also as fine grains (~5 m) along the the late S_2 cleavages (fig. 2.14, 2.15). No direct association was observed between the electrum grains and fluorite. However the late nature of the fluorite and gold in these rocks clearly demonstrates the extensive remobilisation and reprecipitation of gold during deformation at the Henty Prospect.

Other features of the MV are basically similar to those described for MZ.

Some orientated thin sections from MZ and MV were prepared to study the sense of shearing in these rocks (e.g. samples 103961 and 103980) using criteria observed in rotated clasts and pressure shadows adjacent to pyrite (Simpson and Schmidt, 1983). The majority of the determinations indicated a reverse

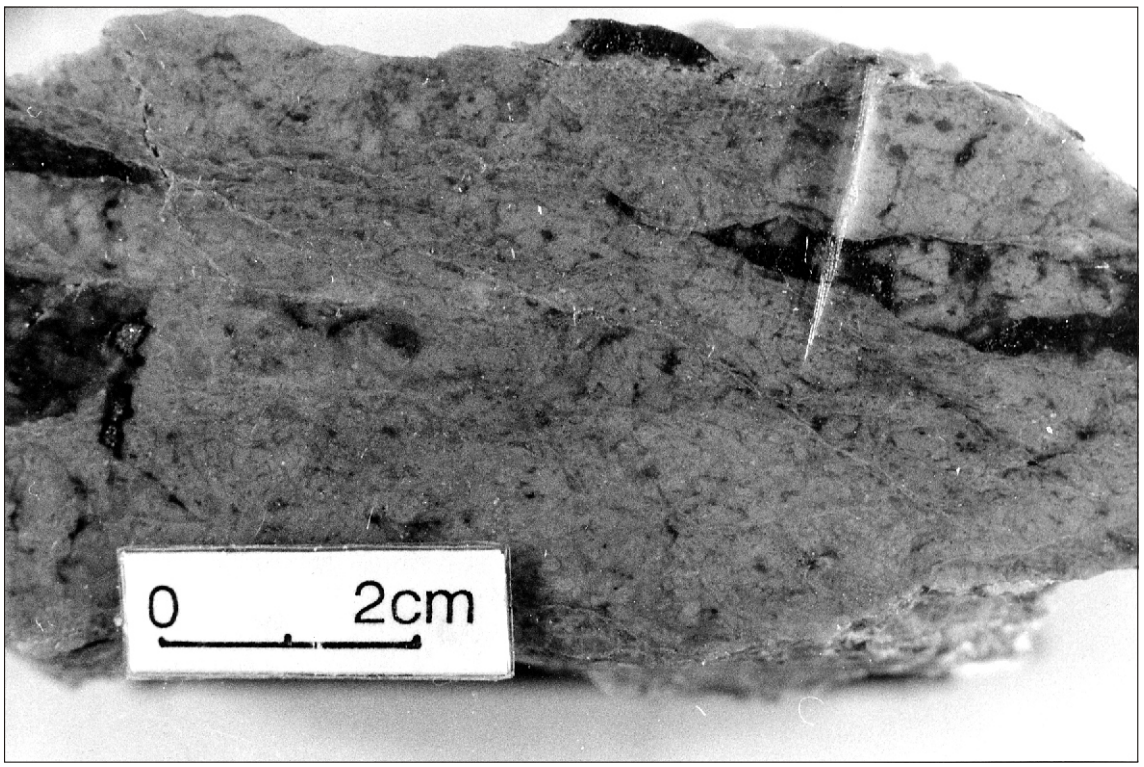

Figure 2.12

Quartz-sericite rock (MV) with boudinaged (shear induced) quartz-sulphides vein. Note thinned ends of the vein along the shearing. Similar vein types also occur in MZ. Sample 103943.

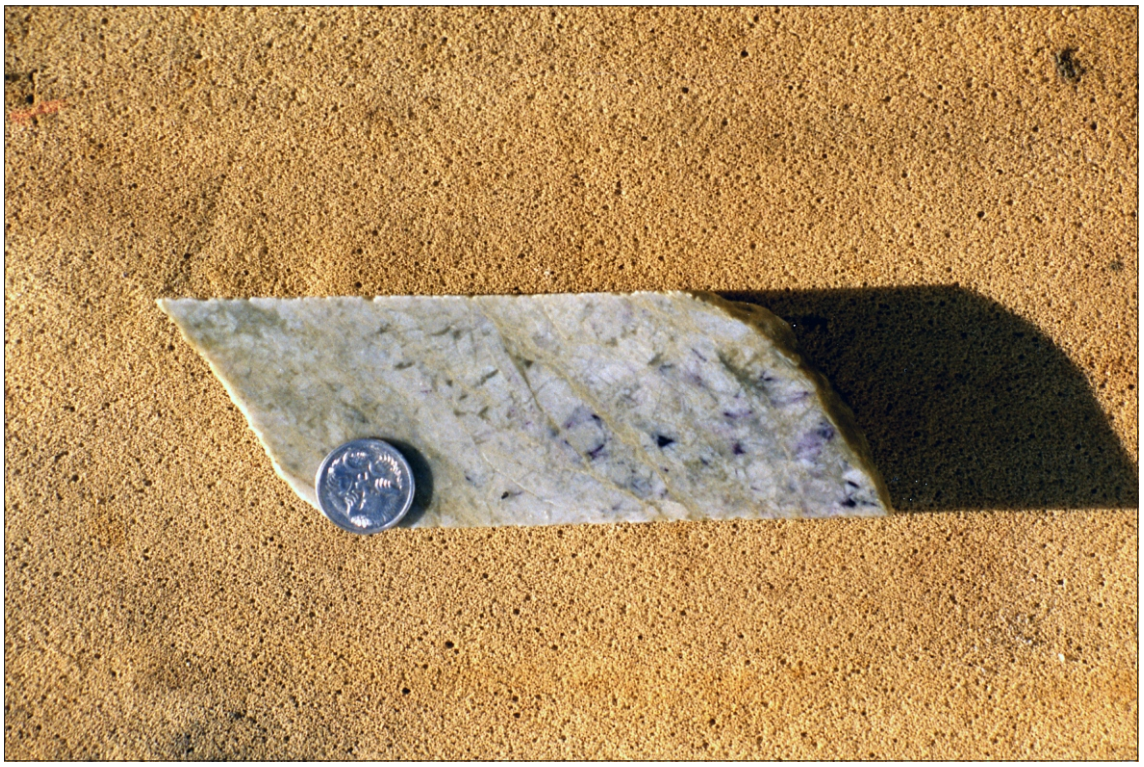

Figure 2.13

Quartz-sericite-fluorite rock. Note the occurrence of extensional fractures filled by fluorite, sericite and quartz. Sample HP 129D, 621 m.

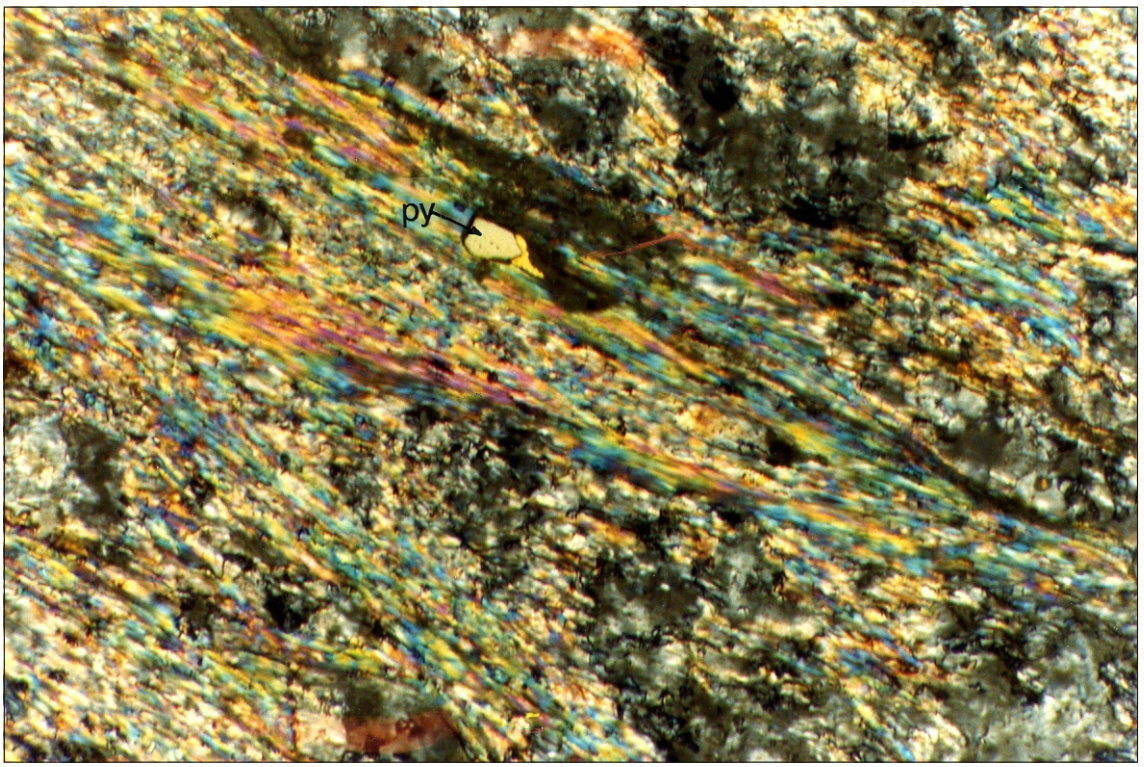

Figure 2.14

Occurrence of electrum (yellow) as pressure shadow adjacent to a pyrite grain along a muscovite-rich sheared zone in MV containing fluorite. Combined reflected and transmitted lights. Sample 104944, FOV 580 390 m .

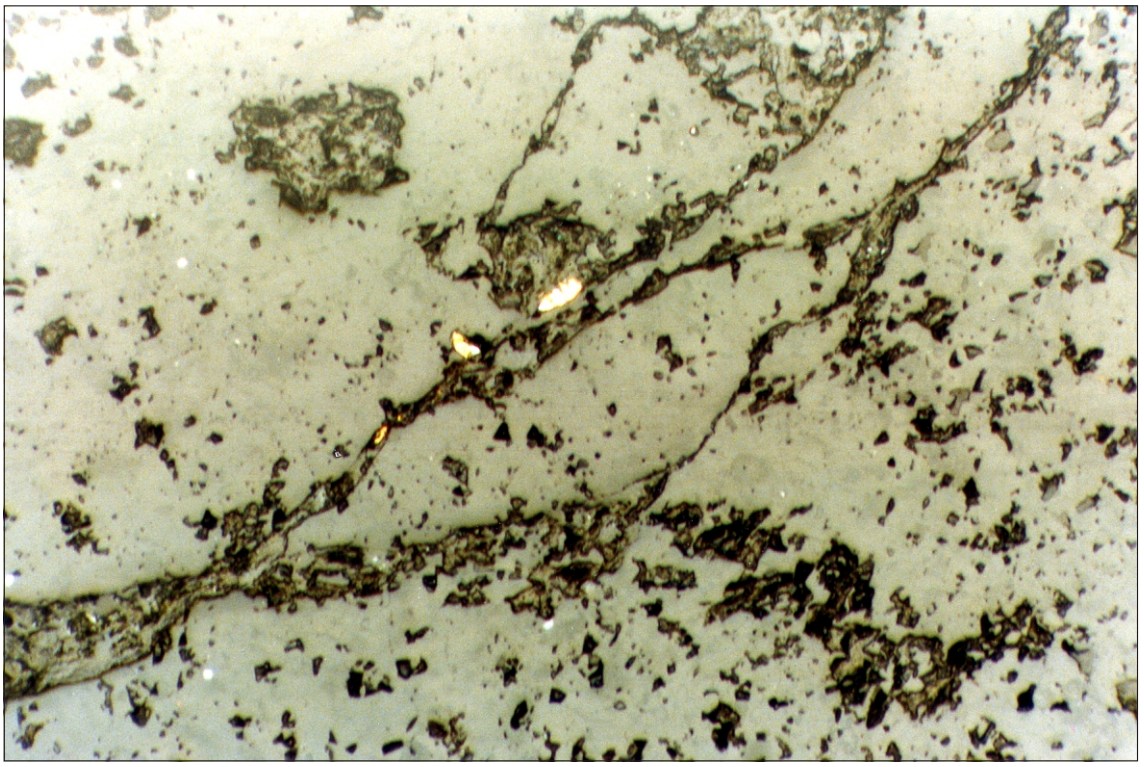

Figure 2.15

Disseminated electrum (yellow) along cleavage plane in a quartz-sericite-fluorite rock. Notice the grain size variations of the gold grains. Reflected light. Sample 104944, FOV 580 390 m.

movement (i.e. east up, west down). However a few exhibit the opposite sense of shear.

(c) MASSIVE QUARTZ-SULPHIDE-GOLD-TELLURIDES (MQ)

This is the main gold-bearing rock at the Henty Prospect. It is characterised by extensively fractured and brecciated, grey, massive quartz occurring as lenticular bodies ranging from a few metres to 50 m long and up to about 8 m wide. Based on recent drilling, this style of mineralisation appears to be vertically continuous up to about 200 metres. MQ lenses are parallel to the general north-trending foliation and in small sections occur as lateral extensions of MV, showing a similar thickness to the MQ. More commonly MQ lenses are enclosed by MV rather than by MZ. There appears to be a sympathetic relationship between the thickness of MQ and those of MV and MZ, and higher gold contents are normally associated with thicker zones of MQ mineralisation. MQ may be subdivided into two mineral assemblages viz:

(1) Massive quartz + sericite muscovite + pyrite

This rock hosts the gold-sulphide-telluride mineralisation. It appears to have been formed by intense silicification of pre-existing volcaniclastic rocks. The rocks have been intensely brecciated and mainly consist of recrystallised, fine-grained cherty quartz with minor muscovite, sericite, pyrite and carbonate. The proportions of the minerals vary widely in different samples, to the extent that some are very similar to MV (i.e. higher sericite contents). There is no evidence of primary textures in some of the clasts (e.g. 103751 and 103965). However the clastic nature of the rocks, and the remnants of S_2 cleavages which have been preserved in some other samples (e.g. 103941), indicate that MQ was probably of a similar original lithology to those of the MV and MZ (fig. 2.16, 2.18 and 2.18*a*). The clasts are up to 10 mm long and have been intensely affected by brecciation, silicification, and multiple veining (breccia veining, fig. 2.16, 2.19). There is also some quartz and feldspar (sericitised or silicified) in the fine cherty groundmass.

Mineralogically, the quartz has been affected by extensive recrystallisation at different stages. The earliest stage of recrystallisation is characterised by fine-grained recrystallised quartz and minor, randomly-oriented fine-grained muscovite flakes. This indicates that at least the early silicification at the Henty Prospect is pre-tectonic. The recrystallised quartz has been affected by another, later stage of recrystallisation or polygonisation and is commonly free of fine flakes of mica. The boundaries between the two stages of recrystallisation, or the early recrystallisation and the later polygonisation, are characterised by stylolitic contacts in which muscovite and, in places, sulphides have been deposited. The massive quartz has been extensively cut by barren clear quartz veinlets about 0.5 to 2 mm wide. The quartz veins are totally recrystallised and often indistinguishable from the massive quartz under the microscope (fig. 2.18).

There is also some network microveining which is confined within the silicified clasts. Fibrous quartz veins showing different directions of elongations are also observed in MQ. All of these vein types also occur in MV.

Sericite contents may vary considerably in MQ. Sericite occurs as matrix, feldspar pseudomorph, small irregular patches and along stylolitic boundaries.

Pyrite occurs as euhedral small crystals (20–300 m) disseminated in the recrystallised quartz or along the discontinuous fractures, remnants of S_2 cleavages, and the stylolites.

Carbonates (mainly calcite) are relatively common and occur as aggregated masses or as veinlets. They are mostly recrystallised and show deformation twinning and bent cleavages. However undeformed (i.e. post-tectonic) carbonate veinlets are also observed. Accessory minerals are similar to those occur in MZ or MV.

(2) Quartz-Sulphide-Gold-Tellurides

This mineralisation is hosted by the massive quartz-sulphides-sericite rocks and occurs in irregular discontinuous microfractures, veinlets, clots and small (millimetric) patches (fig. 2.18*a*, 2.17, 2.20). Quartz is grey to dark blue in colour, shows granular texture, and is mildly strained. The grey-dark blue colour of the quartz is probably due to the occurrence of fine sulphides. The main sulphide minerals include chalcopyrite, pyrite and galena with minor sphalerite. The concentration and proportion of different minerals may vary locally. Chalcopyrite is the main sulphide and displays different occurrences:

(a) along irregular and discontinuous microfractures,

(b) as infillings along with galena in fractured and brecciated pyrite,

(c) along grain boundaries, and

(d) as "chalcopyrite disease" in sphalerite.

Quartz adjacent to the chalcopyrite is mildly strained and rarely exhibits pressure shadows. The etching technique of Kelly and Clark (1975) on chalcopyrite from samples 103937 and 103942 did not show any deformation microstructures such as recrystallisation, deformation, twinning etc. The undeformed nature of the chalcopyrite may indicate the remobilisation and reprecipitation of the chalcopyrite in microfractures and cavities at different stages during deformation. Sulphur isotope studies (Chapter 4) also indicate similar

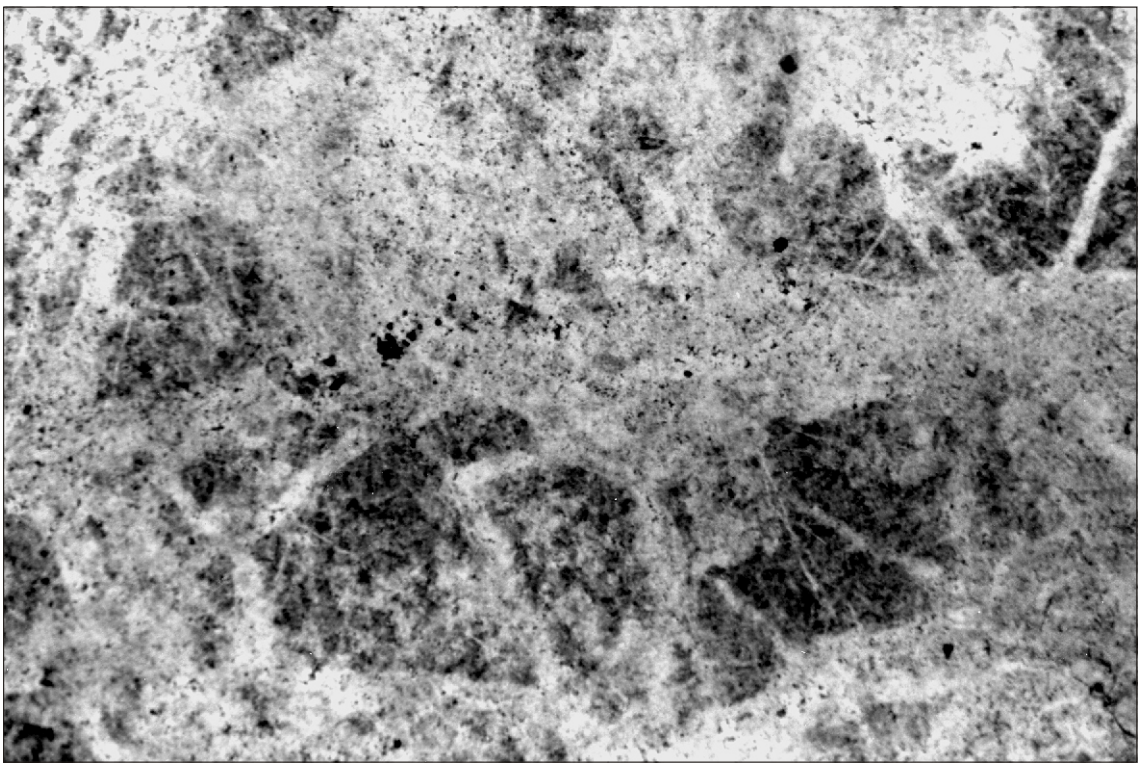

Figure 2.16

Remnants of silicified clasts (dark grey) in fine-grained cherty matrix. Note the intense brecciation and veining in the rock (plain polarised light). Sample 103751, FOV 1.8 1.2 mm.

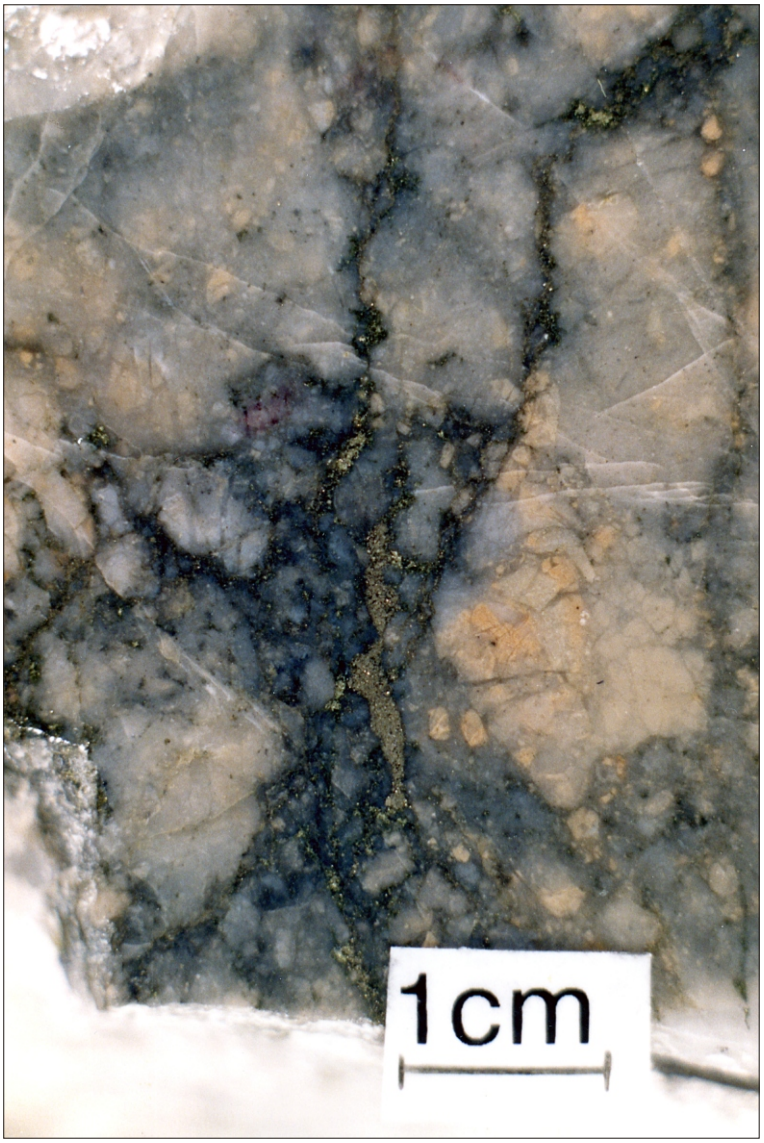

Figure 2.17

MQ and the associated mineralisation in the fractures. Photo illustrates the extensive brecciation of the silicified rock and also the replacement of the silicified rock by late, unbrecciated grey quartz associated with sulphides, gold and tellurides mineralisation. The grey colour of the quartz is probably due to the occurrence of disseminated, fine grains of sulphides. Sample 103934.

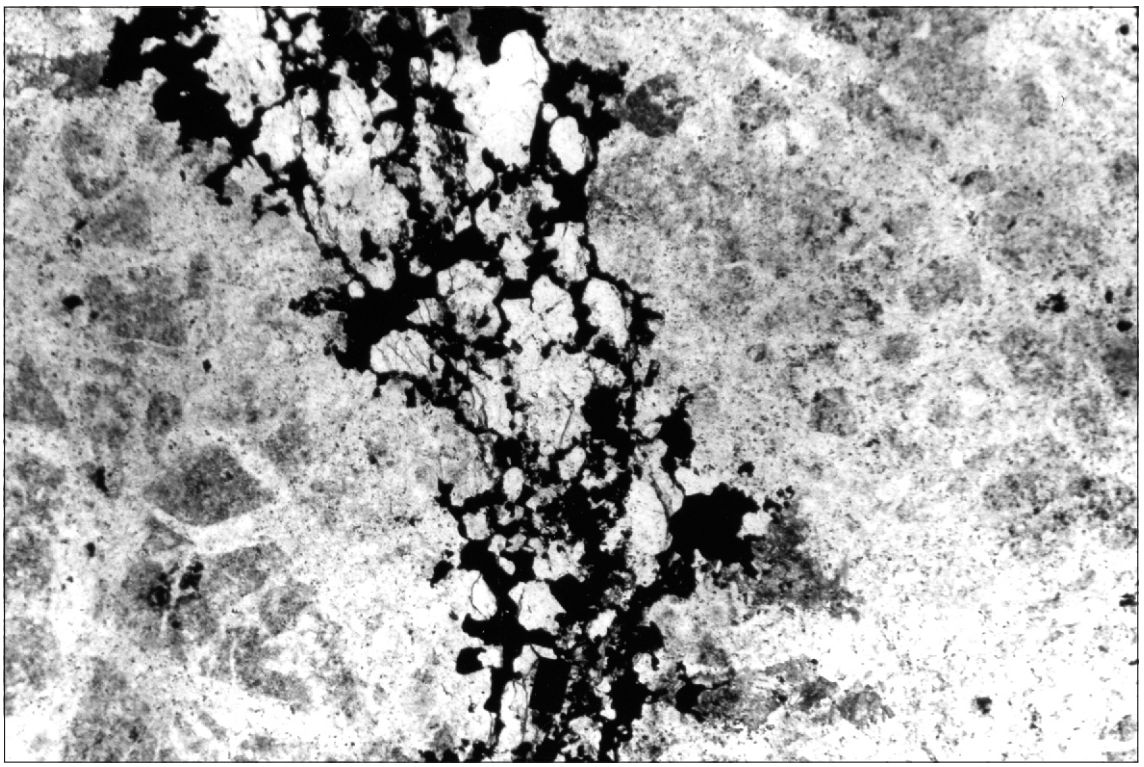

Figure 2.18

Quartz-sulphides as fracture filling in silicified matrix (i.e. MQ). Note the remnants of silicified, finely brecciated clasts and also the veining (breccia veins).
Plain polarised light. Sample 103751. FOV 4.6 3.1 mm.

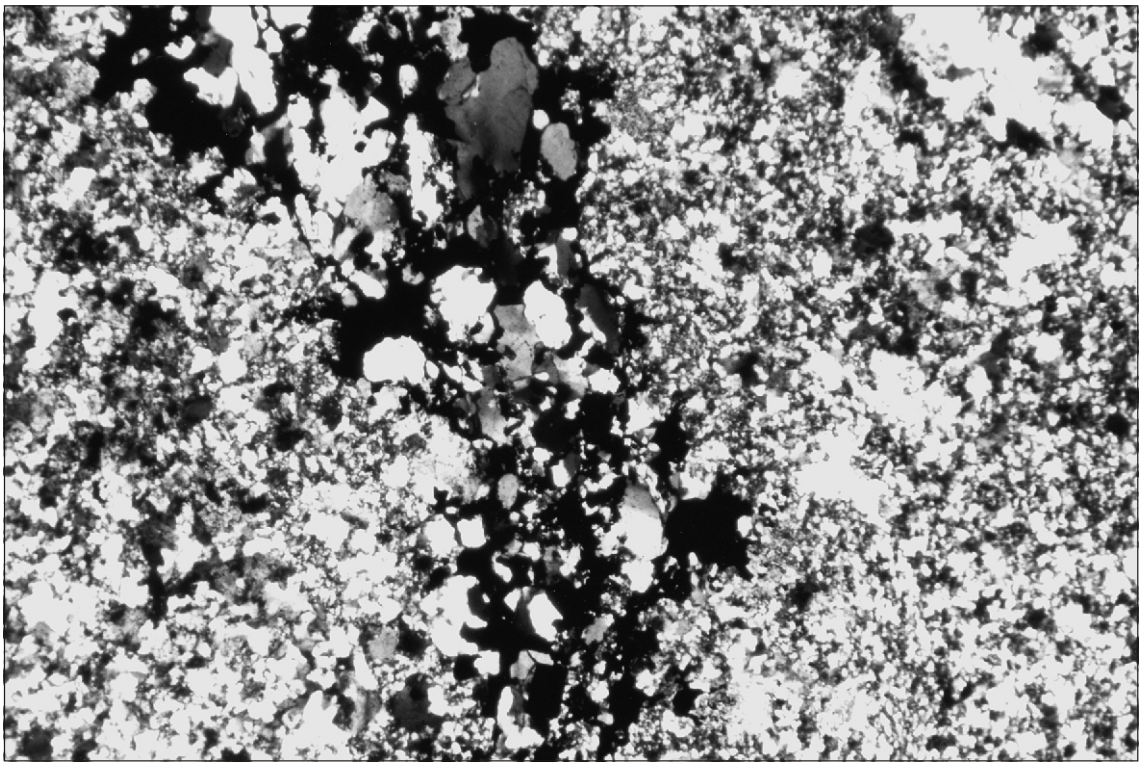

Figure 2.18a

As Figure 2.18, cross polars. Note that the brecciated fragments are indistinguishable from the silicified matrix.

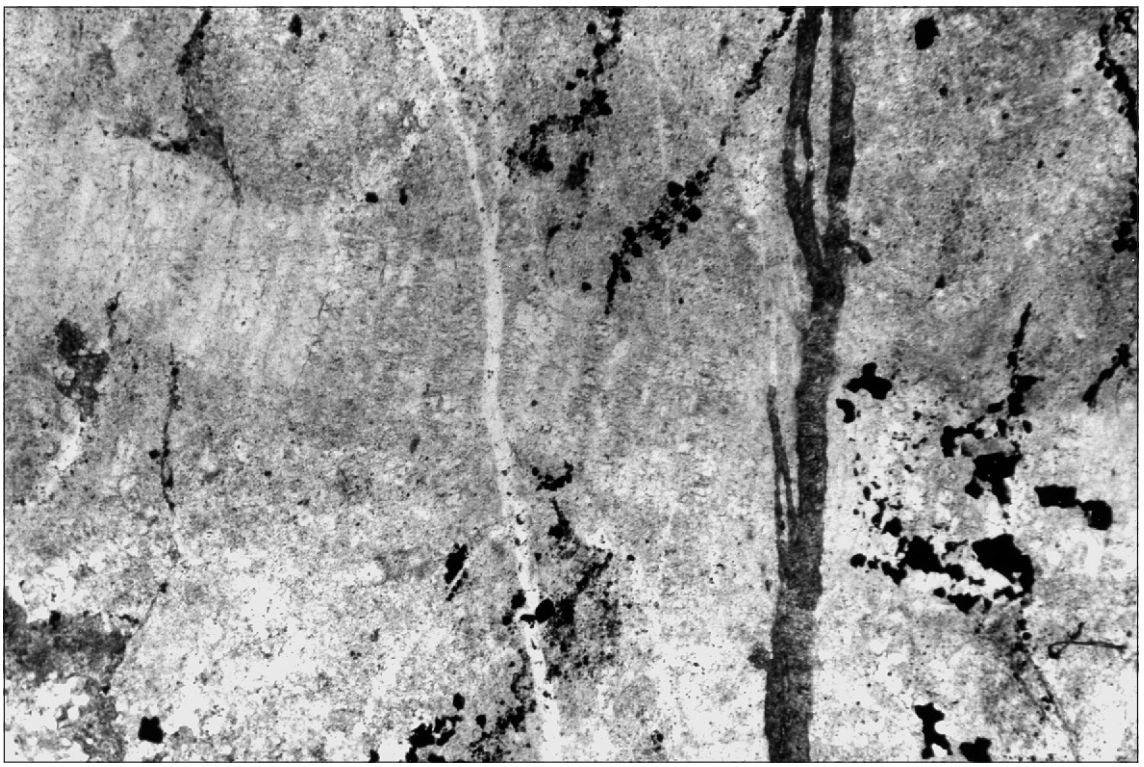

Figure 2.19a. *Plain polarised*.

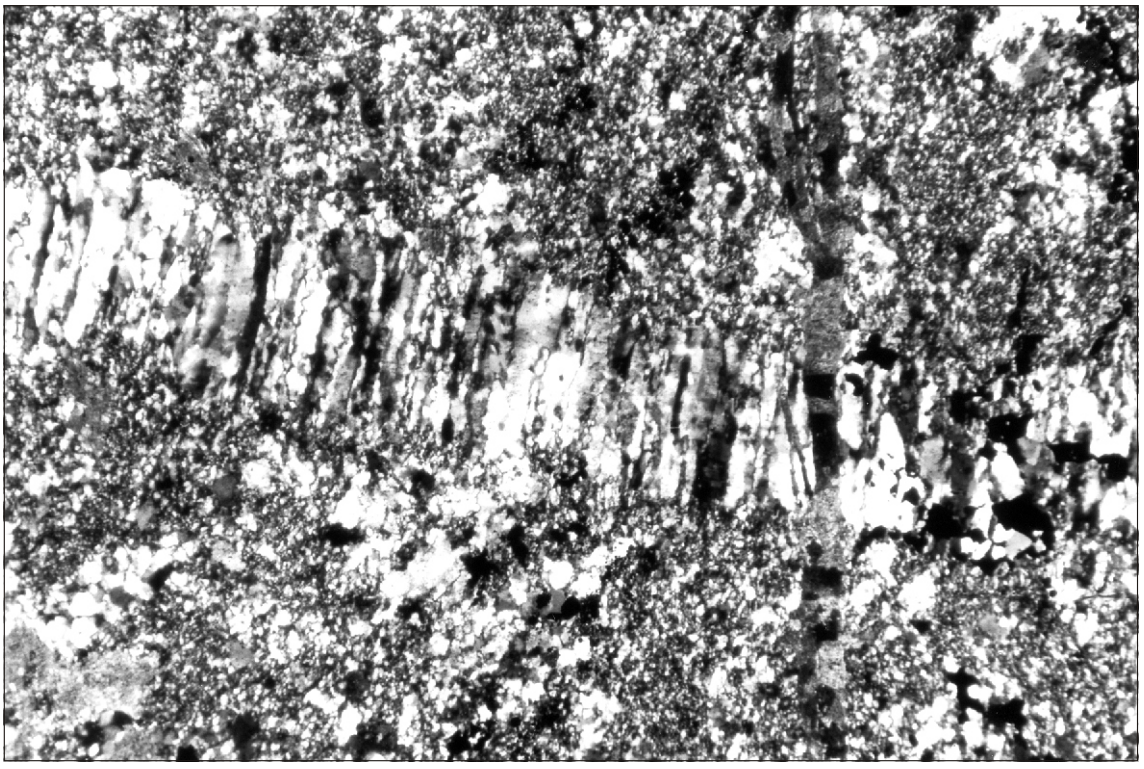

Figure 2.19b *Crossed polars. MQ showing complex history of deformation and alteration:*

(a) multiple veining;
(b) fibrous quartz vein is partially recrystallised and quartz grains show sutured boundaries;
(c) fibrous quartz vein is cut by some veinlets which have been recrystallised and are indistinguishable from the silicified matrix;
(d) there are two types of sulphides,
(1) parallel to sub-parallel thin layers of fine-grained pyrite which are cut by fibrous quartz vein and appear to define the remnants of S_2 cleavages,
(2) patch of sulphides mainly chalcopyrite associated with fibrous quartz vein;
(e) silicified matrix appears to have been affected by polygonisation;
(f) occurrence of late undeformed carbonate veinlet (dark grey).

Sample 103751. FOV 1.8 1.2 mm

Figure 2.20

Pyrite-gold veinlet in MQ. Note the coarse electrum grains (deep yellow). DDH HP 140, 555.6 m.

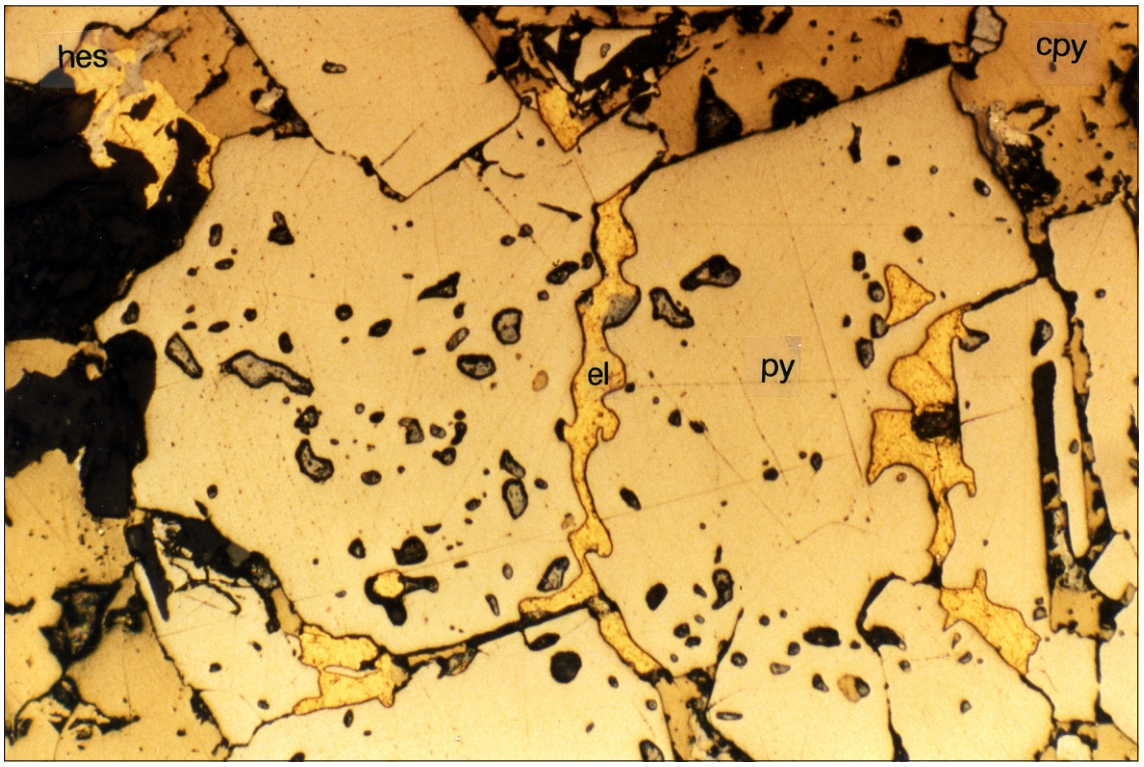

Figure 2.21

Occurrence of electrum (el) along the fractures and pyrite (py) grain boundaries. Note the close association of gold with chalcopyrite (cpy) and hessite (hes). Sample 103934. FOV 580 390 m.

sources of sulphur for the sulphides of different stages at the Henty Prospect.

Electrum is mainly associated with chalcopyrite, galena and tellurides and rarely pyrite, either as inclusions or in contact with them in the microfractures (see also Division of Mines and Mineral Resources Report 1990/12). The occurrence of gold associated with a pyrite veinlet was only observed in DDH HP 140 (fig. 2.20). Electrum may also occur as inclusions in quartz or carbonate (fig. 2.22). The occurrence of gold in the massive quartz is characteristically similar to the occurrence of galena and chalcopyrite (mainly fracture-fillings; fig. 2.21), which indicates that the gold has probably been remobilised along the grain boundaries or into the microfractures, which were subsequently annealed during later stages of recrystallisation.

Te-bearing minerals qualitatively identified by microprobe analyses include Ag-telluride (hessite?, Ag_2Te), Pb-telluride (altaite, PbTe), and Bi telluride (tellurbismuth?, Bi_2Te_3). These minerals are mainly associated with gold, chalcopyrite and galena, and occur as infillings in microfractures, at grain boundaries, or as inclusions in galena. The occurrence of Te-bearing minerals is not limited to the massive quartz and they may be observed as late-forming (i.e. remobilised) minerals in the other types of mineralisation. Ag-bearing minerals identified to date include electrum and the Ag-bearing telluride. However other minerals such as chalcopyrite, sphalerite, and specifically galena may contain significant proportions of Ag in the Henty Prospect.

(d) MASSIVE PYRITE-CARBONATE-QUARTZ GOLD TELLURIDES (MP)

This style of mineralisation occurs to the east of the deposit and stratigraphically forms the upper parts of the main mineralised zone (fig. 2.1). It is commonly hosted by MZ, however only a thin (<1 m) section of MZ separates MP from the overlying rocks including MA or undifferentiated lavas and volcaniclastic rocks. MP may also be in direct contact with the overlying volcaniclastic rocks (e.g. DDH 129D).

Massive pyrite occurs as lenses mostly less than 50 cm wide and a few metres long. It is at about the same horizon as the carbonate hematite alteration (LL). Massive pyrite is the major component and has been affected by extensive fracturing, brecciation and recrystallisation (fig. 2.24–2.26). The recrystallised pyrite occurs as disseminated fine-grained euhedra ranging from <10 m to >1 mm. Chalcopyrite, galena and carbonate are the major fracture-filling minerals (fig. 2.25 and 2.26).

The staining method of Fleet *et al*. (1988) was used to investigate the possible different generations of pyrite and also the effect of deformation on the massive pyrite. The stained polished thin sections revealed that the massive pyrite consists of zoned, colloform and framboidal types which have been intensely fractured and finely brecciated (fig. 2.23 to 2.26). The zoned pyrite has been partially dissolved or overgrown by late (i.e. syn-tectonic) cubic pyrite (fig. 2.26). Some early (pre-tectonic) pyrite is characterised by colloform centres passing outward into euhedral crystals (fig. 2.24). The zonation may be characterised by distinctly different colours, which appear to reflect the differences in the As contents of the different zones (e.g. Taheri and Green, 1990). The As variations may indicate the fluctuations in As content of hydrothermal fluid during the formation of the massive pyrite. The framboidal pyrite is characterised by rounded shapes consisting of many small (~2–5 m) primitive-looking grains (fig. 2.23). The late (recrystallised) cubic pyrite shows no zoning and occurs as disseminations, fracture-fillings or overgrowths on early, pre-tectonic pyrite. The cubic pyrite appears to be syn-tectonic as it commonly has adjacent pressure shadows of quartz, muscovite or carbonate.

The massive pyrite may exhibit alternating bands of semi-massive pyrite with minor carbonate and/or quartz and quartz-carbonate with minor pyrite. The banding has been interpreted to be "exhalative" in origin (e.g. Cowan, 1985). However detailed mineragraphic examination showed that the early, pre-tectonic pyrite has been affected by processes of recrystallisation, and may have remobilised to form a structurally-controlled vein system along the cleavage planes and sheared zones (fig. 2.29).

Carbonate occurs as:

(a) infillings between recrystallised euhedral pyrite crystals,

(b) partially recrystallised syn-tectonic veinlets showing deformation twining,

(c) pressure shadows on pyrite,

(d) clasts up to few centimetres long which show extensive recrystallisation, and

(e) late, post-tectonic, moderately deformed to undeformed veinlets.

Quartz is mostly recrystallised and micro-granular in banded pyrite lenses. It occurs as infillings between recrystallised pyrite grains, as pressure shadows, and as late veinlets cutting the massive pyrite.

Muscovite is less common than carbonate and quartz in the massive pyrite lenses and occurs mainly as coarse grains (up to 200 m) in close association with recrystallised pyrite. It has commonly been affected by deformation showing bent cleavage planes.

Galena and chalcopyrite are relatively common, but mainly minor constituents. They occur as fracture fillings and disseminated intergranular blebs up to

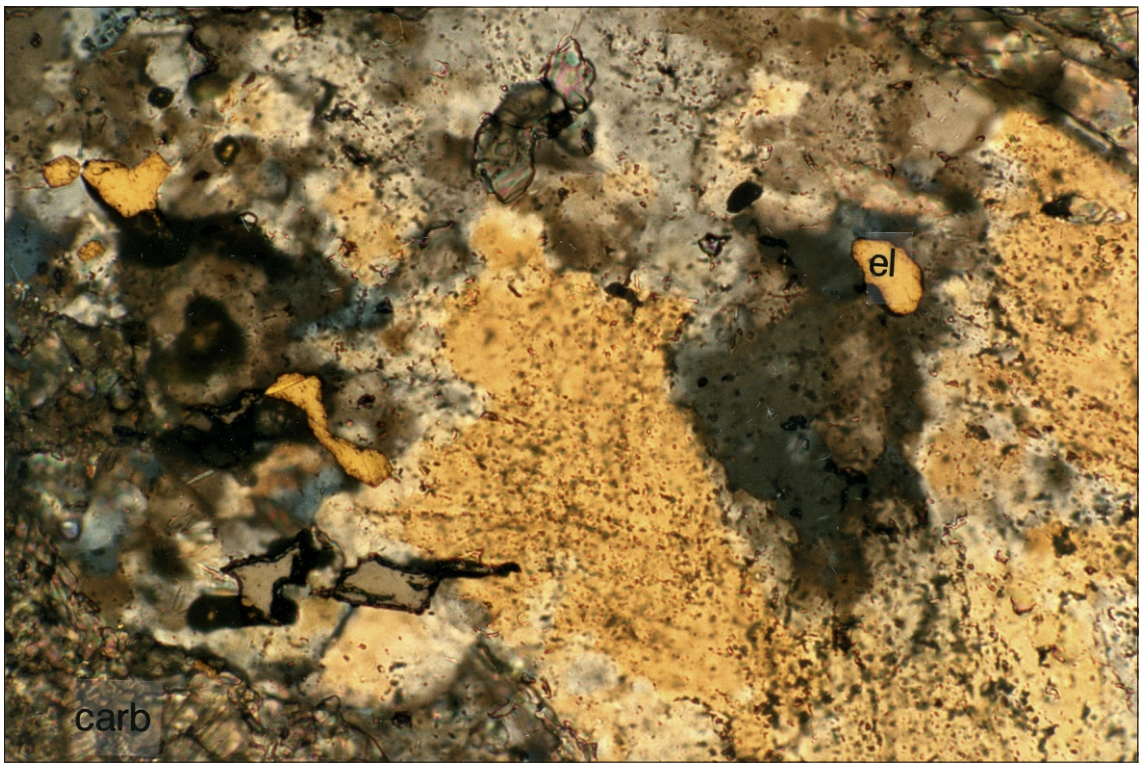

Figure 2.22

Disseminated electrum (el) associated with coarsely recrystallised quartz and carbonate (carb). Note the occurrence of deformed, partially recrystallised carbonate (carb). Sample 103773. FOV 580 390 m.

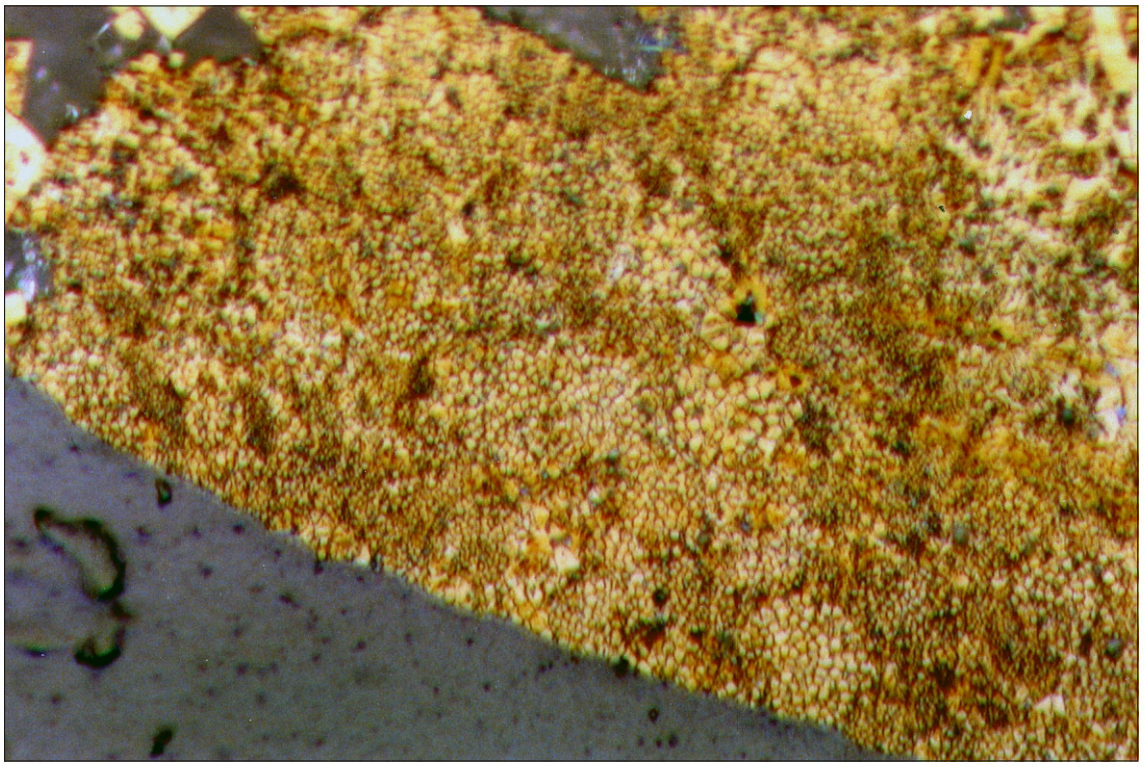

Figure 2.23

Etched massive pyrite showing framboidal texture. Note the circular nature of each aggregate. The grey-brown areas are carbonate. Sample 103953, FOV 230 153 m.

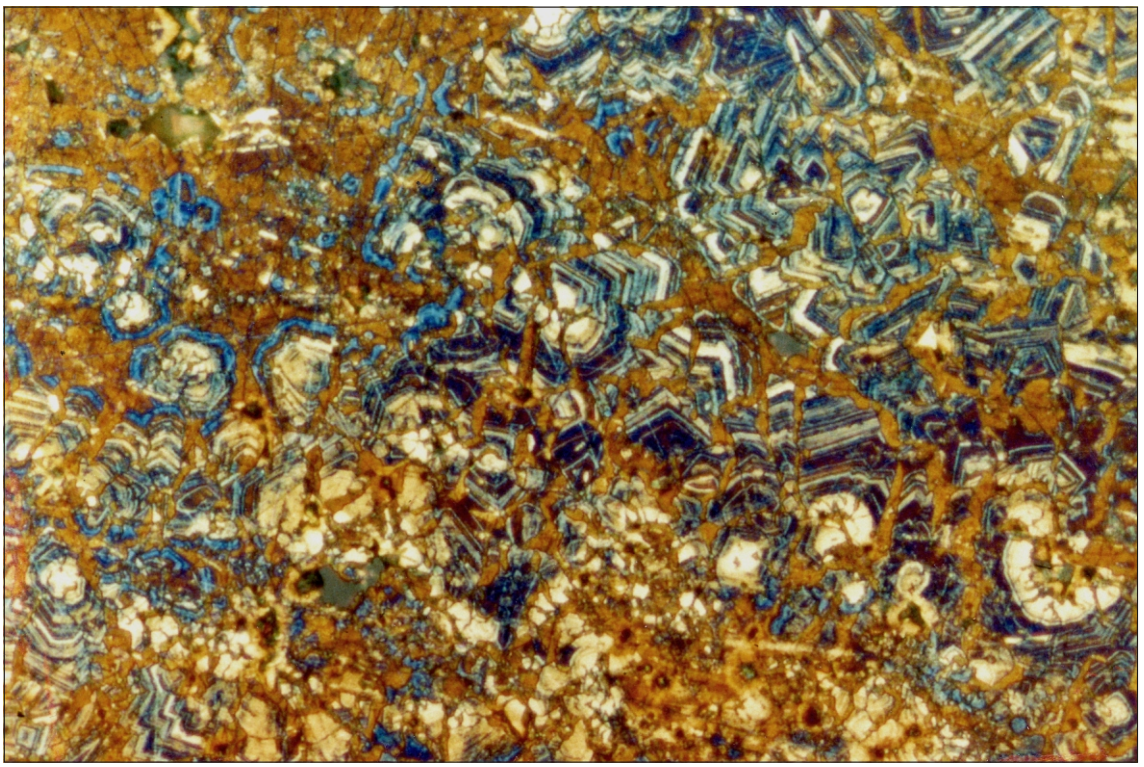

Figure 2.24

Etched massive pyrite showing finely brecciated, early formed zoned and colloform pyrite grains, infilled or partially replaced by late pyrite (dark yellow). Note euhedral zoned overgrowth of colloform pyrite grains. The different colours of the zones reflect variations in As contents of pyrite (see text for detail). Sample 103738, FOV 475 210 m.

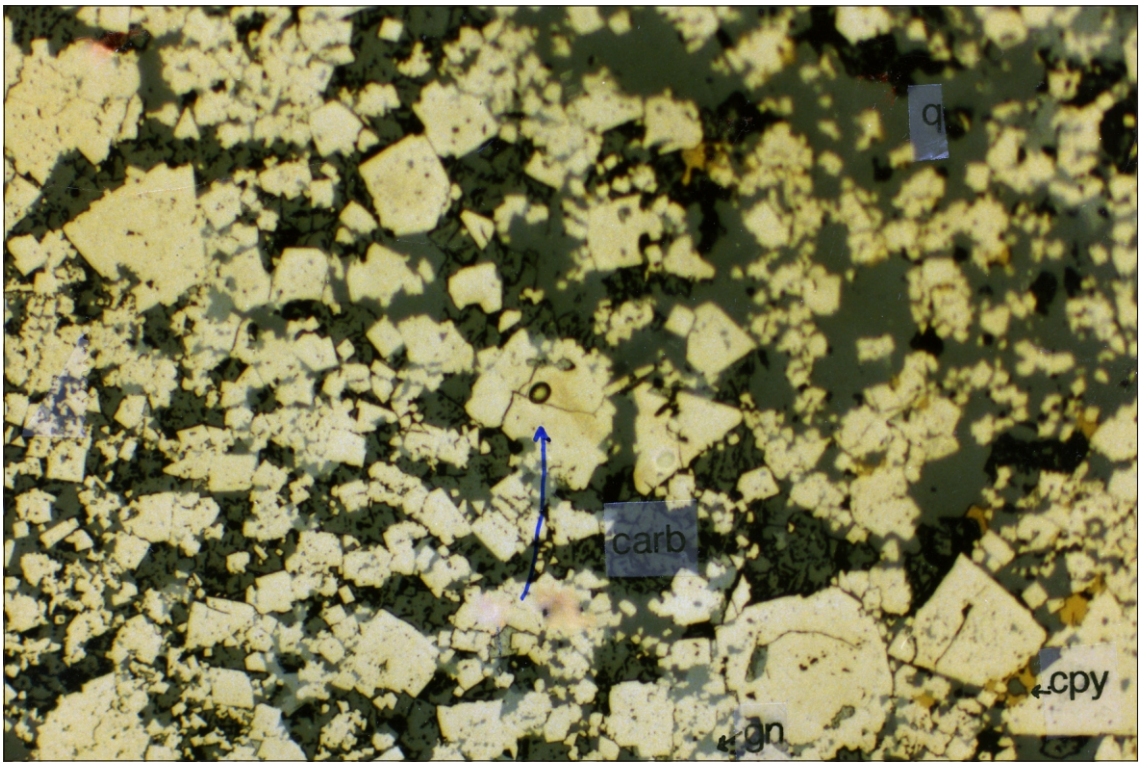

Figure 2.25

Recrystallised pyrite in quartz-carbonate with minor chalcopyrite (cpy) and galena (gn). Groundmass consists of quartz (q) and carbonate (carb). The circle shows the area used for microprobe analysis. See Figure 2.26 for detail. Sample 103950, FOV 1.8 1.25 mm.

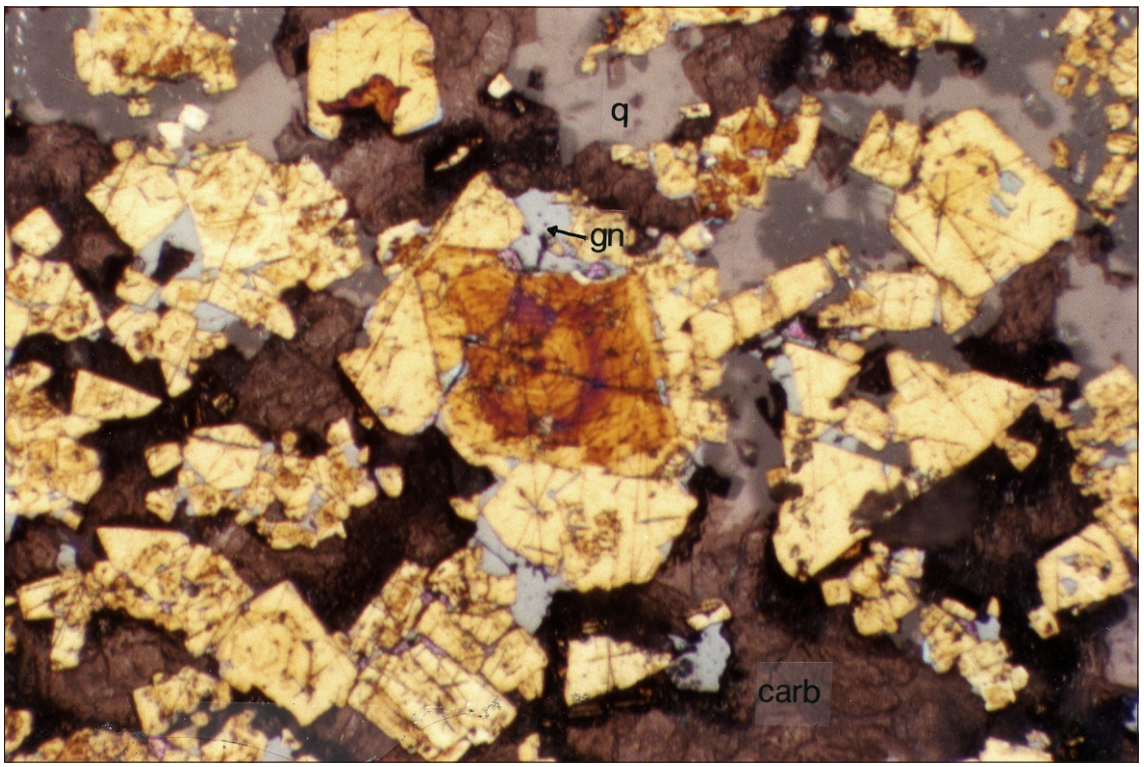

Figure 2.26

Zoned pyrite (etched) overgrown by late pyrite. Note that the early-formed pyrite grains are brecciated, partially dissolved and replaced by pyrite and galena (gn). The etched zoned pyrite grain in the centre is the same grain as in Figure 2.25 which was used for ion microprobe analysis. See Table 4.1 for sulphur isotope results. FOV 580 390 m .

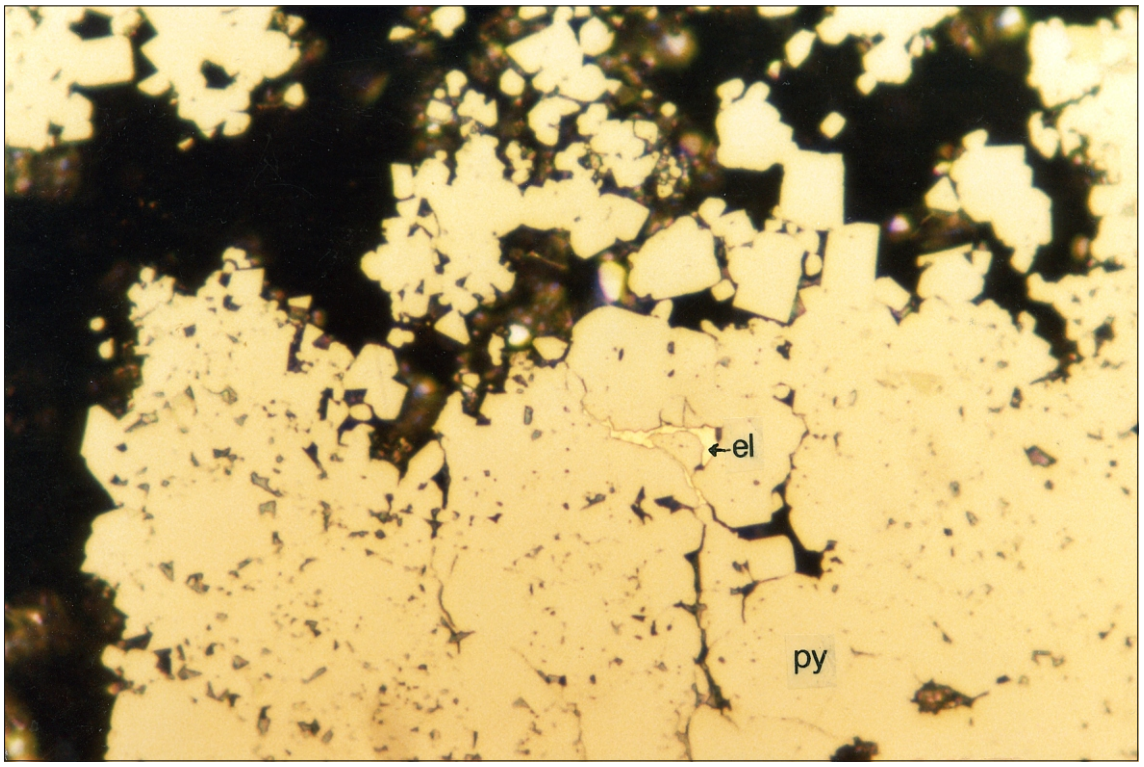

Figure 2.27

Electrum (el) as fracture filling in massive pyrite (py). Note the occurrence of disseminated euhedral pyrite in carbonate. Sample T8820, FOV 580 390 m.

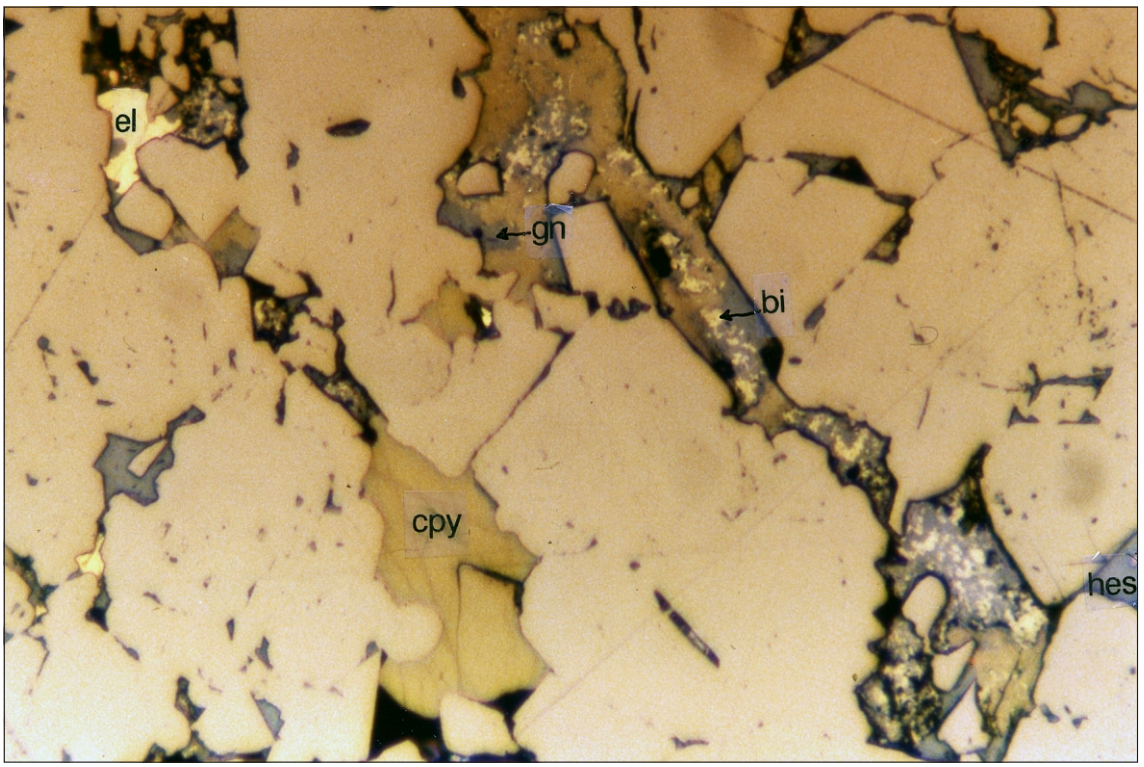

Figure 2.28

Occurrence of electrum (el), galena (gn), chalcopyrite (cpy), hessite (hes) and bismuthinite (bi) along the fractures in massive pyrite. Sample T8819, FOV 230 153 m .

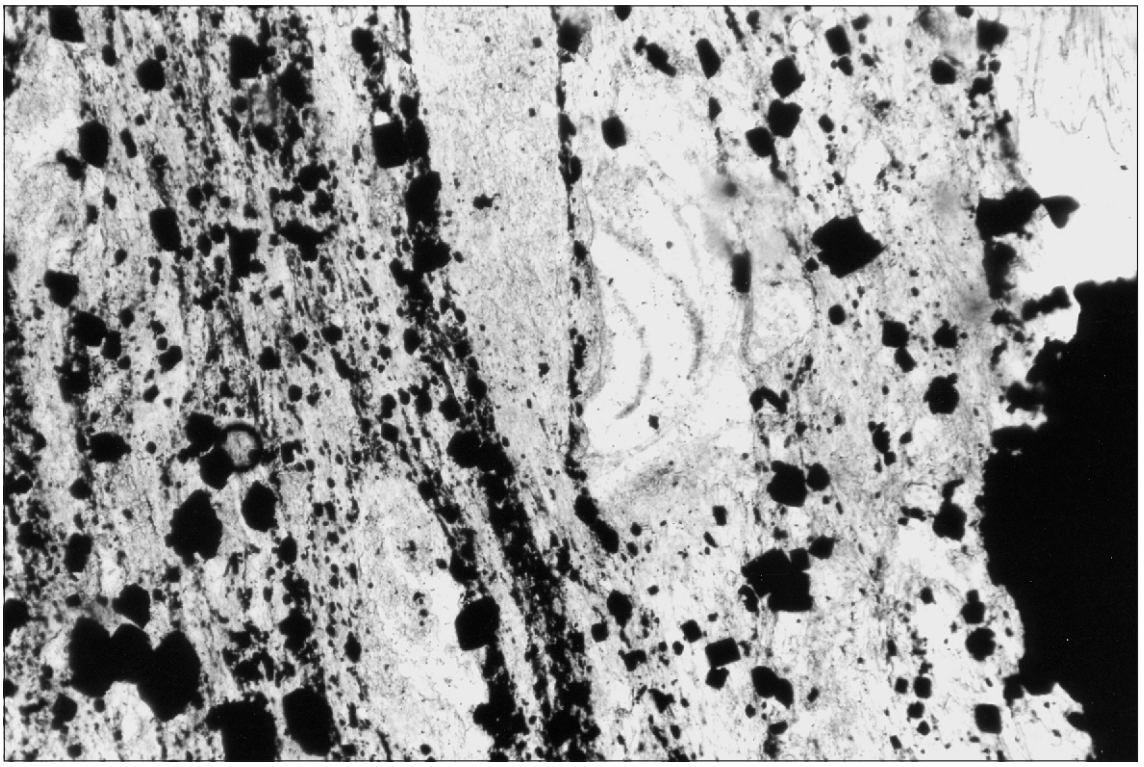

Figure 2.29

Tectonically banded pyrite associated with muscovite and quartz truncating a silicified clast showing relict perlitic structure of the host rock. Note also the euhedral, recrystallised nature of the pyrite grains along the cleavages. Plain polarised light. Sample 16778, FOV 1.8 1.2 mm.

200 m long. They may also occur as small (<1 mm) semi-massive patches enclosing pyrite grains.

Electrum grains are rare in the massive pyrite. They mainly occur in close association with chalcopyrite in microfracture fillings (fig. 2.27, 2.28). They also occur in carbonate or as small grains (2–10 m) in pyrite, which are probably among the earliest electrum grains at the Henty Prospect.

Tellurides are rare and are closely associated with gold, chalcopyrite and galena (microfracture filling, fig. 2.28). Silver telluride (hessite?, Ag_2Te), and Pb-telluride (altaite, PbTe) were positively identified by microprobe analyses (e.g. sample T18819). Bismuthinite was positively identified by microprobe analyses in sample T8819. It occurs as fine grains (~1 m) in microfractures filled with galena and chalcopyrite (fig. 2.28). Sphalerite is not a common sulphide and mainly occurs as chalcopyrite diseased, remobilised veinlets and disseminations in association with galena and chalcopyrite. It may also encloses disseminated euhedral pyrite.

Similar textural relationships between pyrite, chalcopyrite, galena and tellurides have been observed throughout the mineralised zones at the Henty Prospect. The typical relationship with pyrite as the early-formed, brecciated phase and the other minerals occurring as fracture-fillings may reflect the different ductilities of minerals under stress, or it might be the result of a process of dissolution and reprecipitation during deformation. Brittle failure of pyrite during deformation (naturally or experimentally) has been described to be the major deformation mechanism (e.g. Graf and Skinner, 1970; Atkinson, 1975). Other sulphides such as galena, chalcopyrite and sphalerite appear to be more ductile during deformation (e.g. Bruce, *et al.*, 1977; Roscoe, 1975; McClay, 1980; Kelly and Clark, 1975; Salmon *et al.*, 1974).

At the Henty Prospect the etching studies have clearly demonstrated that pyrite has behaved in a brittle manner showing extensive fracturing and brecciation, and some grains have been recrystallised. In contrast chalcopyrite, galena, gold and tellurides have possibly been remobilised and localised in microfractures and grain boundaries during deformation. The paucity of pressure shadows on chalcopyrite, galena and sphalerite may also be indicative of ductile behaviour of these minerals rather than their being late-formed (post-tectonic) minerals.

SUMMARY

The main features of the main mineralised zone may be summarised as follows:

(1) Petrographically, MZ, MV, and MQ appear to have originally been epiclastic rocks of dominantly felsic lava provenance.

(2) The MQ alteration and mineralisation cuts out sharply at depth. This indicates that the mineralisation is highly unlikely to be of dominantly mesothermal origin.

(3) The mineralised rocks have been affected by at least two generations of cleavages (S_1 and S_2) with S_1 cleavages being dragged into or overprinted by the later (Devonian) S_2 cleavage. The early mineralisation has been affected by the early S_1 cleavage (early mineralisation pre-dates Devonian cleavages).

(4) The hydrothermally altered zones are asymmetric relative to MQ or any other mineralised zones, implying that the alteration zones are not envelopes to a vein system.

(5) Volumetrically, MZ represents the largest proportion of the mineralised zones followed by MV and MQ, with MP being the smallest. The intensity of silicification increases from MZ to MQ.

(6) The MV zone occurs as lenticular bodies within or adjacent to MZ, and the same relationship is observed for MQ relative to MV (i.e. the zones are not independent units).

(7) MQ mineralisation is a lateral extension of MV in some places, which indicates that MQ may represent a more silicified version of MV.

(8) There appears to be a general relationship between the overall thickness of the MZ zone and those of MQ and MV in that the wider zones of MZ correspond to thicker lenses of MV and MQ. This indicates that MV, MQ, and MZ were probably formed by the same hydrothermal event in which the thicker mineralised zones have resulted from the interactions of higher volumes of hydrothermal fluids with the rocks (i.e. closer to feeder zones).

(9) Early silicification is characterised by the occurrence of totally recrystallised quartz with disseminated, randomly oriented, fine-grained muscovite and therefore pre-tectonic, and is a common feature in MZ, MV, and MQ.

(10) The intensity of fracturing and veining increases with increase in the degree of silicification within the mineralised rocks, reflecting competency contrasts during deformation.

(3) QUARTZ-CARBONATE-SERICITE-FELDSPAR PYRITE (SC)

This rock type mainly occurs in the northern part of the mineralisation and was exposed in the sill. The rocks are the same as MA (i.e. altered epiclastic rocks) which have been affected by more intense carbonate alteration. The carbonate is deformed, recrystallised and occurs as veinlets of different generations, and as small patches replacing the matrix and some of the clasts. Other features are similar to those observed in MA.

(4) MASSIVE CARBONATE-HEMATITE (LL)

This style of alteration is mainly limited to the deeper sections of the prospect and appears to be in the same stratigraphic horizon as the MP mineralisation. It occurs as discontinuous lenses up to 5 m wide of either relatively pure carbonate with minor hematite or with quartz, sericite and pyrite. The carbonate is strongly deformed and recrystallised and commonly exhibits deformation twinning and bent and kinked cleavage planes (fig. 2.30). It varies in occurrence from veinlets of possible different generations to a massive form associated with minor hematite. Massive pyrite lenses occur rarely in these rocks (e.g. DDH HP13). Original textures of the rocks with high proportions of carbonate have largely been obliterated by extensive veining, brecciation and silicification but there are positively some remnants of rounded clasts which have been completely silicified.

(5) MINOR MINERAL ASSEMBLAGES

There are some mineral assemblages which are volumetrically less significant. These include:

(a) CHLORITE ALTERATION

This style of alteration has mainly been intersected in deeper drill holes in the southern section of the mineralisation in close association with carbonate-hematite alteration. It occurs as discontinuous lenticular bodies up to about 40 m wide. The rocks are characterised by greenish colour and appear to be chloritised epiclastic rocks.

Two types of chlorite were identified:

(i) pale green chlorite with anomalous blue birefringence, and

(ii) dark green chlorite with a brown birefringence.

The pale green chlorite occurs mainly in the matrix and may show similar grain size to sericite. It also occurs along the shearing, as veinlets, and as irregular patches in the matrix. The pale green chlorite appears to have replaced sericite in the matrix, however in places chlorites and sericite are of the same grain size and show intergrowth relationships. The dark green chlorite appears to occur mainly as veinlets and along the cleavages. Some veinlets are characterised by relatively coarse chlorite flakes (~300 m).

The different occurrences of the chlorites in these rocks may simply reflect the effect of mobilisation and reprecipitation for the layered silicates during deformation. Chemically the pale green chlorite is higher in FeO and lower in MgO and SiO_2 than dark green chlorite (Appendix 2). Applying the six component chlorite geothermometer of Walshe (1986), a temperature range of 285 to 329°C was obtained at 1 kBar. Of these results, analyses from a dark green chlorite from sample 103956 gave temperatures of 239, 285 and 303°C, whereas a pale green chlorite from sample 103954 gave temperatures of 321 and 329°C. Experience from elsewhere in Tasmania suggests that chlorites with brown birefringence have been subjected to re-equilibration with metamorphic fluids. The scattered data from sample 103956 in terms of calculated oxidation conditions during formation would tend to support this (Appendix 2). The data from sample 103954 probably reflect peak metamorphic temperatures in the range 320–330°C, and are in good agreement with the empirical geothermometer of Cathelineau and Nieva (1985) and the fluid inclusion temperatures from the late quartz tension gashes. Temperatures of around 300°C are consistent with the fluid inclusion results from quartz gashes (see fluid inclusion section for detail) and may indicate Devonian deformation temperatures at the Henty Prospect.

Carbonate may also occur in the rocks in similar ways to those observed in the other hydrothermally-altered rocks. However there is no specific association between carbonate and chlorites in these rocks. Other features of the rocks are similar to those observed in the rocks of moderate alteration (i.e. MA).

(b) MASSIVE TO SEMI-MASSIVE SULPHIDE-QUARTZ-CARBONATE (MS)

This style of mineralisation occurs as small band massive sulphide lenses up to 200 mm wide in MZ just below MP mineralisation. The rocks consist of pyrite, sphalerite, galena, chalcopyrite, quartz and carbonate, and muscovite. Sphalerite has been recrystallised and partially replaced by chalcopyrite along the cleavages, fractures and on contact with chalcopyrite. The grain boundaries of the recrystallised grains are mostly filled with small fluid inclusions(<2 m). However sphalerite is one of the most mobile minerals at the Henty Prospect, as it may occur along the cleavage planes and as pressure shadows adjacent to pyrite in the other mineralised rocks. Gold is rare and is associated with chalcopyrite in 'diseased sphalerite' or along fractures in association with chalcopyrite and galena. Similar features are also observed in the mineralised veins (fig. 2.31–2.34). Muscovite is associated with sulphides and has been affected by

deformation, showing bent cleavage planes. Some massive sulphides exhibit banding which is likely to be of tectonic origin. In general, textural relationships between the minerals are very similar to those described for MQ and MP mineralisation.

(c) FUCHSITE-SERICITE ALTERATION

This alteration is not common at the Henty Prospect. It occurs as small zones (a few metres wide) and is not restricted to any particular stratigraphic horizons. It displays sharp contacts against adjacent rocks and may represent altered mafic dykes. Petrographic examination suggests that the rocks were originally andesitic, which is also indicated by one analysed sample from the sill (see Chapter 5 for details). Moderately altered samples (e.g. 3034) show a typical andesitic texture with feldspar phenocrysts up to 2 mm long and minor quartz phenocrysts(~0.5 mm). The matrix consists of sericite and fuchsite which have commonly been replaced by carbonate. Fuchsite also occurs in the sheared zones in these rocks.

(d) QUARTZ GASH-SULPHIDES GOLD TELLURIDES

Quartz gashes are best exposed in the sill and are associated with the late (Devonian or younger) small faults (fig. 2.35). They are up 3 m long and 300 mm wide but thin away from the faults. The quartz is extensively fractured and moderately strained. It occurs as coarse grains associated with galena, chalcopyrite, pyrite, and rarely gold and tellurides.

The sulphides, mainly galena and chalcopyrite occur in microfractures and as small patches. Paragenetically all the minerals belong to the same stage of mineralisation (i.e. post-tectonic) and the minerals exhibit similar features to those described for mineralisation in the massive quartz (MQ), except that the sulphides are characteristically coarser grained and no pressure shadows are observed adjacent to the euhedral pyrite grains. Etching of sample 103784 also indicated that the pyrite grains are undeformed and structureless in contrast to the zoning, colloform or framboidal textures observed in the massive pyrite. The occurrence of similar minerals in the MQ alteration and in the quartz gashes may indicate that the mineralisation in the quartz gashes is the result of remobilisation of the minerals from the main mineralised zone and their consequent syn-deformational reprecipitation in the fault-related fractures. Recent lead isotopic data (Carr and Dean, 1990) also indicate a Cambrian lead source for galena in the quartz gashes.

(6) QUARTZ-FELDSPAR (AS)

Quartz-feldspar rocks mainly occur to the east of the MA (i.e. above MA stratigraphically) either in direct contact with MA or with less altered Tyndall Group volcaniclastic rocks and lavas (RGC classification) away from MA. The rocks may also occur as relatively thin (a few metres) discontinuous bodies within the mineralised zones (e.g. DDH HP 140). The rocks range from a few metres to over 30 m thick, and may be continuous over 300 m vertically.

The rocks are grey to milky in colour with a cherty appearance. Semi-quantitative XRD results (Appendix 7) of samples from different drill holes and also from the sill showed that the rocks mainly consist of subequal proportions of feldspar and quartz, with dolomite as a minor but widespread mineral.

The samples taken from the sill consist of quartz and feldspar phenocrysts ranging from 300 m to 2 mm and comprising 10 to 20% of the rock in an albitised and silicified matrix. Dolomite occurs mainly in late undeformed veins and also as small deformed patches in the matrix. Some of the feldspar phenocrysts have been replaced selectively by albite aggregates. The rocks have been affected by fracturing, brecciation and veining and are weakly mineralised (<0.5%). The veinlets are mostly quartz and carbonate. The quartz in the veinlets is totally recrystallised and is often microscopically indistinguishable from that in the matrix. The brecciated fragments appear to have been healed by quartz and rare dolomite. However the fragments are not readily distinguishable, as they are similar mineralogically and texturally.

Mineralisation mainly occurs along the microfractures and as disseminations. Sulphides include a dominant pyrite phase with fine grains of galena, chalcopyrite, sphalerite and possibly traces of tellurides. The gold content is normally below detection limit (<0.008 ppm, RGC analyses), but in hand specimen the grey varieties of the rocks are very similar to the massive quartz- muscovite-pyrite rocks which host the gold-tellurides mineralisation (MQ, fig. 2.36), especially low sulphide varieties of the MQ. However the rocks are texturally homogeneous and appear to be altered lava, in contrast to the massive quartz (MQ) alteration which is free of feldspar and is probably of epiclastic origin.

It is possible that some thin sections of the MQ alteration zones may have been mistaken for AS. This was revealed in DDH HP 140, in which an X-ray diffraction scan revealed no feldspar in a low-gold content interval of MQ considered in preliminary core logging to be part of the AS zone. The AS alteration characteristically contains dolomite as the sole carbonate whereas in the MQ mineralisation calcite is common. The zones are also distinctly different in concentration of same trace elements (see Chapter 5).

Petrographic observations on one sample from 'undifferentiated lavas and volcaniclastics' (RGC classification), intersected adjacent to the AS zone in drill hole 129D (sample 104927), indicated that the rock is basically a quartz-phyric lava with a

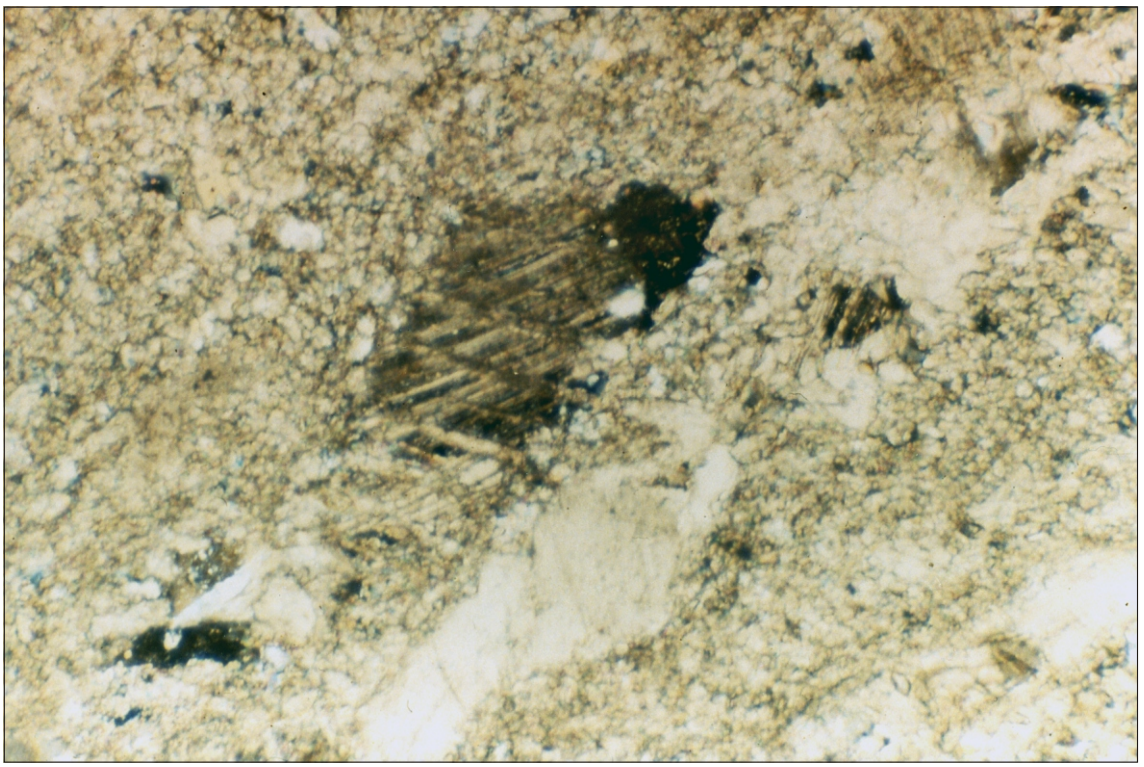

Figure 2.30

Massive carbonate showing extensive recrystallisation, deformation twining and veining.
Sample 103783, FOV 1.8 1.2 mm .

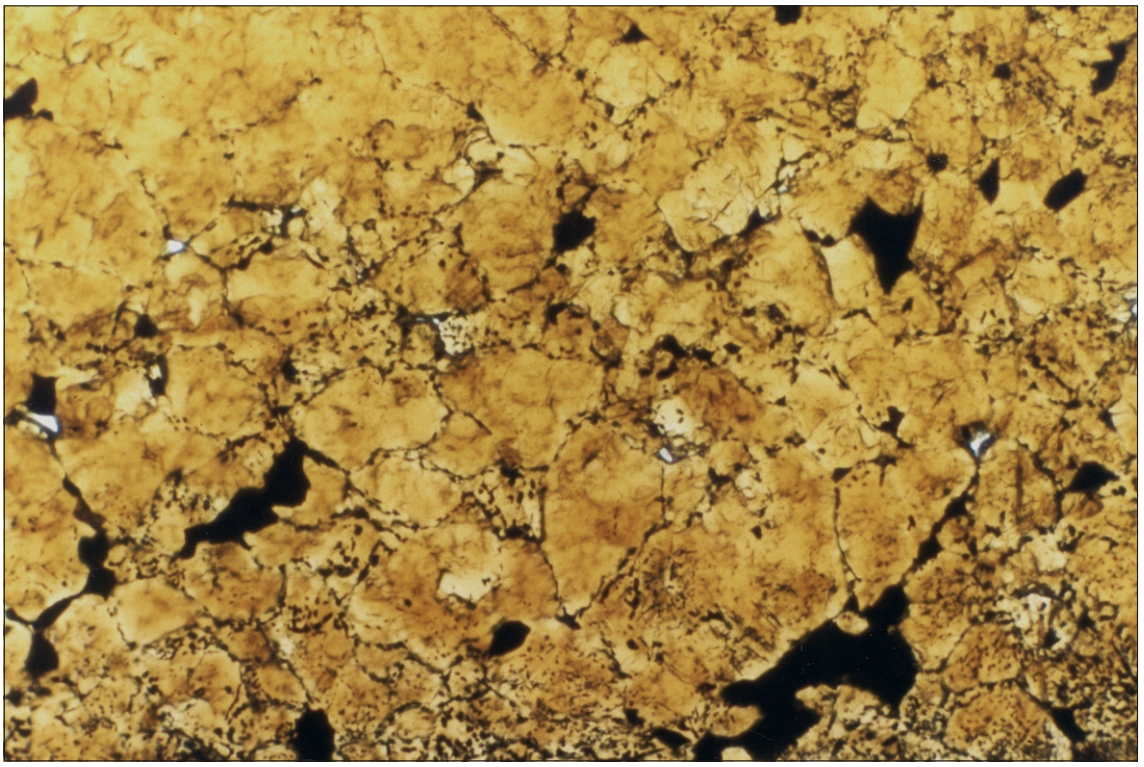

Figure 2.31

Recrystallised sphalerite showing triple boundaries between the recrystallised grains.
The dark grain boundaries are due to the occurrence of small fluid inclusions.
Transmitted light. Sample 103775. FOV 580 390 m.

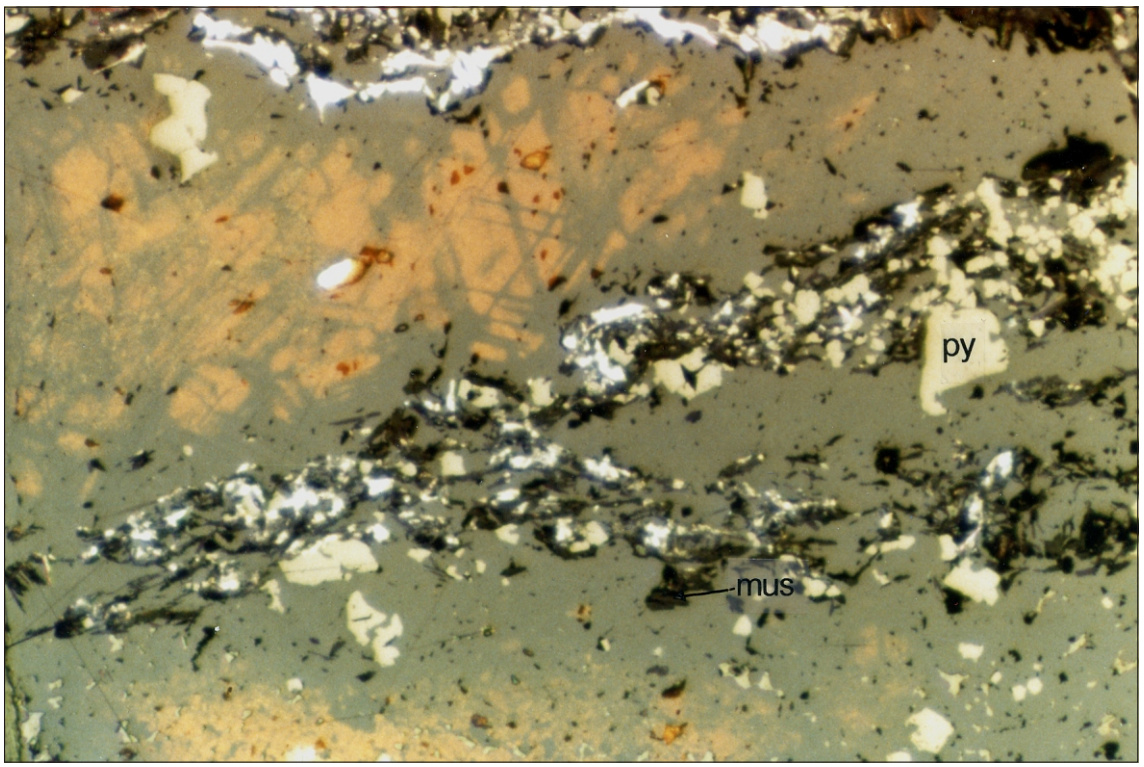

Figure 2.32

Replacement of deformed sphalerite (brown) by chalcopyrite (i.e. chalcopyrite disease), pyrite and muscovite (mus) along cleavage planes. Note the occurrence of deformation twinning in sphalerite. Reflected and transmitted light. Sample 103765. FOV 710 475 m.

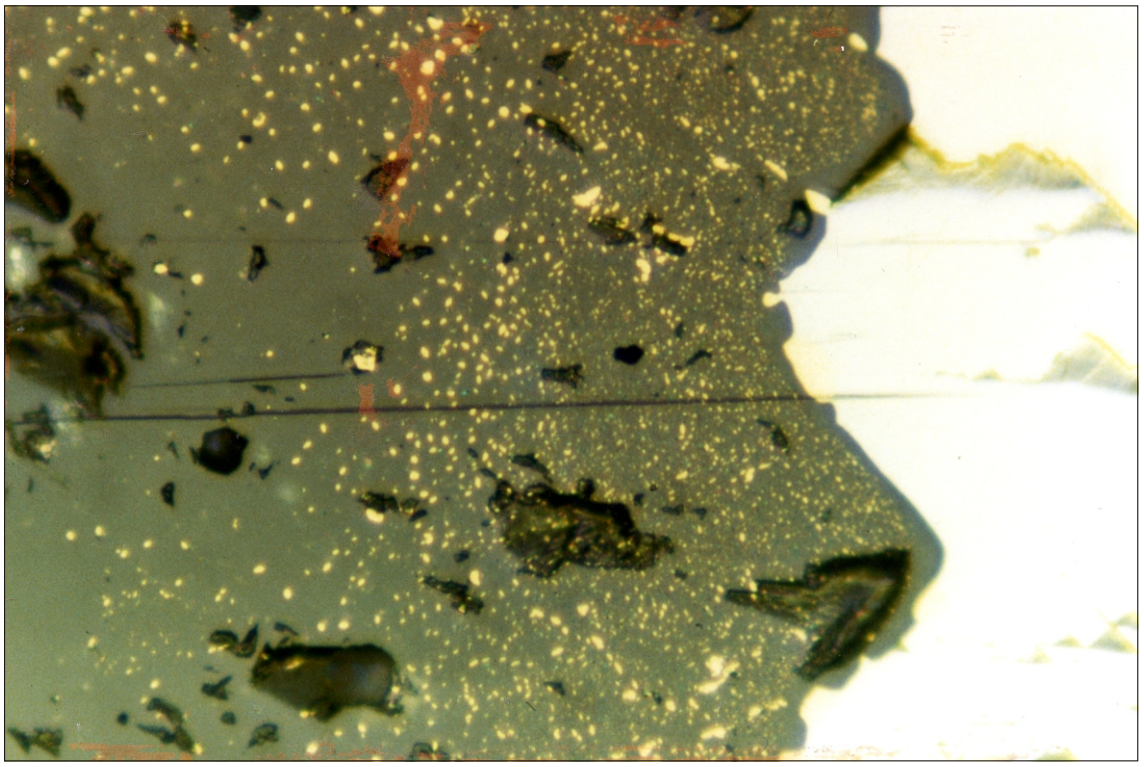

Figure 2.33

Sphalerite showing 'chalcopyrite disease' on the margin. Note the intensity of chalcopyrite replacement decreases towards the centre. The surface is coated by a late chalcopyrite-free sphalerite. Sample 103775. FOV 230 150 m.

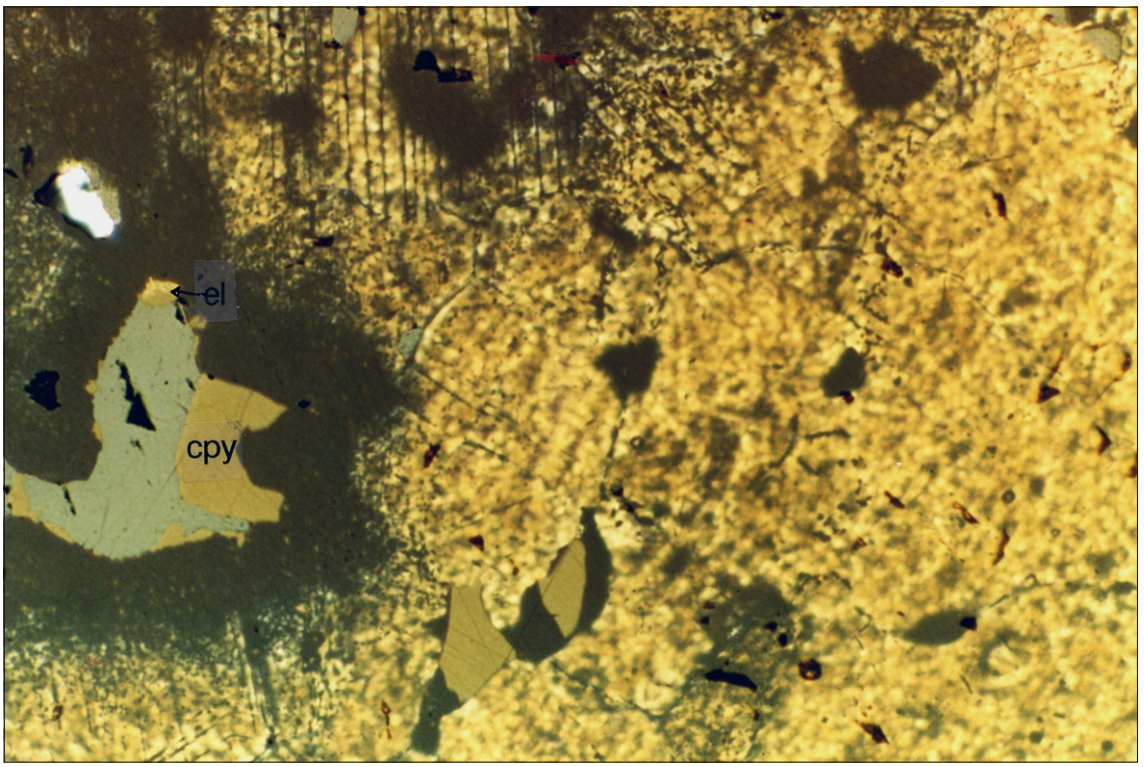

Figure 2.34

Replacement of sphalerite (light brown) by chalcopyrite (dark, 'chalcopyrite disease'). Note the association of gold (Au) with chalcopyrite (cpy) and galena (gn) in diseased sphalerite. Combined reflected and transmitted light. Sample 103775. FOV 230 150 m.

Figure 2.35

Quartz gash cutting through MQ and MV. Most of fractures in MQ are filled with fine grains of sulphides and quartz. Note deformed nature of quartz gash (i.e. bent and fractured). Photo also shows the extensive remobilisation of sericite as it has filled a late-formed fracture affecting the quartz gash, MV and MQ (upper left). The patch of sulphide in quartz gash is chalcopyrite (photo taken in the sill).

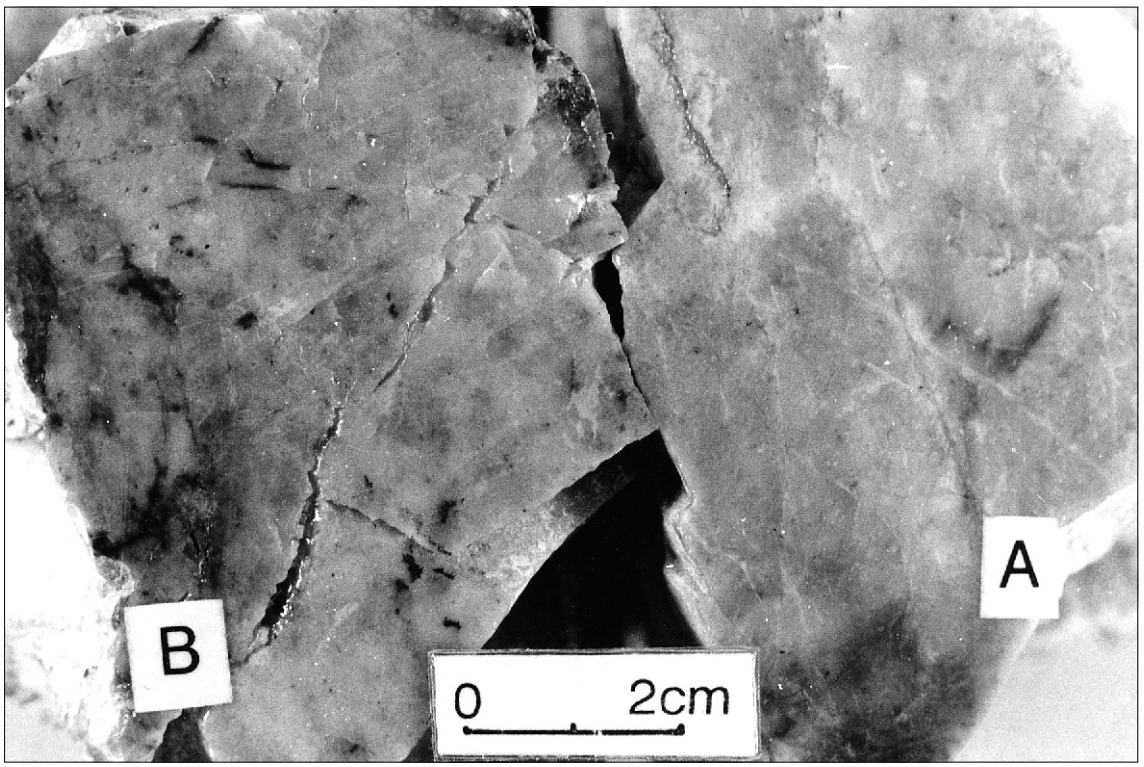

Figure 2.36

Hand specimens of massive quartz-sulphides (MQ, B) and quartz-feldspar rocks (AS, A). Note the similar appearance of the rocks. Samples SF33C and NF32-33E.

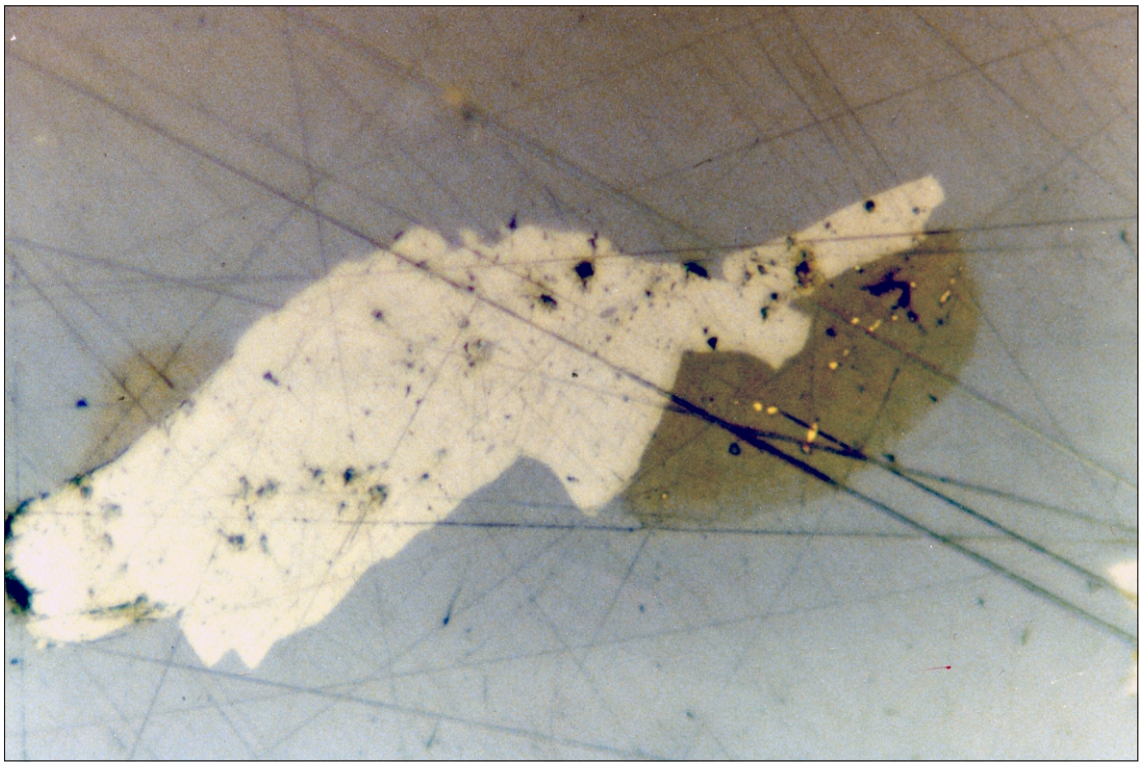

Figure 2.37

Occurrence of fine electrum grains (yellow) in hessite. Hessite and tellurbismuth (cream) are hosted by galena.Sample 103937. FOV 230 150 m.

completely sericitised matrix. The rock shows autobrecciation and flow banding. No feldspar phenocrysts were observed in this rock, however these were probably replaced by quartz and sericite as there are some elongate patches of cloudy quartz and fine cherty clasts of similar size to the quartz phenocrysts which could represent silicified feldspar grains. In general this rock shows a similar texture and size of phenocrysts to those in AS, and the two may represent the same primary lithology. If so they may have acted as a cap for the mineralisation. However this can only be verified by a systematic, detailed petrochemical investigation of the relevant rocks.

DISTRIBUTION, GRAIN SIZE AND CHEMISTRY OF ELECTRUM

Electrum grains vary in colour, depending on their silver content, from pale to deep yellow and are mainly associated with chalcopyrite, galena and tellurides regardless of the host rocks or styles of alteration. Electrum mainly occurs along discontinuous microfractures and pyrite grain boundaries. It may also occur along the cleavages in galena, in fine voids, and as inclusions in quartz, carbonate, pyrite, chalcopyrite, galena and tellurides. The electrum inclusions in tellurides have probably been exsolved from the pre-existing gold tellurides during deformation. This process may also explain the lack of gold tellurides at the Henty Prospect. In DDH HP 140, a rare association between coarse grains of electrum (up to 1 mm) and a pyrite veinlet in MQ was also observed (fig. 2.20).

Electrum grains are mainly irregular in shape, occur as fracture-fillings (e.g. fig. 2.21), and vary widely in size ranging from <1 m to about one millimetre. Consequently any conventional technique involving the construction of histograms based on measured grain sizes from polished sections must be interpreted with great care, as a one millimetre equant electrum grain is volumetrically equivalent to about eight million grains of 5 m diameter. A normal sized thin section may not represent the true distribution of electrum grains for a particular drill core interval of a mineralisation style. This is illustrated in Figure 2.37, in which about 20 electrum grains ranging in size from 1 to 2 m were observed in a hessite grain of about 60 m in size from a quartz gash in which the gold content is relatively low. On the other hand thin sections prepared from gold-rich intervals may not contain any electrum grains, mainly due to the nugget effect. This was experienced in an MQ sample (T20140), in which two polished thin sections were prepared from a gold-rich interval (>100 g/t) but no electrum grain was observed. The coarser electrum grains may also be lost during thin section preparation.

MQ, as the main gold-bearing rock, exhibits the whole spectrum of the grain sizes, and most gold-rich intervals appear to contain relatively coarse electrum grains. This makes the conventional technique even less reliable at the Henty Prospect. An alternative method, such as that suggested by K. Henley (pers. comm. to R. Bottrill) which involves dissolution of certain amounts of gold-bearing rocks (depending on gold concentration) in hydrofluoric acid and then measuring the electrum grains (unaffected by the acid), may statistically provide more reliable results. In addition we have introduced bias by examining some styles of mineralisation (e.g. massive pyrite, late tension gash veins) out of proportion to their occurrence in the mineralised zone.

Figure 2.38 is a histogram which shows the distribution of the measured electrum grains in the different styles of mineralisation, excluding those grains that can be observed with the hand lens or naked eye in the drill core (i.e. >300 m). In general, the histogram indicates that most electrum grains in MQ are in the range of 5 to 15 m. The rarity of the large electrum grains is probably due to the nugget effect, and intersections with lower gold contents (~10–15 g/t) may only contain the common electrum grain size range (i.e. 5 to 15 m). It also indicates that electrum grains in MP, MS and the quartz gashes are relatively smaller than those in MQ. Obviously more measurements may change the shape of the histogram as discussed above.

Preliminary electron microprobe results from electrum grains in the different mineralisation styles (Appendix 3) indicate that the grains vary in fineness and may contain minor mercury. The colour of the electrum grains containing high silver contents are pale yellow; these grains are commonly observed as inclusions in hessite. Similar grains occur rarely in late (post-tectonic) carbonate veins. However in general, silver-rich electrum grains (fineness <600) are relatively scarce, and the main gold-bearing rocks (i.e. MQ) at the Henty Prospect are characterised by gold-rich electrum grains (fig. 2.39).

The electrum grains in MQ and late quartz are uniform in composition, ranging from 800 to pure gold, and are free of mercury. However only one grain of pure gold was identified. Electrum grains in the massive pyrite and the late carbonate veins are relatively lower in Au and may contain minor mercury.

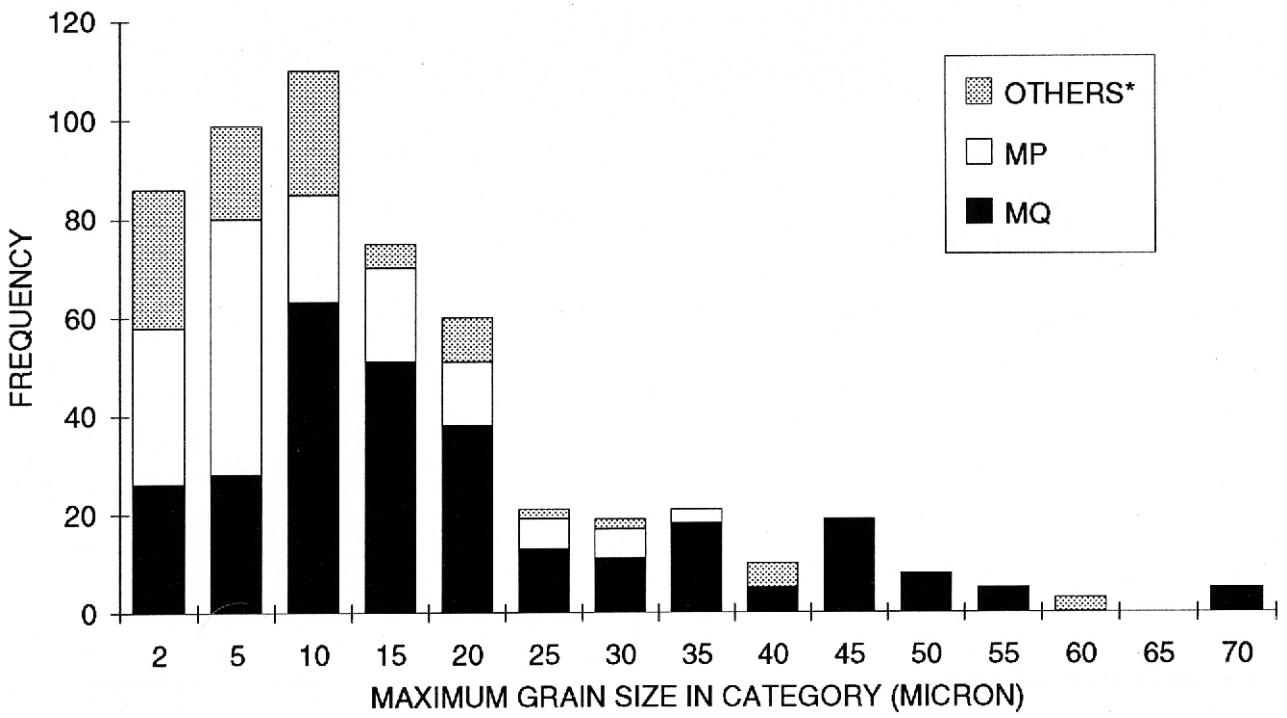

Figure 2.38

Frequency distribution of electrum grains for the different styles of mineralisation

The compositions of electrum grains associated with base metals appear to vary, depending on the paragenesis of the grains, and they may have been affected by different stages of remobilisation and reprecipitation. Mercury only occurs in silver-rich electrum grains and its concentration may correlate with silver, as it reaches up to 2 wt% in an electrum grain with 52 wt% silver (Appendix 3). A similar relationship has been noticed from some other deposits (R. S. Bottrill, pers. comm.). The occurrence of mercury-bearing electrum grains in paragenetically late, post-tectonic carbonate veins or in the massive pyrite mineralisation may indicate that the occurrence of mercury in electrum is mainly temperature dependent, as the electrum in massive pyrite is paragenetically different from that in late carbonate veins and exhibits distinctly different mineral associations and grain size. However both types could have been formed at similar (probably low) temperatures. More analyses of electrum grains are required to establish the relationships between the compositions of the electrum grains and their associations with the different mineralisation styles in more detail.

Co, Ni, Se, AND As IN PYRITE

Co-Ni

Co and Ni contents of pyrite appear to vary in sulphide deposits of different origin (e.g. Fleisher, 1955; Mercer, 1976; Bralia *et al.*, 1979). Volcanic-hosted massive deposits in Tasmania and elsewhere are characterised by a relatively high content of cobalt and also high cobalt/nickel ratios (e.g. Loftus-Hills and Solomon, 1976).

Pyrite grains from late quartz-sulphides veins, massive sulphides (MS), and massive pyrite-carbonate-quartz (MP) were analysed by a SX Cameca microprobe at the University of Tasmania. The detection limits for Co, Ni, Se, As, were 60, 60, 38, and 44 ppm respectively. Values obtained from the massive pyrite were from different parts of a porous massive pyrite, whereas individual pyrite grains were used for each analysis in the other samples. None of the samples were stained for the microprobe analysis.

The following interpretation is based on limited number of analyses, and further work is required to vindicate the results. The cobalt content of pyrite varies widely, ranging from <60 to 1140 ppm (Appendix 4). Massive pyrite is characterised by a high content of Co with an average of 469 ppm. Ni content ranges from <60 to 260 ppm. In a broad sense the Ni concentration appears to be independent of the morphology of the pyrite.

The high Co and high Co/Ni values in the massive pyrite may indicate the original (pre-metamorphic) values and fall within the field of massive sulphide deposits (fig. 2.40). However Co appears to have been removed from pyrite during recrystallisation. The lack of correlation between the types of pyrite (i.e. recrystallised vs massive) and the Ni concentration may, on the other hand, indicate that Ni concentration was largely unaffected by recrystallisation.

Se

S/Se values have also been used to investigate ore genetic processes, and Se appears to be more

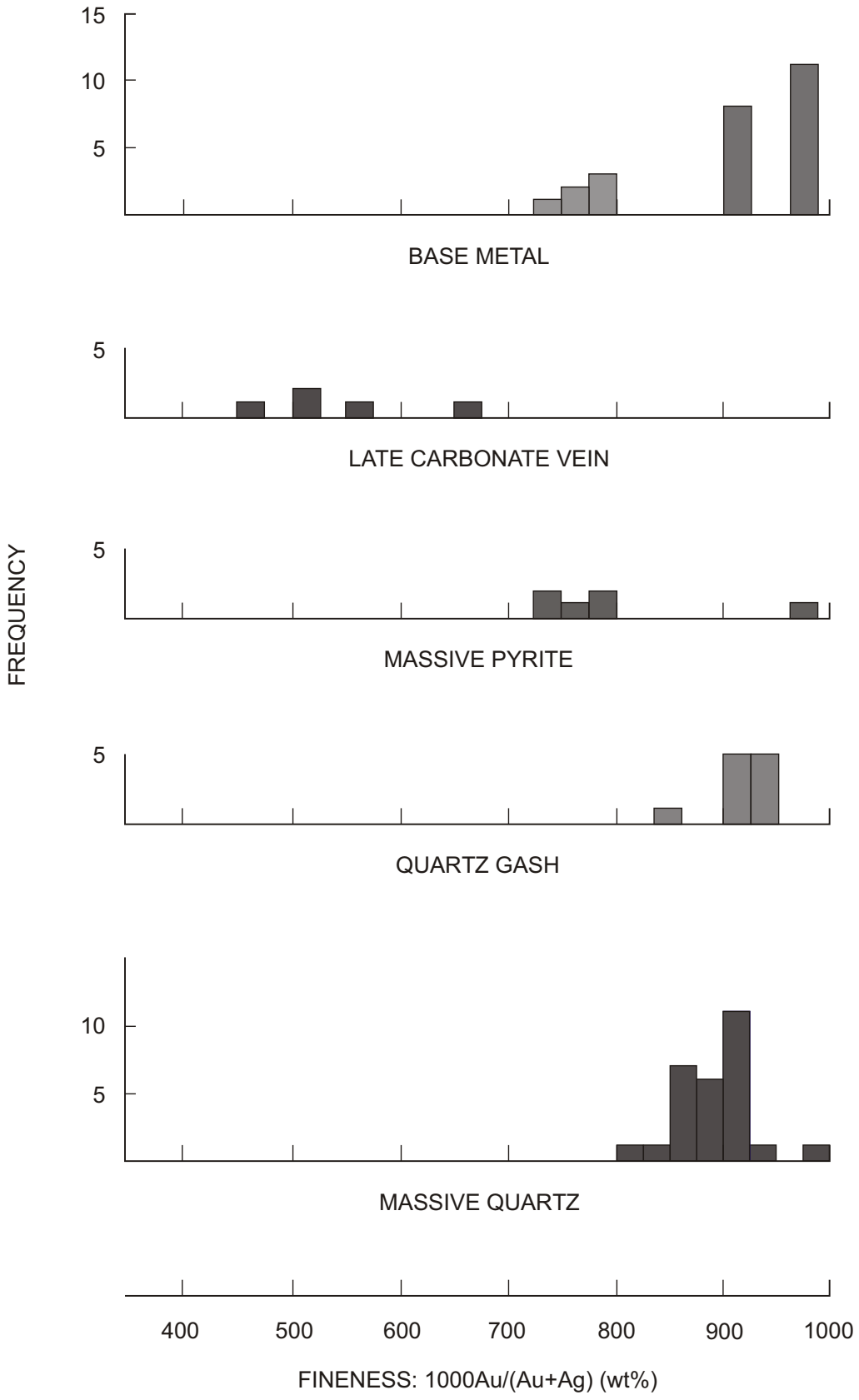

Figure 2.39

Fineness histogram for electrum grains in different hydrothermally altered rocks

common in pyrite of volcanic origin (e.g. Willan and Hall, 1980; Edwards and Carlos, 1954; Yamamoto, 1976). S/Se in pyrite of exhalative origin is generally <22 000 and in sedimentary pyrite >100 000 (Stanton, 1972). However S/Se ratios are considered to be less reliable than Co/Ni ratios, as there are high and low S/Se values from similar provinces (Willan and Hall, 1980) and the ratios may be affected by the temperature, fO_2, and pH of solution.

The selenium values at the Henty Prospect range from <44 to 870 ppm, with higher values being mainly from massive pyrite. Se shows a broad positive correlation with Co content in the analysed samples (Appendix 4). In general the S/Se ratios are similar to values in massive pyrite of exhalative origin.

As

Arsenic appears to be common in all types of analysed pyrite, however the concentrations appear to vary widely within each sample (Appendix 4). Arsenic may occur as submicroscopic arsenopyrite grains or as substitution of As for S in the pyrite structure. The solubility of As in pyrite appears to be less than 0.6 wt% and is temperature independent (Clark, 1960). Therefore a high content of As in a sample may be due to the occurrence of fine-grained arsenopyrite. As-rich pyrite may occur as microscopic zones in early-formed (pre-tectonc) massive pyrite or it may occur as overgrowths and fracture-fillings causing colour variations within individual pyrite grains of etched pyrites (e.g. Taheri and Green, 1990; Fleet *et al.*, 1988).

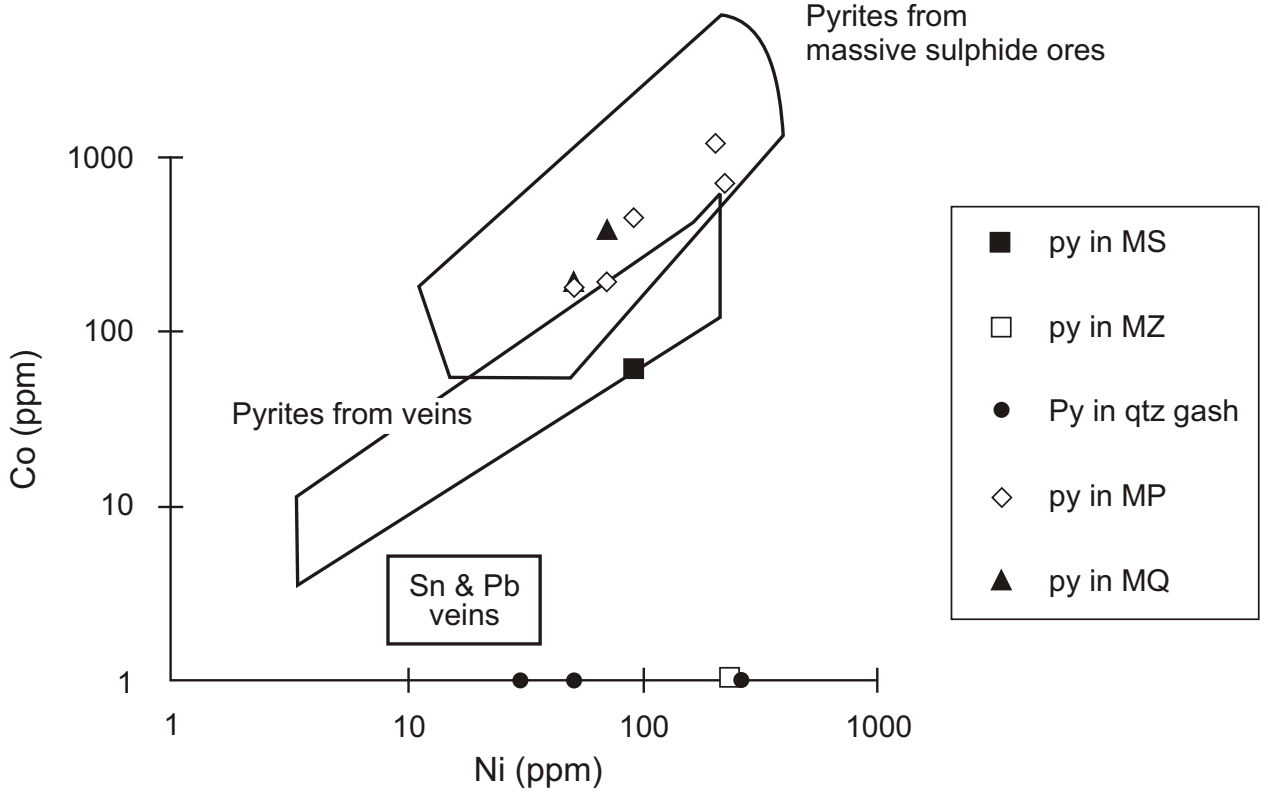

Figure 2.40

Ni-Co diagram for pyrite from the hydrothermal altered rocks. General fields for massive sulphides are also indicated. Data from Willan and Hall (1980), Bralia (1979), and Loftus-Hills and Solomon (1967).

CHAPTER 3

Fluid Inclusions

INTRODUCTION

During processes of crystal growth, recrystallisation or fracture healing small proportions of the fluid medium may be trapped as fluid inclusions. Fluid(s) may be trapped either during crystal growth in growth irregularities to form **PRIMARY** fluid inclusions or at some later time by processes of recrystallisation to form **SECONDARY** fluid inclusions. **PSEUDO- SECONDARY** fluid inclusions are those formed along the fractures during the growth of a crystal.

Most of fluid inclusions range in size from 3 to 20 m, however museum specimens with fluid inclusions larger than one millimetre are known (e.g. Hidden, 1882; Rankin and Greenway, 1978).

Compositions of fluid inclusions vary widely. The major solvents are H_2O and less commonly CO_2, and the major solute ions include Na, K, Ca, Mg, Cl, SO_4 and HCO_3, with Li, B, Al, Fe, F, Mn, and Si being as minor solute ions. Major constituents in inclusions with organic liquid or gas include H_2, CH_4 and C_2H_6, as well as a variety of high molecule weight compounds.

Fluid inclusions normally have a vapour or gas bubble which may move constantly under the effect of a thermal gradient or of gravity. The volume coefficients of thermal expansion for minerals are less than the water by up to three times. Therefore upon cooling, a fluid inclusion which has been formed as homogeneous fluid at elevated temperatures will shrink more than the host mineral, and when the total vapour pressure of the fluid is more than the pressure in the inclusion, a bubble will nucleate and grow. The process can be reversed simply by heating the fluid inclusion to the temperature at which the bubble disappears (i.e. homogenisation temperature). This was first suggested by Sorby (1858).

The salinity of fluid inclusions (wt% NaCl equivalent) can be estimated by freezing the fluid inclusions and measuring the depression of the freezing points of the inclusions. This is just an estimate, as other solute ions such as Mg, Ca, etc. may also be present in the fluid. There are many methods (non-destructive and destructive) to determine the compositions of the fluid inclusions and these have been explained in detail by many workers (e.g. Roedder, 1984). For more recent micro-analytical techniques the reader is referred to the journal *Geochemica et Cosmochemicha Acta*, Volume 54, 1990.

In general fluid inclusions can be utilised in defining the possible environment of ore formation (e.g. epithermal, mesothermal), and in studies of physicochemical conditions of ore-forming fluids. They can also be used in igneous and metamorphic terrains, in oil exploration, in active geothermal systems, and in many other fields.

FLUID INCLUSIONS AT THE HENTY PROSPECT

The following preliminary and incomplete fluid inclusion study was undertaken during the early stage of the project but was not continued, mainly because fluid inclusion studies were not considered to be essential for the project by the RGC geologists. Therefore a systematic, detailed work may provide more information regarding the formation temperatures and compositions of the ore-forming solutions.

Fluid inclusion petrography of some 35 fluid inclusion sections from the massive quartz-sulphide-gold rocks (MQ) and the quartz gashes, as well as the polished thin sections and thin sections, revealed that only the fluid inclusions in quartz from the late quartz gashes and late (post-deformation) carbonate veins were useful for microthermometry measurements. The lack or rarity of primary fluid inclusions is due to the extensive fracturing, brecciation and recrystallisation which have destroyed almost all of the primary fluid inclusions in quartz, fluorite, carbonate and sphalerite. Therefore the standard criteria used in distinguishing primary from secondary fluid inclusions (Roedder, 1984) cannot be applied readily in deformed rocks, and it may be more appropriate to use terms such as "primary looking", "early formed" or "early secondary" fluid inclusions for those which may be classified as primary fluid inclusions in a deformed mineral.

Fluid inclusions in quartz from the massive quartz-sulphide-Au rocks are very small (<2 m) and occur mainly along the fractures. Quartz formed during the earliest stage of crystallisation (Chapter 2) is free from fluid inclusions, and the deformation appears to have caused the migration of the inclusions to sub-grain boundaries. Fluid inclusions in fluorite from sample 104912 appear to have been affected by necking down processes, and have variable vapour to liquid ratios. Fluid inclusions in sphalerite from the massive sulphides are very small and mainly occur along the grain boundaries, however it is possible to obtain some information regarding the temperatures and compositions of fluid inclusions in some sphalerite grains.

Only five polished sections (Appendix 5) from the late quartz gashes were found useful for fluid inclusion studies. There are basically three types of fluid inclusions in the late quartz gashes:

Type A: Two phase (liquid + vapour) inclusions with vapour to liquid ratios of less than 0.1 and ranging in size from <2 to 10 m. The inclusions occur in fractures and grain boundaries, and are clearly of secondary origin.

Type B: Two phase fluid inclusions with high vapour to liquid ratios (0.4 to 0.6), and may show a dark meniscus around the vapour bubble which probably indicates the occurrence of minor vapour CO_2 in these inclusions. These inclusions are randomly distributed and appear to be independent of fractures.

Type C: Three phase fluid inclusions consisting of aqueous solution (L_{H2O}), liquid CO_2 (L_{CO2}) and vapour $CO_2 + H_2O$ ($V_{CO2+H2O}$). The fluid inclusions range in size from 2 to 20 m and are relatively consistent in their phase ratios with 35 to 50 vol% liquid plus gas CO_2. Almost all of the large fluid inclusions (~10 m) have been affected by necking down and some exhibit decrepitation clusters (Swanenberg, 1980; Roedder, 1984). Decrepitation clusters result from partial decrepitation of large inclusions, and are characterised by the occurrence of small satellite inclusions around the larger original inclusions. They may be formed either by heating of the inclusions above their homogenisation temperatures or by a drop in external pressure.

The most reliable and primary-looking fluid inclusions occur immediately next to sulphides, in particular galena and chalcopyrite in the late quartz gashes. These fluid inclusions appear to have been protected by the ductile behaviour of the sulphides from the later deformation phases. This is clearly exhibited in thin section, in which quartz adjacent to the sulphides is commonly the least strained. The number of the primary-looking fluid inclusions decreases sharply away from such areas by overprinting by later-formed low temperature secondary fluid inclusions in more intensively deformed quartz. Analytical Method

The microthermometric measurements were conducted on a modified (Fluid Inc) US Geological Survey, using 60 to 150 m doubly polished sections. Temperatures were calibrated against a set of synthetic fluid inclusion standards at temperatures -56.6°C, -21.2°C, -10.7°C, 374.1°C and 573°C (Appendix 5). The homogenisation and salinity measurements can be duplicated within +0.1 to +0.2°C.

Fluid inclusion composition – freezing experiments

A few freezing measurements on type A inclusions indicate low salinities (~3 equiv. wt% NaCl, Appendix 5). Salinity measurements in CO_2-bearing fluid inclusions (types C and possibly B) using the melting points of ice are inaccurate (Collins, 1979; Hollister and Burruss, 1976; Poty *et al.*, 1978). This is due to the formation of clathrate (CO_2, 5.75 H_2O) upon freezing. However the melting of CO_2 hydrate may be used for salinity measurements provided no other gas species are present.

Freezing measurements on a few type B fluid inclusions were not successful, mainly due to the small sizes of the inclusions. Large (>4 m) three-phase fluid inclusions (type C), including some necked-down inclusions, were used for freezing experiments. Necked-down fluid inclusions may be used for salinity measurements provided no phase changes (e.g. formation of daughter mineral) occurs before necking down.

Melting points of CO_2 hydrate are very difficult to measure. This is because of the isotropic character of the hydrate and the similarity of its refractive indices to those of aqueous solutions. Therefore, the crystal may be almost invisible depending on the refractive index of the aqueous solution. The best technique in measuring the melting point of CO_2 hydrate is by a slow warming rate of about 0.2°C per minute and rapid cooling at a temperature close to melting of CO_2 hydrate. If the temperature at which the rapid cooling is applied is below the melting point of CO_2 hydrate, then the gas hydrate will grow and deform the gas-liquid boundary or a rapid movement of gas bubble is indicated. This process is continued sequentially incrementing temperature by 0.2 to 0.5°C until rapid cooling does not cause any changes in the inclusion. The measurements can be duplicated by this method to 0.2°C. The procedure is actually similar to that described by Roedder (1962, 1963) for the melting measurements of ice in the fluid inclusions.

The CO_2 in the fluid inclusions appears to be pure, as the melting point of CO_2 (solid) was different by + 0.2°C from that of pure CO_2 (i.e. -56.6°C, Appendix 5). The melting temperatures of clathrate for the fluid inclusions were consistent, ranging from 5.0 to 5.5°C, an average depression of about 4.5°C from the melting of CO_2 in a CO_2–H_2O system (i.e. +10°C). The salinity of aqueous phase consistent with this depression is about 8.5 wt% NaCl (Appendix 5).

Homogenisation data

Fluid inclusion homogenisation temperature data is shown in Figure 3.1. Type A fluid inclusions exhibit a wide range of homogenisation temperatures (110–192°C). However fluid inclusions occurring in the same fracture show similar homogenisation temperatures.

Type B fluid inclusions homogenised to liquid in the range of 244 to 331°C. CO_2 phases (liquid and vapour) in type C inclusions homogenised to liquid upon heating within a narrow range of 27.9 to 29.1°C

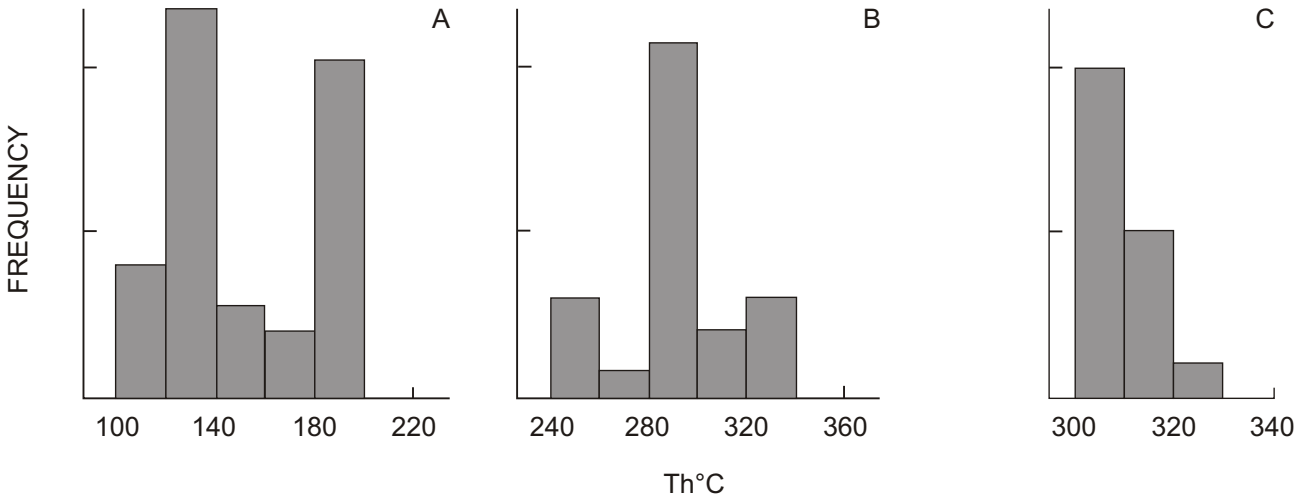

Figure 3.1

Homogenisation temperature histograms for types A1, A2 and A3 fluid inclusions

(Appendix 5). The final homogenisation temperatures (to liquid) range from 304 to 325°C, with more than 70% of population falling in the range of 290 to 330°C. One inclusion homogenised to vapour.

Many fluid inclusions decrepitated prior to homogenisation, probably as a result of high internal pressures generated in CO_2-bearing fluid inclusions during heating or because the inclusions had leaked. However all of the inclusions used for heating experiments had relatively consistent phase ratios.

Discussion

Because of the limited data and incomplete nature of the work any interpretations should be treated with caution. Type A fluid inclusions appear to have been derived at different times and possibly from different fluid sources, as fluid inclusions in each fracture appear to be characterised by a very narrow range of homogenisation temperatures but are distinctly different from other fractures. This is consistent with the petrographic observation in that the rocks have been affected by different generations of veining.

Type B and C fluid inclusions exhibit a similar range of homogenisation temperatures. However there are not sufficient criteria to explain the distributions of the CO_2-bearing fluid inclusions by fluid immiscibility in the system H_2O-CO_2-NaCl. A minimum pressure estimate can be made if compositions, bulk densities and volume proportions of fluid inclusions are known.

Density of the CO_2 phase can be estimated from homogenisation temperatures using the experimental solvus of the pure CO_2 system (after Roedder, 1965). Bulk density may then be estimated by knowing the density of the aqueous solution and visual estimate of volume proportions of the CO_2 phase (liquid plus vapour) and aqueous solution at room temperature (after Burruss, 1981*b*). The estimated average densities for the CO_2 phase and the bulk of the fluid (CO_2 + H_2O) for type C fluid inclusions are 0.6 and 0.85 g/cm^3 respectively.

The mole fractions of H_2O, CO_2 and NaCl may also be estimated using the techniques described by Burruss (1981). The estimated average mole fractions for H_2O, CO_2 and NaCl are 0.86, 0.12 and 0.02 respectively. Considering the above estimated bulk density and the mole fractions and using the calculated densities of fluids in the ternary system H_2O-CO_2-NaCl as isochors on a pressure-temperature diagram (Bowers and Helgeson, 1983) a minimum pressure of around 800 bars is indicated at a temperature of 320°C. The maximum temperatures obtained from chlorite geothermometry (~320°C, Chapter 2) are similar to the homogenisation temperatures of types B and C fluid inclusions. If the results obtained by chlorite geothermometry are considered to be reliable, then the similarity in the temperatures indicates that the homogenisation temperatures for types B and C inclusions represent true formation temperatures (i.e. CO_2-bearing fluid inclusions are on a two-phase immiscibility curve). In this case the quartz gashes have probably formed at temperatures of about 320°C and a pressure of around 800 bars.

CHAPTER 4

Stable Isotopes

INTRODUCTION

The geological, petrological and fluid inclusion evidence points to the importance of syn- to late-deformational events as important controls of the immediate site of gold mineralisation. On a broader scale, the geological setting, textural and whole-rock geochemical data point to a probable Cambrian age for the basic alteration mineral assemblages which exert a control on the location of gold mineralisation.

As with the other geological and geochemical data, the stable isotopes of oxygen, sulphur and carbon may be subject to varying degrees of overprinting of Cambrian events by Devonian deformational events. However by comparing results from the Henty deposit with the extensive data base now available from a wide range of Devonian and Cambrian mineral deposits in western Tasmania, valuable insights can be gained into the genesis of the Henty ore. By necessity, much of this evaluation is interpretive and is based on empirical comparison between data from Henty and other deposits.

Elements used in stable isotope studies include C, H, O, S, B and N, of which the isotope variations of carbon, oxygen, hydrogen, boron and sulphur are used in ore genesis studies. Some of the common features of these elements include low atomic mass, abundance in nature and relatively large mass differences between the abundant and rarer isotopes. The proportion of the rare isotopes (e.g. ^{34}S, ^{18}O) are still sufficient for accurate measurements by mass spectrometry.

Application of stable isotope geochemistry to the earth sciences was first discussed by Urey (1947). Interpretations of the data to ore genesis were relatively limited until recent work by Rye and Ohmoto (1974), Talyor (1974 and 1979), Ohmoto and Rye (1979), Ohmoto (1986) and others which have increased our knowledge of the factors governing variations in ratios of stable isotopes in nature. For example Ohmoto (1972) showed that the large variations in ^{34}S values of sulphides in ore deposits can be due to the variations in oxidation states of hydrothermal fluids rather than being solely due to biogenic processes (e.g. Jensen, 1967). The interpretation of stable isotope data is being increasingly modified with the development of new analytical techniques (e.g. ion microprobe, Eldridge *et al.*, 1987) and our better understanding of the processes responsible for formation of different ore deposits. Stable isotope data need to be interpreted in conjunction with other geological information such as structural setting, mineralogy, paragenesis, phase relationships, geochemistry, and fluid inclusion studies. If this is done then useful information may be gained regarding the temperature of formation, sources of carbon and sulphur, origins and redox states of ore-forming fluids, and evolution of hydrothermal fluids in ore deposits.

SULPHUR ISOTOPE

Conventional Technique

Sulphur isotope values were determined according to the method of Robinson and Kusakabe (1975) using a VG Micromass 602 mass spectrometer at the University of Tasmania. The data are reported as per mil (‰) deviation from $^{34}S/^{32}S$ values of the Troilite in Canyon Diablo Troilite (CDT). The error on the internal standards (Broken Hill galena and Tullah galena) are less than 0.1‰.

Analyses were carried out on 34 sulphides from the different styles of mineralisation. Some of the analysed samples are from the same core samples as those selected by Yeats (1989), however the results obtained through this study are consistently heavier by up to 1.2‰. The analyses should be randomly repeated in order to establish which set of data are the more accurate. However this discrepancy will not change the overall interpretation of the sulphur isotope data.

Table 4.1 shows the combined results of this study and those from Yeats (1989) which were not repeated in this study. The sulphide minerals analysed include pyrite, chalcopyrite, galena and sphalerite. The sulphur isotope values range from 6.92 to 14.4‰, with nearly 80% of the population falling in the range of +8 to +13‰ (Table 4.1, fig. 4.1). The average value is +10.1‰ with a standard deviation of 1.7‰. There is no apparent systematic change in ^{34}S values with respect to alteration style, locality or type of occurrence. The sulphur isotope values are plotted as histograms for the different styles of mineralisation in Figure 4.1. The three major mineralisation styles, including massive pyrite, massive quartz-sulphides-gold, and quartz-sericite-sulphides, exhibit very similar ranges, with averages and standard deviations ranging from +9.66 to 9.96‰ and 1.4 to 2.0‰ respectively (fig. 4.2).

Ion Microprobe Analyses

Detailed mineragraphy of etched pyrites in the massive pyrite-carbonate-quartz assemblage revealed that pyrite occurs in four distinct different morphologies:

(1) cubic (recrystallised),

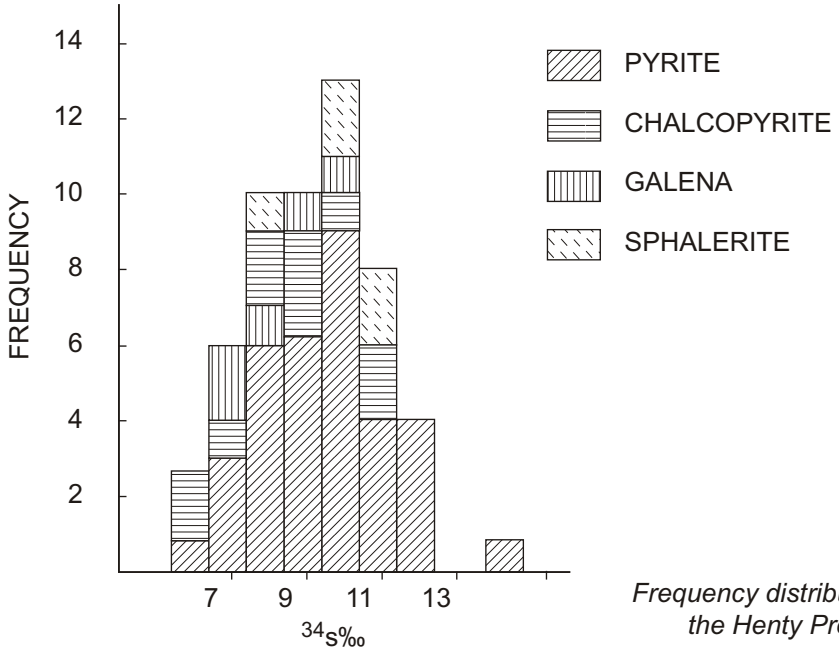

Figure 4.1

Frequency distribution of sulphur isotope values at the Henty Prospect (data from Table 4.1)

(2) strongly zoned,

(3) framboidal, and

(4) colloform (Chapter 2).

Given the fine-grained textures, sulphur isotopic data using the conventional technique will only represent bulked isotopic compositions of two or more pyrite types. Therefore it was essential to use a technique in which the sulphur isotope compositions of the different types of pyrite could be individually analysed. In particular it was necessary to determine whether the late-stage syndeformation cubic pyrite, possibly temporally associated with gold-chalcopyrite mobilisation and concentration, could be distinguished isotopically from the earlier, presumably Cambrian syngenetic or syn-diagenetic stage. This was achieved through analyses by C. S. Eldridge using the SHRIMP ion microprobe at the Australian National University. Three polished thin sections from the massive pyrite samples were prepared and etched (see Chapter 2 for more detail) for the analyses. Areas of interest were then marked with circles which were at least 30 m in diameter, close to the minimum beam width of the ion microprobe. The craters created by the beam are about 5 m deep.

The ion microprobe and the technique used for sulphur isotopic analyses have been discussed by Compston *et al.* (1984) and Eldridge *et al.* (1987) respectively. A total of ten analyses were obtained from the morphologically different pyrite types (Table 4.1, fig. 4.2). The sulphur isotope data range from 4 to 15 per mil. A similar range is also indicated by the conventional technique. However there is no correlation between the different types of pyrite and the sulphur isotope values (Table 4.1).

DISCUSSION

Possible sources of Sulphur

The texture of the massive pyrite at the Henty Prospect is consistent with a pre-deformational Cambrian origin. The Henty Prospect is one of several deposits along the Henty Fault Zone. Therefore the relationship between the sulphur isotope values from the Henty Prospect with other deposits along the Henty Fault needs be discussed.

Figure 4.3 is a cross section along the Henty Fault showing the calculated position of the Granite Tor Granite (Leaman and Richardson, 1989) and the general mineralogy, range, mean and standard deviations of the sulphur isotope values for some of the deposits located along the Henty Fault Zone between the Mt Farrell Mining District and the Henty Prospect. According to Taheri and Green (1990) in the Tullah–Sterling Valley area there is a correlation between the position of the underlying Granite Tor Granite and the distribution of sulphides and the sulphur isotope values. Isotopically light sulphur values are from deposits occurring at shallow depth right above the crest of Granite Tor ridge, and are mineralogically characterised by pyrrhotite, pyrite, arsenopyrite, chalcopyrite and gold. Lead-silver-zinc dominated deposits with higher ^{34}S values occur on both sides of the ridge at a greater depth (fig. 4.3). The deposits with low sulphur isotope values and high temperature mineral assemblages have been interpreted to indicate a greater proportion of magmatic sulphur whereas the higher ^{34}S values from the lead-silver-zinc deposits are indicative of a more substantial input from dissolved Cambrian sulphides or sulphates. However neither the mineralogy nor the sulphur isotope values at the

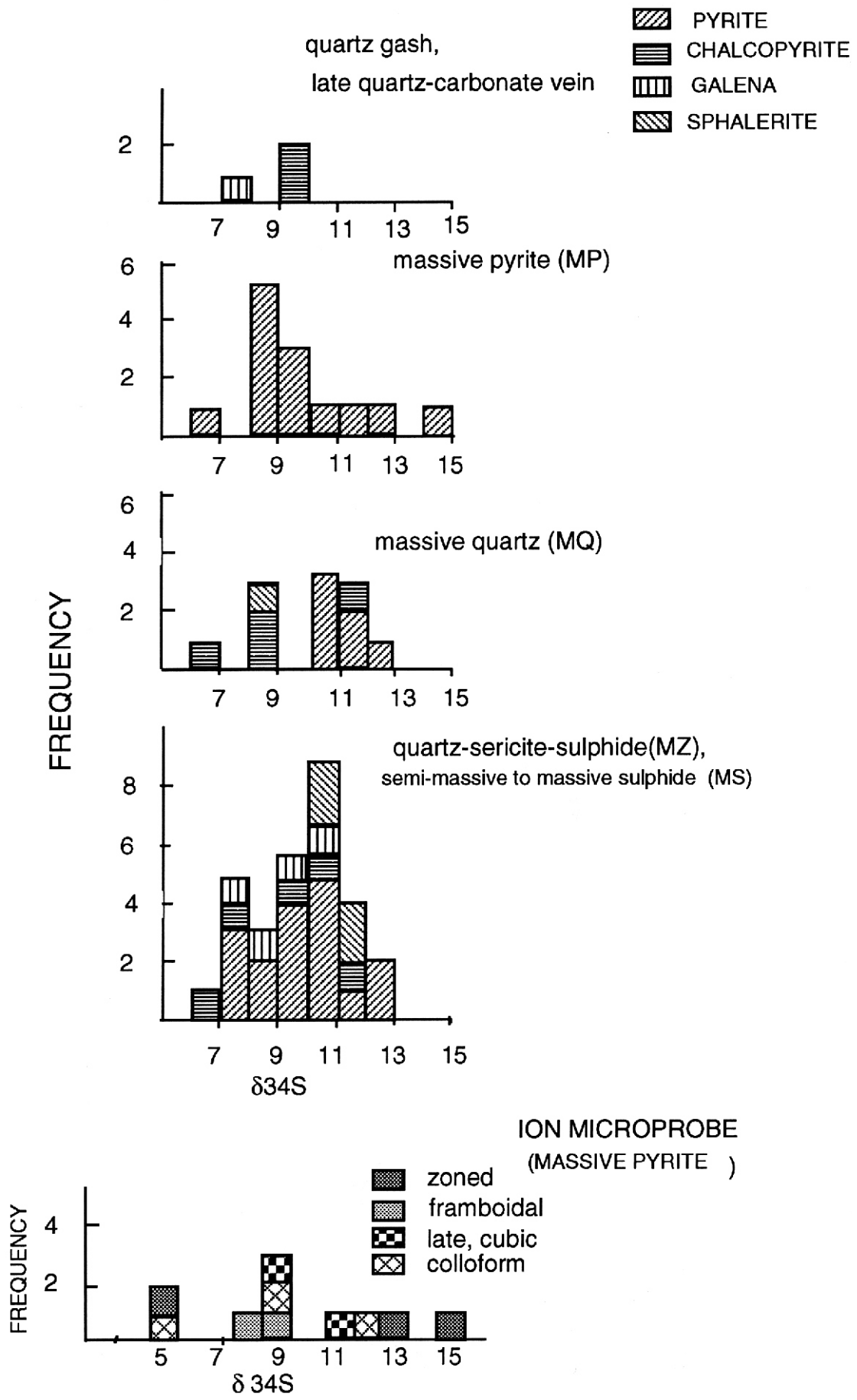

Figure 4.2

Frequency distribution of ^{34}S values for different types of mineralisation, Henty Prospect (data from Table 4.1)

Table 4.1

Sulphur isotope data, Henty Prospect

DDH	*Depth (m)*	*Cat. No.*	*RGC No.*	*Rock type*	*Sulphide*	*^{34}S (‰)*
HP4	250.1	103736	T17739	q-sulphide in MZ	py	10.56
HP4	258.7	103737	T17740	q-sulphide in MZ	cpy	10.89
HP4	260.7	103738	T17741	MP	py	12.51
HP7	373.00	103745	T17701	MS	py	9.71
HP19	282.7	103752	T17728	MQ	py	11.57
HP19	184.8	103753	T17729	q gash-cpy	cpy	9.80
HP20	144.4	103754	T17710	MP	py	9.33
HP24	120.8	103758	T17720	q-sulphide in MZ	gn	7.87
HP24	125.4	103762	T17723	MP	py	8.77
HP26	112.2	103764	T17734	MQ	cpy	6.92
HP26	112.2	103764	T17734	MQ	py	10.75
HP28	326.3	103765	T17724	MS	gn	10.75
HP28	326.3	103765	T17724	MS	py	12.24
HP28	326.3	103765	T17724	MS	sph	11.98
HP31	334.5	103768	T17738	MP	py	9.77
HP32	164.1	103769	T17730	MZ	py	10.46
HP42	602.8	103772	T17745	q-sulphide in MZ	cpy	11.33
HP42	611.1	103776	T17749	MZ	py	11.28
HP47	441.8	103781	T17705	MS	sph	11.46
HP47	441.8	103781	T17705	MS	py	12.16
HP47	441.8	103781	T17705	MS	gn	8.72
HP47	441.8	103781	T17705	MS	cpy	9.96
HP51	128.4	103784	T17784	q gash-gn-cpy	cpy	9.49
HP51	128.4	103784	T17784	-	gn	7.46
HP51	129.8	103786	T17704	MQ	cpy	8.32
HP57	669.4	103792	T17753	q-sulphide in MZ	py	7.90
HP57	675.3	103793	T17754	q-sulphide in MZ	py	7.90
HP96A	590.65	104926	T20139	MZ with banded pyrite-qtz-carb	py	8.49
HP129D	636.1	104934	T20146	banded MS-q	sph	10.65
HP129D	638.0	104930	T20147	MP	py	11.74
HP129D	650.5	104903	T20152	q-carb. sulphide vein	sph	7.25
HP129D	612.85	104906	T20140	MQ	py	11.87
HP129D	641.5	104928	T20149	MP	py	9.45
HP129D	640.15	104929	T20148	MP	py	14.14
SF33	-	103926	-	MP	py (zoned)	15*
SF33	-	103926	-	MP	py (zoned)	13*
SF33	-	103926	-	MP	py (late, cubic)	11*
SF19-20	-	103950	-	MP	py (zoned)	4*
SF15-16	-	103953	-	MP	py (framboidal)	8*
SF15-16	-	103953	-	MP	py (framboidal)	9*
SF15-16	-	103953	-	MP	py (colloform)	4*
HP4	260.7	103738	T17741	MP	py (colloform)	12*
HP4	260.7	103738	T17741	MP	py (colloform)	9*
HP4	260.7	103738	T17741	MP	py (late, cubic)	9*
HP7	373	-	-	MS	py	9.48**
HP9	135.2	-	-	MS	py	7.97**
HP13	597.6	-	-	MP	py	11.39**
HP17	157.9	-	-	MP	py	6.30**
HP17	159.1	-	-	MP	py	8.54**
HP19	282.1	-	-	MQ	py	12.18**
HP19	287.7	-	-	MQ	py	10.72**
HP19	284.8	-	-	MQ	cpy	8.91**
HP20	144.4	-	-	MP	py	8.84**

Table 4.1 (continued)

DDH	*Depth (m)*	*Cat. No.*	*RGC No.*	*Rock type*	*Sulphide*	*^{34}S (‰)*
HP31	333.5	-	-	MP	py	8.64**
HP32	138.5	-	-	MZ	py	10.64**
HP42	603.6	-	-	MQ	cpy	11.06**
HP47	434.2	-	-	MQ	py	10.29**
HP47	434.2	-	-	MQ	sph	8.92**
HP47	439.9	-	-	MZ	py	9.74**
HP47	441.7	-	-	MS	py	10.8**
HP47	441.7	-	-	MS	gn	9.80**
HP47A	443	-	-	MS	sph	10.63**
HP49a	922.6	-	-	MZ	py	9.94**
HP49A	941.4	-	-	MZ	cpy	7.18**
HP49A	942.3	-	-	MZ	cpy	6.15**
HP53	165.4	-	-	MZ	py	10.88**
HP55	165.5	-	-	MP	py	8.25**

* Ion microcprobe results
** Data from Yeats (1989)

cpy	chalcopyrite	carb	carbonate
gn	galena	MZ	quartz-sericite-sulphide
q	quartz	MP	massive pyrite
sph	sphalerite	MQ	massive quartz
py	pyrite	MS	massive sulphide

All values are in ‰ relative to Canyon Diablo Troilite
Analytical precision 0.1‰.
Analyses for this study by R. N. Woolley.

Henty Prospect correlate with the above spatial zoning, and interpretation of gravity data by Leaman and Richardson (1989) indicates that granite lies at a depth of about 8 km at the Henty prospect. This indicates that the mineralisation probably formed under different physicochemical conditions from the other deposits along the Henty Fault Zone.

Magmatic (uncontaminated) sulphur isotope values are likely to be between +3 to -3‰ and the magmatic hydrothermal fluid derived from this magma will have ^{34}S values in the range of -3 to +7‰ (Ohmoto and Rye 1979). Pyrite or sphalerite formed from such a magmatic hydrothermal fluid at temperatures between 200 and 300°C may have ^{34}S values ranging from larger than +8 to ~-30‰, depending on the redox reactions between the fluid and the country rocks, the fO_2, and the original ^{34}S values of the melt. Therefore there is a possibility of involvement of magmatic sulphur at the Henty Prospect. The magmatic sulphur can either be derived directly from a magmatic fluid or through leaching of magmatic sulphides or sulphates from the rocks beneath the ore horizon. The former is highly unlikely because of the depth to granite. It is possible that the leaching process may have had a significant input to the sulphide sulphur of the Henty Prospect. However the overall ^{34}S values are distinctly higher than those from the major Tasmanian Devonian magmatic hydrothermal ore deposits. They are even higher by approximately two per mil than those at the Lakeside and the Sterling Valley tin prospects, which probably had multiple sulphur sources (fig. 4.4).

A possible source for the heavy sulphur isotope values is Cambrian seawater (^{34}S seawater ~30‰, Claypool *et al.*, 1980) in which the circulation of seawater through the rocks beneath the ore horizon at elevated temperatures probably resulted in the formation of H_2S by leaching of magmatic sulphides from the rocks and reduction of seawater sulphate by Fe-Mg minerals containing ferrous iron such as hornblende and chlorite. Such a seawater-dominated hydrothermal fluid would have its H_2S content buffered by pyrite solubility and its ^{34}S value governed by the proportions of rock – seawater-derived sulphur as well as the redox state of the fluid (e.g. Ohmoto *et al.*, 1983; Solomon *et al.*, 1988). Obviously high water/rock ratios lead to higher ^{34}S values because of the greater contribution of seawater sulphur. However the consistent and the relatively low to moderate sulphur isotope values at the Henty Prospect are consistent with a relatively high rock-sulphur input, and that the solution remained relatively constant in terms of fO_2 or temperature during the formation of the deposit. The few sulphur isotope data which fall outside the common isotopic range (8–12‰) may have been formed under slightly different oxygen fugacities. The sulphur isotope values from the quartz gashes and the recrystallised pyrites (ion microprobe analyses) fall in the middle of the isotopic range and probably reflect the dissolution, isotopic homogenisation and reprecipitation of sulphide during deformation. Dissolution and reprecipitation processes of Cambrian sulphides are

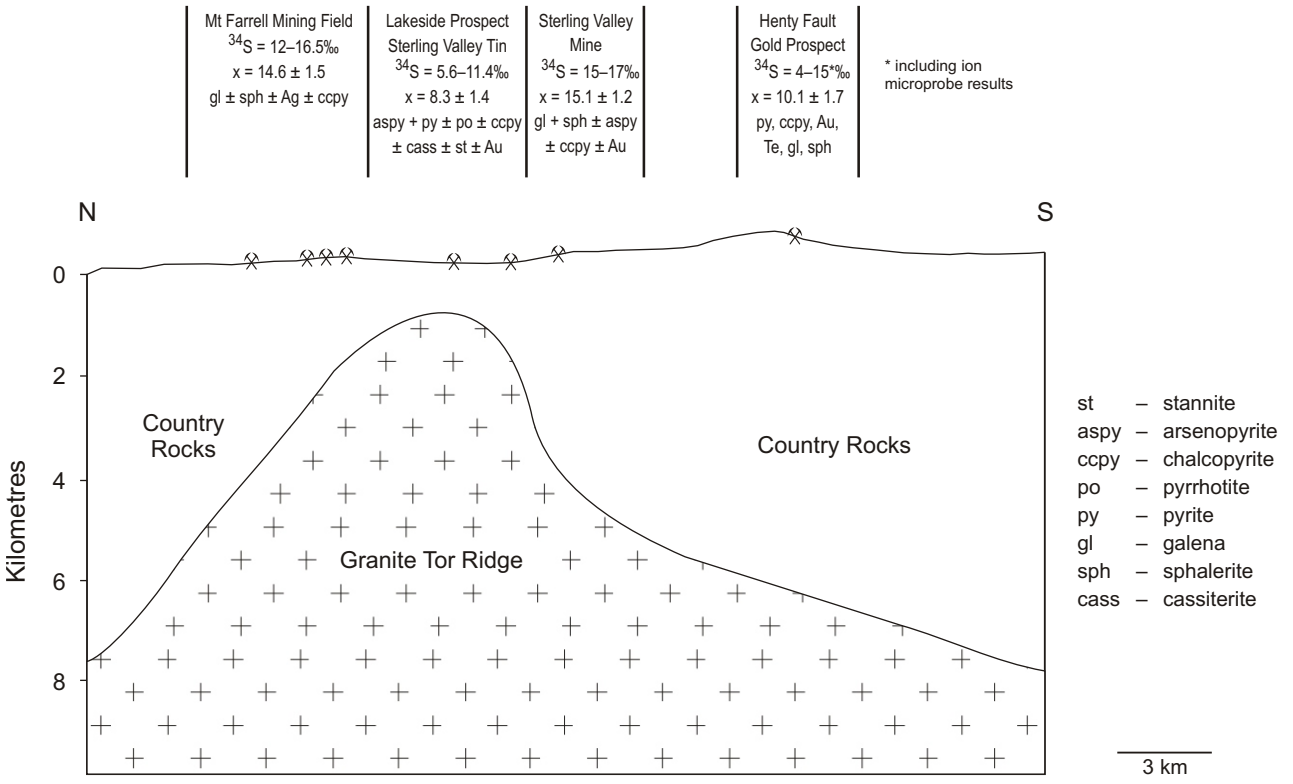

Figure 4.3

Spatial relationships between ^{34}S values and mineral assemblages, and the intrusion of the Granite Tor Granite along the Henty Fault, western Tasmania (modified after Taheri and Green, 1990)

also supported by Cambrian lead isotope values of galena in quartz gashes (Carr and Dean, 1990).

The sulphur isotope values at the Henty Prospect do not exhibit any particular similarity to the other Cambrian stratiform deposits hosted by the Mt Read Volcanics, as each deposit appears to be characterised by its own ^{34}S values (i.e. different sulphur sources, water/rock ratios, or different physicochemical conditions; fig. 4.4). The relatively low ^{34}S values at Que River and the Cambrian deposits at Mt Lyell suggest the involvement of mafic to intermediate rocks beneath the ore body, with relatively higher contents of magmatic sulphur to those in predominantly felsic terrains (Rosebery, Hercules) which have higher mean ^{34}S values and reflect a higher proportion of seawater sulphur. The mineralogy of these deposits suggest that the seawater sulphate component had been totally reduced to H_2S during deposition of the bulk of the Rosebery ore, and an inferred increase in ^{34}S values of the sulphides in the deposit through time was interpreted to reflect a progressive depletion of the disseminated magmatic sulphur source.

However the barren pyritic deposits such as Chester and Basin Lake are characterised by low (negative) ^{34}S values, which are believed to reflect formation temperatures that are too low to affect inorganic reduction of seawater sulphate (less than 20°C). In summary it is concluded that:

(1) The texture of massive pyrite and the overall range of the sulphur isotope values are consistent with those of a Cambrian VMS system.

(2) The sulphides of probable Devonian origin in the deposit (i.e. sulphides in late tensional veins, late euhedral pyrite) have a range of ~9 to 11‰ (excluding galena). Although the data are sparse, these values are not inconsistent with a source for this sulphur from a mixed Devonian magmatic and leached Cambrian sulphur source (e.g. Lakeside, Taheri and Green, 1990). However the fact that the late sulphides have ^{34}S values near the mean for the deposit as a whole indicates that it is unnecessary to appeal to any additional Devonian sulphur source and that the minerals may have been merely derived by dissolution, homogenisation of sulphur, and reprecipitation of Cambrian sulphides during deformation.

Figure 4.4

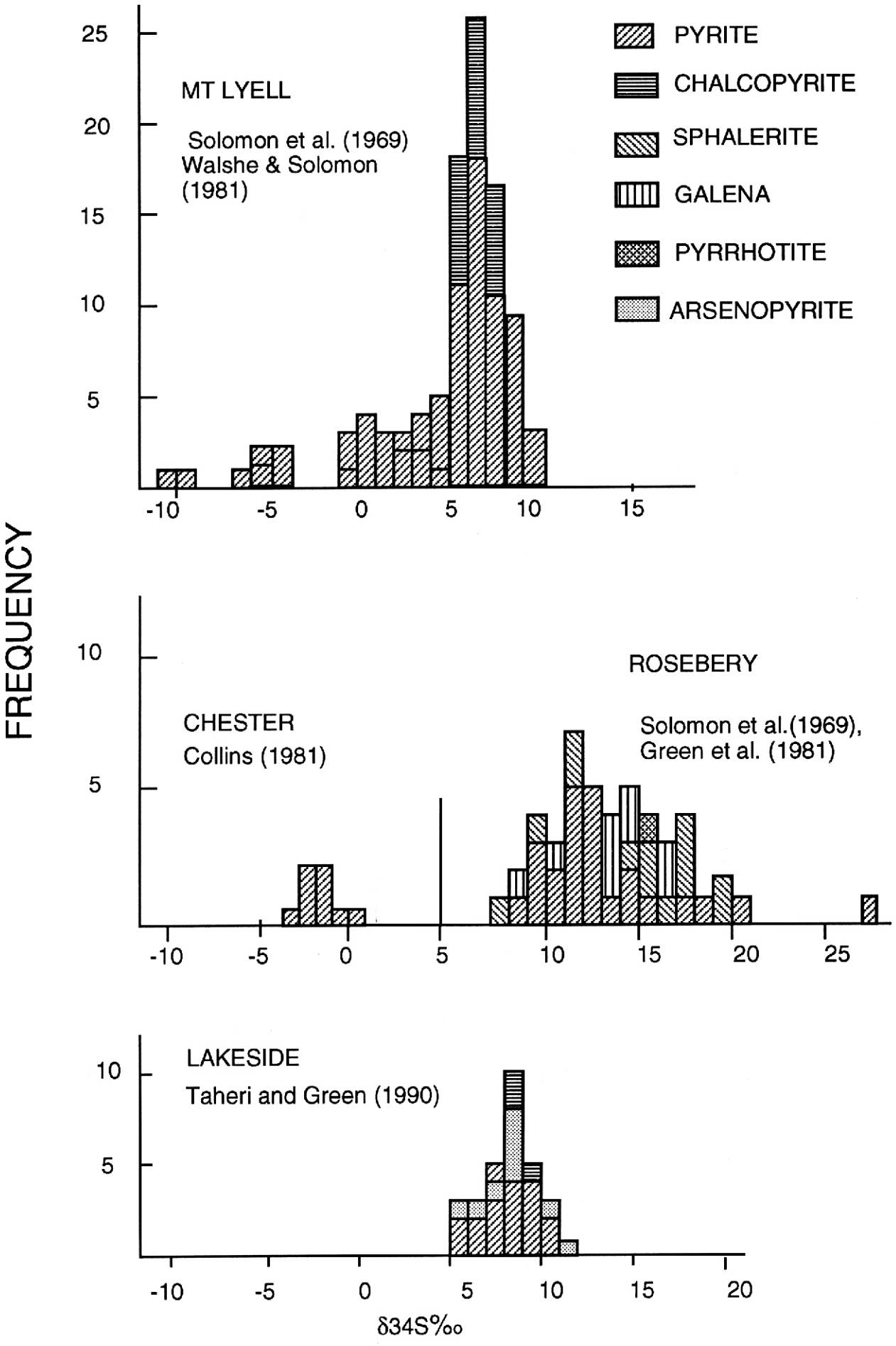
FREQUENCY
MT LYELL
Solomon et al. (1969)
Walshe & Solomon
(1981)
PYRITE
CHALCOPYRITE
SPHALERITE
GALENA
PYRRHOTITE
ARSENOPYRITE
25
20
15
10
5
-10
-5
0
5
10
15
CHESTER
Collins (1981)
ROSEBERY
Solomon et al.(1969),
Green et al. (1981)
10
5
-10
-5
0
5
10
15
20
25
LAKESIDE
Taheri and Green (1990)
10
5
-10
-5
0
5
10
15
20
δ34S‰

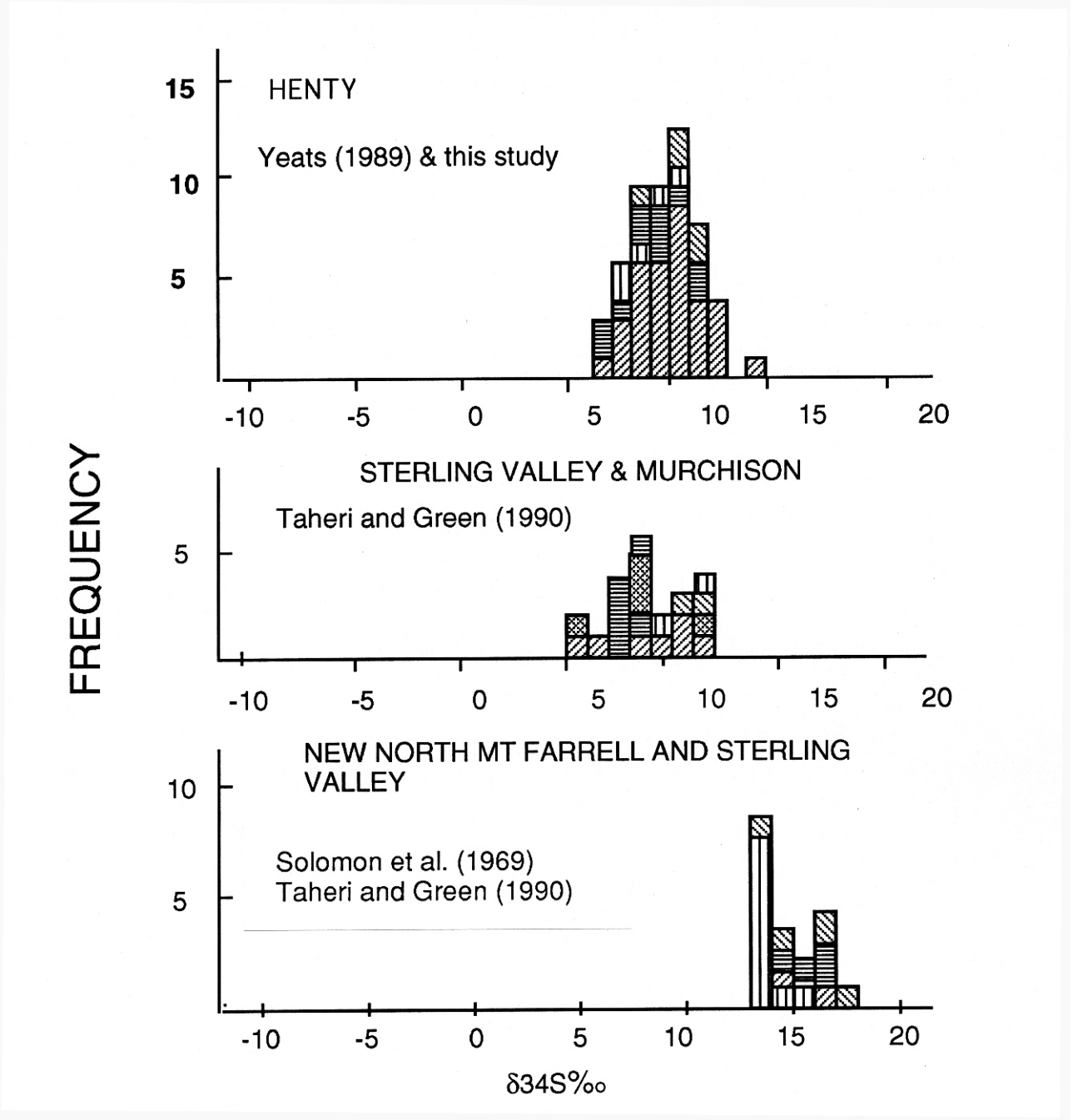

Figure 4.4

Frequency distributions of sulphur isotope compositions of sulphides from the Devonian deposits along the Henty Fault Zone (Lakeside, Sterling Valley Tin, Murchison, New North Mt Farrell) and some of the Cambrian stratiform ore bodies including the Henty Prospect.

CARBON AND OXYGEN ISOTOPES OF CARBONATES

Seventeen calcite samples from LL, MA, MZ, MV, MQ, MS, and late veins, and one dolomite sample from a vein, were analysed for carbon and oxygen isotope analyses. The results from this work, along with those obtained by Yeats (1989), are shown in Table 4.2.

The oxygen isotope values show a narrow range of 9.4 to 13.1‰ with an average and standard deviation of 10.2 and 0.8. The carbon isotope values show relatively more variations, ranging from -3.6 to +0.7‰, including the samples from veins in the Central Volcanic Complex (CVC) and a dolomite vein (Table 4.2, fig. 4.5).

Discussion

A marine sedimentary origin for the carbonates is unlikely as the oxygen isotope values are lower than those of Cambrian limestone (fig. 4.5). Deposition of carbonates from Devonian magmatic fluid is also improbable as discussed above. Therefore the likely source of the fluid appears to be of hydrothermal origin.

The oxygen isotope values of hydrothermal Devonian and Cambrian carbonates appear to show comparable ranges (Khin Zaw and Large, 1990, fig. 4.5), although the majority of the Devonian ^{18}O values are relatively higher than those in the Cambrian. It should be mentioned that the above statement is based on limited number of analyses, and further detailed work is needed to establish more statistically reliable data, and also to investigate the extent and effect of the isotopic exchange between the Cambrian sedimentary carbonate and the Devonian fluid, as some isotopically heavier oxygen isotope values may have been originated by such an isotopic exchange (e.g. Taheri, 1986).

The oxygen isotope values of the carbonates at the Henty Prospect generally fall within the Cambrian field, however the values exhibit narrower range and are isotopically lighter than those from the Devonian hydrothermal deposits. The carbon isotope values also show similar but narrower distributions than those obtained from VMS deposits such as Rosebery, Hercules (Khin Zaw and Large, 1990) and Hellyer (Green, unpublished data), and are isotopically heavier than the Devonian carbonates from Cleveland (Collins, 1981), Renison Bell (Patterson *et al.*, 1981) and the Sweeneys mine (Taheri, 1986, fig. 4.5).

The oxygen isotope values at the Henty Prospect are uncommonly uniform for most of the samples of the different styles of the mineralisation. This may be explained in three ways:

(i) the values may simply indicate that the samples have been taken from a small area within or on the fringes of a relatively low temperature mineralisation and that the recrystallisation has occurred in solid state without any significant input of externally derived fluids,

(ii) the mineralisation is of metamorphic or mesothermal origin which has been formed at relatively high temperatures (300–350°C), and

(iii) the carbonate has gone through extensive isotopic exchange with the later Devonian fluid.

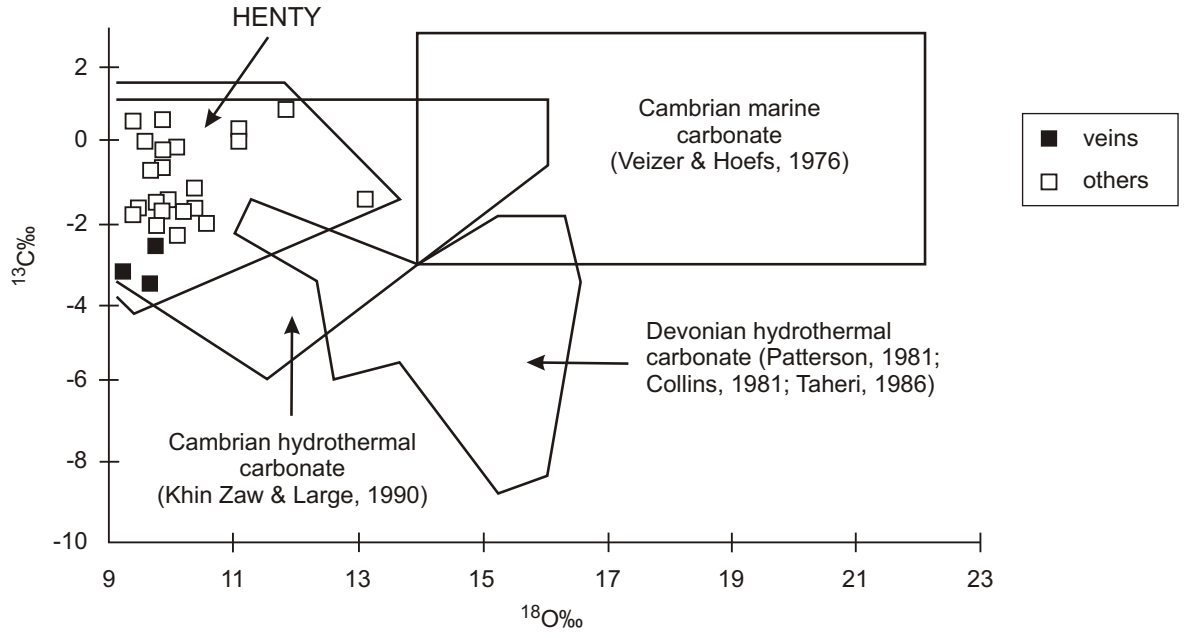

Figure 4.5

^{18}O vs ^{13}C diagram showing the general field for Cambrian marine carbonates and Cambrian and Devonian hydrothermal carbonates

Table 4.2

Carbon and oxygen isotope data

Field No.	*RGC No.*	*DMR No.*	*Rock type***	*^{13}C*	*^{18}O*	*T°C*	*^{13}C fluid*
HP 24, 120.8 m	T17720	103758	QB in MZ	-0.7	9.9	193	-0.7
HP 44, 117.0 m	T17744	103780	LL	0.2	11.1	172	-0.4
HP 47, 445.7 m	T17707	103783	LL	-0.2	10.1	189	-0.3
HP 57, 669.4 m	T17753	103792	QB in MZ	-0.1	11.1	172	-0.7
HP 57, 679.0 m	T17755	103794	LL	-1.2	10.4	184	0.2
HP 57, 680.8 m	T17756	103795	LL	0.2	9.4	202	0.4
HP 47, 445.3 m	T17706	103782	LL	-1.9	9.4	202	-1.6
HP 42, 606.1 m	T17747	103774	MQ	-1.7	9.8	195	-1.6
HP 42, 607.0 m	T17748	103775	MZ	0.7	11.8	161	0.3
SF 33C	-	104947	dolomite vein	-3.6	9.7	261	-2.1
NF 30-31W	T21867	103964	SC	-2.1	10.6	181	-2.5
HP 96A, 558.6 m	T20138	104932	quartz sulphides	-1.5	10	192	-1.5
HP 129D. 646.2 m	T20151	104949	altered epiclastic rocks	-1.8	9.9	192	-1.8
HP 129D, 650.5 m	T20152	104903	quartz-carbonate vein	-2.0	9.8	193	-2.0
NF 13-14W	-	104948	SC	-2.2	9.8	195	-2.1
NF 6-7W	T21834	103925	SC	-2.4	10.1	189	-2.5
HP 96A, 583.5 m	T20135	104916	MQ	-0.1	9.6	199	0.1
HP 13, 588.8*	-	-	LL	-1.7	10.4	184	-1.3
HP 13, 589.8*	-	-	LL	0.4	9.9	193	-0.4
HP 13, 590.1*	-	-	LL	-1.5	13.1	144	-3.2
HP 13A, 587.3*	-	-	LL	-0.8	9.7	197	-0.7
HP 47, 446.3*	-	-	LL	-1.8	10.2	188	-1.9
HP 47, 447.3*	-	-	LL	-1.6	9.8	195	-1.5
HP 47A, 447.35*	-	-	LL	-1.7	9.5	200	-1.5
HP 49A, 933.5*	-	-	LL	-0.3	9.9	193	-0.3
HP 71, 266.3*	-	-	carbonate vein in CVC	-2.7	9.8	195	-2.6
HP 77, 258.1*	-	-	carbonate vein in CVC	-3.3	9.3	205	-3.0

* Yeats, 1989

** For abbreviations see Appendix 1

^{13}C values reported as ‰ vs the PDB standard

^{18}O values reported as ‰ vs the SMOW standard

Table 4.3

Oxygen isotope analyses, Henty Prospect

Sample No.	*Cat. No.*	*RGC No.*	**Description*	*$^{18}O‰SMOW$*	*$^{18}O‰$ fluid*	*T°C*
SILICA-FELDSPAR-SERICITE-CARBONATE ALTERATION (SC)						
NF 30-31W	103964	-	pink, massive (q + fls + ser)	10.7	0.2	200
NF 16-17E	103973	T21877	pink, massive (q + fls + ser)	10.5	0.1	"
NF 22-23W	103976	-	pink, massive (q + fls + ser + carb)	10.4	0.5	"
SILICA-FELDSPAR ALTERATION (AS)						
HP 17, 160 m	103750	T17709	pink, massive (q + fls + minor carb)	11.2	0.9	200
HP 6, 318.1 m	103744	T17760	pink, massive (fls + q + minor ser)	10.8	1.1	"
SF 32-33W	104909	-	grey, massive (fls + q)	9.8	-0.1	"
SF 33C	104908	T2015	quartz + fls + gl + carb (carb. dissolved)	10.0	- 1.1	"
MASSIVE QUARTZ ALTERATION (MQ)						
HP 42, 606.1 m	103774	T17747	grey, massive (q + carb)	12.6	-0.5	200
NF 20-21E	103923	-	grey, massive (q)	13.4	-1.3	"
NF 32-33W	103927	-	grey, massive (q + carb)	2.9	-0.8	"
NF 13E	103934	-	grey, massive	13.7	-1.66	"
NF 3-4B	103979	-	grey, massive (q + carb)	12.9	- 0.9	"
HP 96A, 583.5 m	104905	T20137	grey, massive (q + ser)	12.2	4.9	"
NF 7-8W	104911	-	grey, massive (q + carb)	12.7	0.6	"
NF 7-8W	104911	-	grey, massive (q)	12.5	0.4	"
HP 129D, 612.85 m	104906	T20140	grey, massive (q + carb)	12.1	0.1	"
NF 38C	103938	T21848	grey, massive (q + carb)	11.9	0.1	"
QUARTZ-SERICITE (MV), QUARTZ-SERICITE-PYRITE						
HP 96A, 573.45 m	104901	T20134	quartz in MV	11.8	-0.3	200
HP 129D, 622.5 m	104902	T20143	quartz in MV	11.7	-0.4	"
HP 129D, 650.5 m	104903	T20152	quartz in altered volcaniclastic rocks (q + ser + py)	11.7	-0.4	"
QUARTZ GASH, LATE QUARTZ-CARBONATE VEIN						
HP 24, 117.7 m	103755	T17716	quartz gash	12.9	5.6	300
HP 24, 117.8 m	103761	T17717	quartz gash	12.6	5.3	"
HP 51, 128.4 m	103784	T17702	quartz gash	12.7	5.4	"
NF 13E	103934	-	quartz gash	14.4	7.1	"
NF 12-13E	103935	-	quartz gash	14.3	7.0	"
SF 32.08	103937	-	quartz gash	14.1	6.8	"
HP 129D, 650.5 m	104903	T20152	quartz in late quartz-carbonate vein	12.2	4.9	"

* carb carbonate
fls feldspar
q quartz
gl galena
ser sericite
py pyrite

There is sufficient evidence to reject a mesothermal or metamorphic origin for the mineralisation, and there is no evidence to indicate significant Devonian fluid input at the Henty Prospect (see also mineralisation, oxygen and sulphur isotope sections). If the fluid from which the carbonates have been formed is assumed to be of seawater origin (i.e. $^{18}O = 0‰$), then formation temperatures of around 200°C may be calculated for most of the samples (Table 4.2). However this assumption should be considered cautiously for the carbonate veins, as the dolomite vein showed a higher formation temperature and the other veins were not studied mineralogically (i.e. unknown paragenesis), and may have been formed from a different fluid source and temperatures.

One way to examine the validity of this assumption is to calculate the carbon isotope value of fluid at the calculated temperature, using the carbon isotope values of the carbonate, temperature and the fractionation factors of Rye and Ohmoto (1979). If the values are close to 0%, then the assumption of the seawater-dominated fluid may be justified.

At the Henty Prospect the calculated carbon isotope values of fluid are slightly less than 0‰, with those from the veins being relatively lighter than the others. This may reflect either or both of contribution of magmatic CO_2 and CO_2 derived from oxidation of organic matter in sediments. The lighter carbon isotope values in the veins may indicate different formation temperatures, fluid mixing and most likely a different fluid source.

An independent thermometer, assuming a similar source of fluid and temperature for the massive quartz mineralisation and the massive carbonate (LL), may be applied using the fractionation factor between quartz and calcite (Clayton *et al.*, 1972; O'Neil *et al.*, 1969) at the Henty Prospect. Considering the average oxygen isotopic compositions of MQ and LL (12.7 and 10.1‰ respectively), a fractionation factor of about 2.6‰ gives a temperature of around 200°C, and is consistent with the temperatures obtained by assuming a seawater-dominated source for the fluid (Table 4.2). Further detailed work is required in order investigate the carbon and oxygen isotope variations throughout the deposit and the host rocks, and also to check if the different types of the carbonate veins are isotopically different. In summary, the carbon and oxygen isotope values at the Henty Prospect indicate that the carbonates are probably of Cambrian hydrothermal origin and have possibly formed from a seawater-dominated fluid at temperatures of around 200°C.

OXYGEN ISOTOPE DATA

Twenty-eight samples (drill core and underground) were analysed for oxygen isotopes. The analyses were carried out on massive quartz (MQ), quartz from quartz-sericite (MV) and quartz-sericite-sulphides (MZ) rocks, quartz veins and gashes, a quartz-carbonate-feldspar-galena vein, quartz-feldspar rocks (AS) and pink massive (quartz-feldspar sericite) separates from silica-feldspar-carbonate (SC) alteration. The results are shown in Table 4.3.

The purpose of this preliminary oxygen isotope study was to investigate the possible sources of fluids responsible for the hydrothermal alteration at the Henty Prospect. Whole-rock oxygen isotope analyses, with the exception of quartz-feldspar rocks (AS), were not carried out. This was due to the inhomogeneity of the altered rocks and that a whole-rock oxygen isotope study should be carried out systematically from the most to the least-altered rocks in the area. The RGC geologists did not consider the latter aim to be essential for this project.

The samples were analysed by X-ray diffraction (Appendix 7) because the massive, very fine-grained nature of some of the altered rocks makes distinction of quartz from feldspar and the estimation of the proportions of these minerals very difficult under the microscope.

Quartz from the massive quartz-gold-sulphides was carefully separated to avoid contamination with late-formed quartz veins and gashes. Attempts were also made to separate the recrystallised, early-formed (pre- to syn-tectonic) veinlets from the massive quartz. The proportion of the the early-formed quartz in veinlets after the separation was not more than about 1% of the analysed quartz samples. The samples may also contain minor sericite and/or carbonate (1–2%).

The quartz analysed from quartz-sericite pyrite, tension gashes and quartz carbonate veins was pure. The reproducibility of the oxygen isotope analyses was within 0.2‰.

Massive Quartz-Gold-Telluride-Sulphides

Six underground and five core samples were used for oxygen isotope analysis. The values are very consistent, ranging from 11.9 to 13.7‰ with an average of 12.6‰ and standard deviation of 0.5‰.

Quartz Gashes and Late Quartz Carbonate Veins

Three quartz samples taken from tension gashes exposed in the sill showed uniform values ranging from 14.1 to 14.4‰. It is not clear whether the analysed late quartz from drill core are actually from tension gashes or from quartz veins of possibly different origin. The oxygen isotope values of the quartz from drill core are slightly lower, ranging from 12.2 to 12.9‰.

Quartz-feldspar (AS)

The oxygen isotope values for four analysed samples taken from drill core and the sill are similar, and range from 9.8 to 11.2‰. Sample 104908 is from

a 5 cm quartz-feldspar-carbonate vein occurring adjacent, and parallel to, a massive pyrite lens at SF 33 (centre). The carbonate was dissolved in HCl and the residue gave an oxygen isotope value of 10.0‰, which is similar to those from the quartz-feldspar rock.

Quartz-Sericite (MV) and Quartz-Sericite-Sulphides (MZ)

Oxygen isotope values for three separated quartz samples from these rocks are uniform (11.7 to 11.8‰).

Quartz-Carbonate-Sericite Feldspar (SC)

Three samples from the massive pink parts of the rocks were separated for oxygen isotope analysis. The samples were initially (before XRD) assumed to be fine recrystallised quartz. However XRD analyses revealed that they contained up to 50% feldspar. The feldspar contents appear to vary from 15 to 50% but the oxygen isotope values are very similar, with a narrow range of 10.4 to 10.7‰.

Discussion

The lack of appropriate mineral assemblages and the rarity of suitable material for fluid inclusion study make the estimation of temperatures for the main mineralising events almost an impossible task. The following is an attempt to discuss the possible sources of the ore-forming solution and the likely formation temperatures for the main alteration assemblages.

If we assume that the early alteration (e.g. massive quartz) occurred at a temperature of about 200°C, then the oxygen isotope values of water in equilibrium with massive quartz is around 0‰ using the quartz-water fractionation factor of Ligang *et al.* (1989, Table 4.3). The choice of seawater oxygen isotope values (~0‰) is based on evidence which suggests that Phanerozoic seawater has been buffered at about 0‰ (e.g. Sheppard, 1986; Muehlenbachs, 1986; Ohmoto, 1986) and that the ^{18}O values of most VMS fluids is also close to 0‰ including Tasmanian VMS deposits (Green, 1986; unpublished data). The validity of a seawater origin for the silicification needs to be discussed further.

The relatively uniform oxygen isotope values are either indicative of original, pre-tectonic silicification (see Chapter 2 for detail) or of homogenisation by metamorphic fluids. The latter seems to be unlikely, as the early silicification pre-dates the deformation and the oxygen isotope values of quartz formed from metamorphic fluids, such as those in tension gashes, are heavier by about 2‰ than those in massive quartz.

Silicification by a Devonian magmatic fluid is also unlikely, considering the pre-tectonic texture of the massive quartz and the depth of the granite in this area (~8 km, Leaman and Richardson, 1989). Therefore it seems unlikely that the involvement of metamorphic or magmatic fluids was significant in the early silicification of pre-existing rocks at the Henty Prospect.

Similar oxygen isotope values are also indicated for the water in equilibrium with the quartz from quartz-sericite sulphides (MV + MZ). This may suggest quartz deposition over an extended history of deposition at constant temperature and with fluid ^{18}O buffered by a large volume of wall rocks. This is not consistent with textural observations, which indicate that at least some of the silicification is pre-tectonic. Systematic work is needed to establish the differences (if any) in the ^{18}O values of quartz showing different texture or paragenesis in these rocks.

It should be mentioned that the silicification of pre-existing rocks (i.e. MQ) is paragenetically and possibly genetically different to the formation of gold-telluride within the fractures of the rock (see Chapter 2 for detail). Therefore the above discussion is strictly related to fluid(s) responsible for the silicification rather than gold-telluride mineralisation. The possible origin of the gold-telluride mineralisation is discussed later in this text.

Samples from feldspar-quartz alteration and the pink, massive quartz-albite sericite separated from the silica-feldspar-carbonate-sericite rocks (SC) are isotopically lighter than those from the massive quartz. However if the fractionation factors (Ligang *et al.*, 1989; Matsuhisa *et al.*, 1979; O'Neil and Taylor, 1969) and the proportions of the minerals are considered, then the oxygen isotope values of water in equilibrium with these rocks at 200°C are very similar to those calculated for the massive quartz, and are around 0‰ (Table 4.3). The similarity of the calculated oxygen isotope values of water in equilibrium with these rocks is at least consistent with the proposition that fluid responsible for the silicification or albitisation was originally from the same seawater source. However there is no mineralogical or textural evidence to support a pre-tectonic alteration for quartz-feldspar rocks, and they could have resulted from a metamorphic fluid at different temperature.

The oxygen isotope values for the late (post-tectonic) quartz include:

(a) tension gashes in the sill which are isotopically the heaviest among the analysed samples, and

(b) drill core (veins or gashes) which show similar values to those from the massive quartz.

The quartz veins and gashes observed in drill core clearly post-date the silicification (see Chapter 2 for detail) and appear to have been formed from typical CO_2-rich metamorphic fluids at temperatures of around 300°C (fluid inclusion data). The oxygen isotope values of water in equilibrium with the

quartz veins or gashes range from 5 to 7‰ at 300°C, and fall well within the values of metamorphic fluids (Sheppard, 1986).

In summary, by using geological, petrological, paragenesis, geochemistry and fluid inclusion data, the preliminary oxygen isotope study at the Henty Prospect indicates that the early alteration, including the silicification and albitisation, probably resulted from the circulation of a seawater-dominated hydrothermal fluid through the rocks at moderate temperatures (~200°C). The late quartz tension gash veins appear to have been formed from CO_2-rich metamorphic fluids at temperatures of around 300°C. Further oxygen isotope analyses, including whole rocks and mineral separates, would be required for a better understanding of the sources of fluids at the Henty Prospect.

CHAPTER 5

Geochemistry

Twelve samples from MZ, MV, MQ, AS and fuchsite alteration (MVF) were analysed for major and some trace elements (Appendix 6). The objects of this preliminary study were to:–

(a) test our petrographic observations regarding the similarity of the original rocks in the main mineralised zone and the likely original rock types of the fuchsite-bearing rocks, and

(b) compare the chemical compositions of the quartz-feldspar rocks to the other hydrothermally-altered rocks at the Henty Prospect.

Petrographic examinations (Chapter 2) suggest that the different hydrothermally-altered rocks in the main mineralised zone have been derived from a common parent. If this is so, then the ratios between immobile elements such as Zr, Ti and Nb should be similar in MZ, MV, and MQ. The immobile nature of these elements has already been shown in some hydrothermally-altered rocks of the Mount Read Volcanics (e.g. Green, 1983; Large *et al.*, 1986).

At the Henty Prospect the Ti/Zr values for the MZ, MV, and MQ are very similar despite their chemical differences. This is shown in Figure 5.1, in which Ti/Zr values have been plotted against SiO_2, Al_2O_3, K_2O, Y, Rb, Mg, and Ba. In general Al_2O_3, K_2O, MgO, Ba, Fe, Rb, Y, and S decrease with increase in degree of silicification from MZ to MQ (fig. 5.1 and 5.2), reflecting the mineralogical changes dominated by the replacement of sericite by quartz and the lower contents of sulphides in MV and MQ. Ga and Ce are higher in the MZ than MV and MQ (fig. 5.3). Nb concentration is low but is similar in MZ, MV, and MQ rocks. The higher contents of Mg in MZ is due to the occurrence of minor fine grains of chlorite. Ce, Th, Mo, Sn, As, Bi, W, Ni, and Co are of low concentrations and do not exhibit any systematic variations in the altered rocks of the main mineralised zone (Appendix 6).

The concentrations of Pb, Cu and Zn may vary widely, mainly due to the erratic distribution of sulphides in all styles of mineralisation. However the concentration of Zn is relatively low, mainly because of the dissolution and removal of sphalerite from the mineralised zones by hydrothermal solutions during metamorphism, rather than being related to a high temperature of mineralisation as stated by Yeats (1989). Our petrographic observations indicate extensive remobilisation of sphalerite in the hydrothermally-altered rocks. Therefore calculation of the zinc ratio (100Zn / Zn + Pb) may not be applicable as a geothermometer at the Henty Prospect, as suggested for VMS deposits in general by Huston and Large (1989). The values, as expected, are low and scattered relative to the Cambrian VMS deposits of western Tasmania (shown in fig. 5.4). There is a general positive correlation between Pb and Cu, as galena and chalcopyrite are closely associated in most of the mineralised rocks (fig. 5.5).

A systematic whole-rock analysis from the most-altered to the least-altered rocks is required to study the chemical variations in the different hydrothermally-altered rocks. However based on our petrographic observations on the moderately-altered rocks (MA) and the geochemical data, it is indicated that the MZ and MV are characterised by the enrichment in K, Cu, Pb, Zn, and by depletion in Na and possibly Sr. MZ alteration is also marked by Fe and S enrichment.

Similar chemical changes have also been observed in altered rocks of the VMS deposits of western Tasmania (e.g. Green, 1990; Jack, 1989). The only analysis from fuchsite-bearing rocks (MVF) clearly indicates a different source rock characterised by relatively high Mg, MnO, CaO and low silica (fig. 5.6).

The compositions of two quartz-feldspar rocks (AS) are characterised by higher Na and Sr and lower Zr, Ti and Fe than those in the main mineralised zone (fig. 5.1, 5.2, 5.6a, b, c, and 5.7). The relatively low concentration of Ti and Zr in the AS alteration may simply indicate that these rocks were originally low in these elements, or that the elements have been depleted passively by silica addition (quartz precipitation in vesicles etc.) rather than by replacement which dominates the chemistry of the MQ alteration facies. This is indicated by the low concentration of elements such as Al in the MQ. The lower Ti/Zr ratios of the AS may indicate a primary compositional difference between this rock type and the epiclastic rocks of the mineralised zone, consistent with our petrographic descriptions, and might indicate that the lavas in the AS are more strongly differentiated (fig. 5.1).

The high contents of Na and Al in the AS alteration indicate that the depletion in trace elements cannot be the result of silica addition alone. Either the extensive alteration was due to extensive silicification and albitisation (or formation of precursor zeolites) involving replacement of K by Na, or it is the result of alkali exchange with relatively weak silicification. In the former case, the depleted concentration of trace elements could be due to simple dilution related to the addition of Si, Na and Al. In the latter case the low trace element

concentrations reflect a very different primary composition of the rock, as also suggested by the higher Zr/TiO_2 ratio of these rocks compared with those from the main mineralised zone (fig. 5.8).

On a Ti-Zr plot, unaltered rocks from the Tyndall Group (from Corbett and Solomon, 1989) show a scattered trend, with most samples displaying a weak decrease in Zr content with increase in Ti. Samples from the MQ, MV and MZ alteration styles show positive correlation between Ti and Zr, cutting the trend for the unaltered rocks and a high angle and projecting towards the origin (fig. 5.7). This positive correlation is typical of the effects of hydrothermal alteration of a fairly homogeneous parent rock (Finlow, Bates and Stumpfl, 1981).

The inference is that Ti and Zr behave as immobile elements during alteration and their concentrations reflect gross addition or depletion of other elements from the parent rocks. Samples plotting above the igneous fractionation trend have had a net depletion of other components; those plotting below it have had a net addition of material.

Two of the three samples of MZ and one sample of MQ plot above the primary trend, indicating a net removal of material. Samples from the MV alteration zone and one sample from the MQ show net addition of material, largely silica, but it is clear from the graphs that the spectacular concentration of SiO_2 in the MQ alteration were the result of replacement of other oxides by silica and not simply due to addition of silica.

Tyndall Group lavas have Ti contents as low as 1100 ppm and Zr down to 165 ppm (Corbett, *in* Corbett and Solomon, 1989). Low TiO_2 contents have also been recorded from some intrusive quartz porphyries in the Hellyer area (Corbett and Komyshan, 1985). Using the Zr/Ti vs Nb/Y plot of Winchester and Floyd (1977), the rocks from the main mineralised zone and AS fall in the rhyodacite-dacite field whereas those from fuchsite-bearing rock are indicative of an andesitic rock (fig. 5.8). The results are consistent with the petrographic observations, however further work is required for statistically more reliable conclusions. If the unusual composition of the AS lava is validated, this could provide a useful tool for stratigraphic correlation purposes.

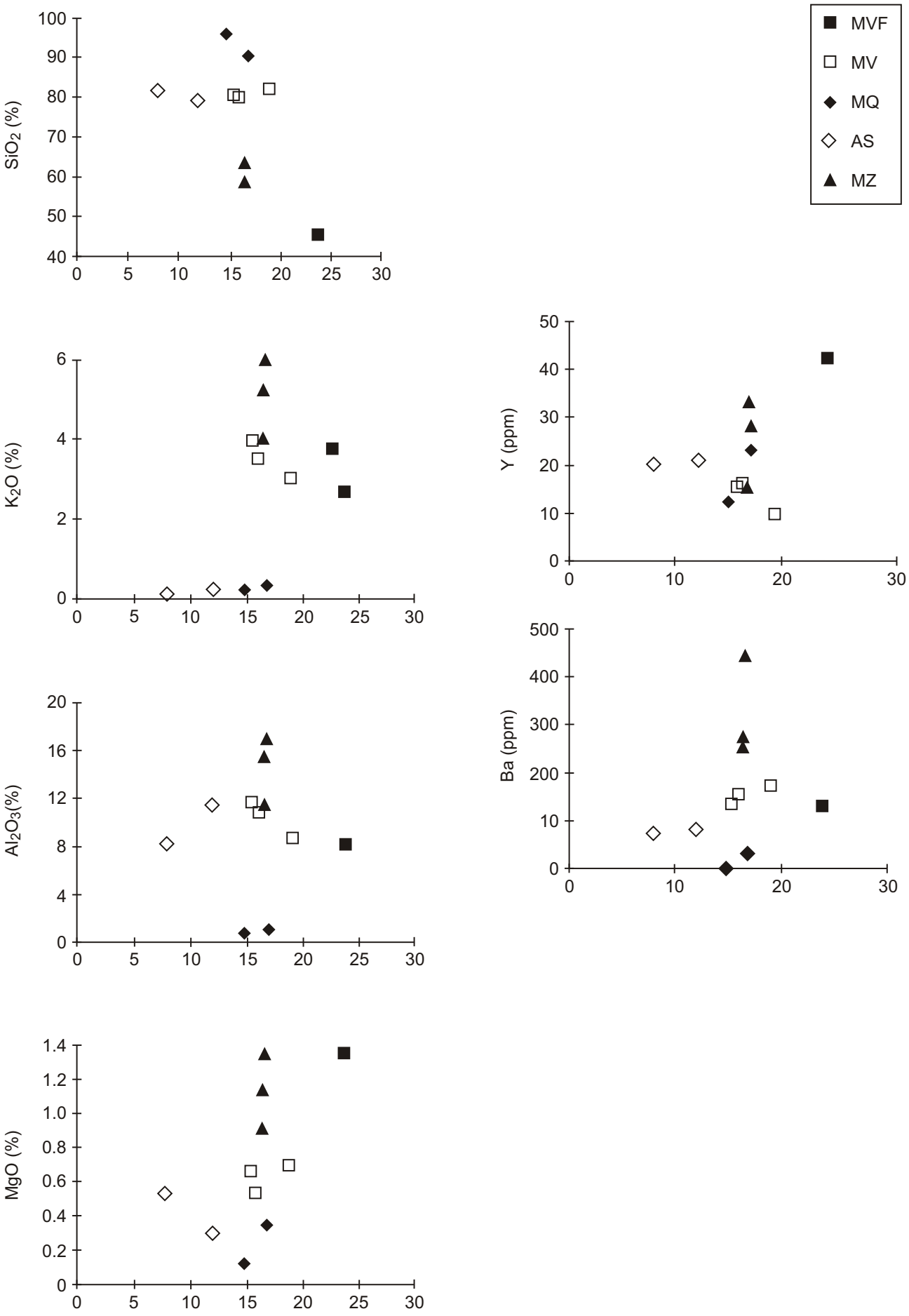

Figure 5.1

Variation of SiO_2, K_2O, Al_2O_3, MgO, Y and Ba with Ti / Z

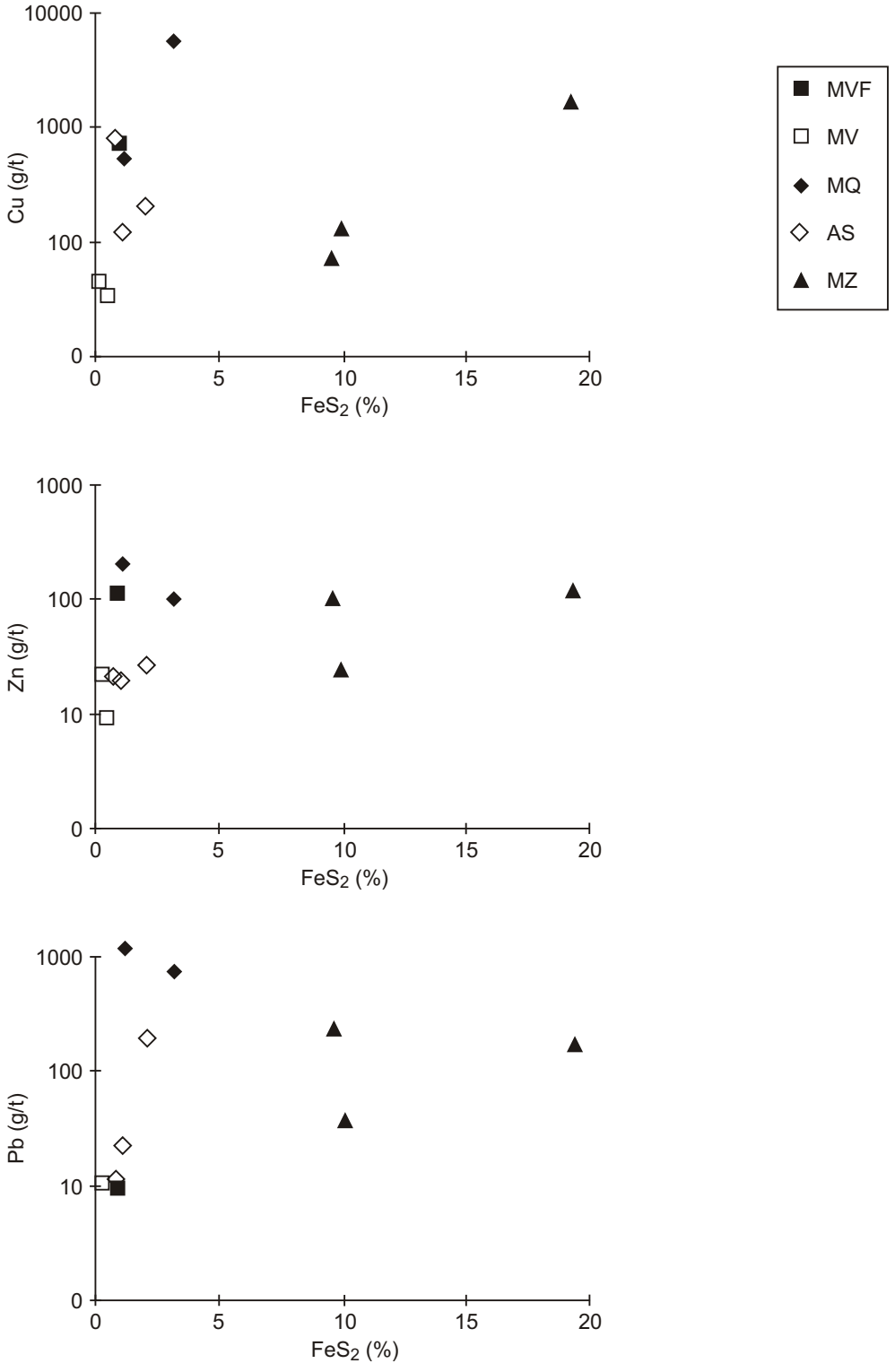

Figure 5.2

Variation of Cu (a), Zn (b) and Pb (c) with FeS_2

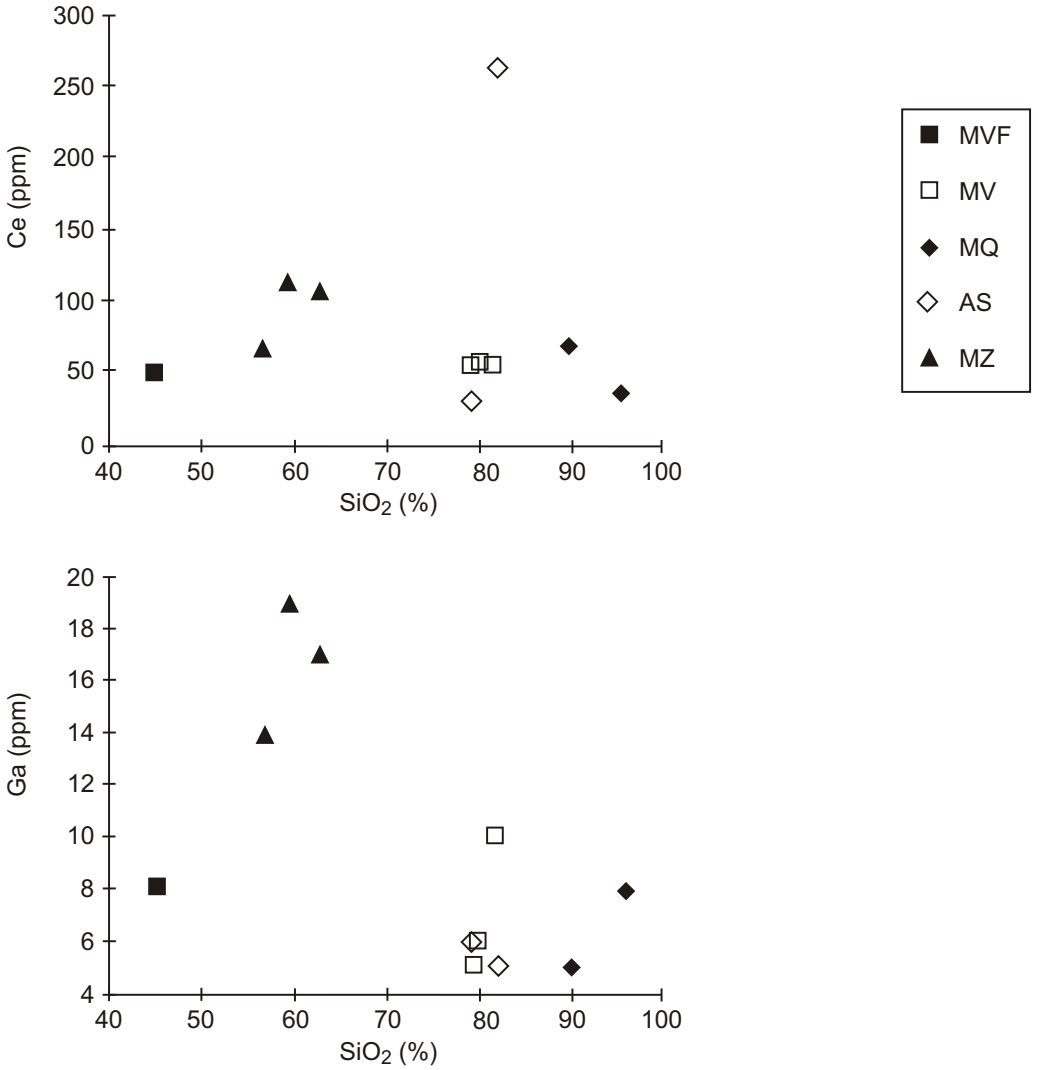

Figure 5.3

Variation of Ce and Ga with SiO_2

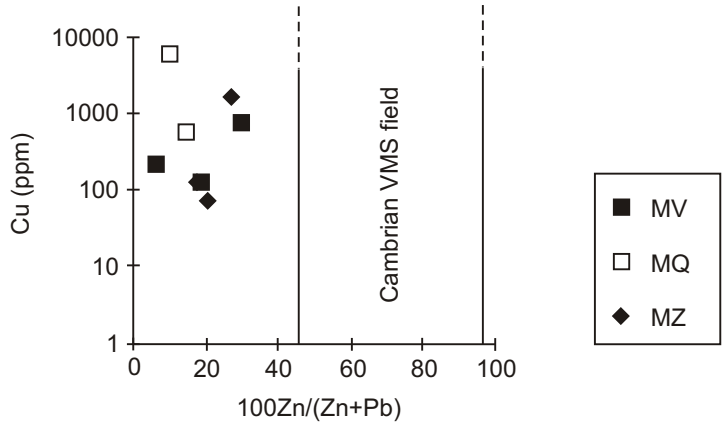

Figure 5.4

Zinc ratios vs Cu plot. Note the high zinc ratios for Cambrian VMS deposits from western Tasmania (after Huston and Large, 1990)

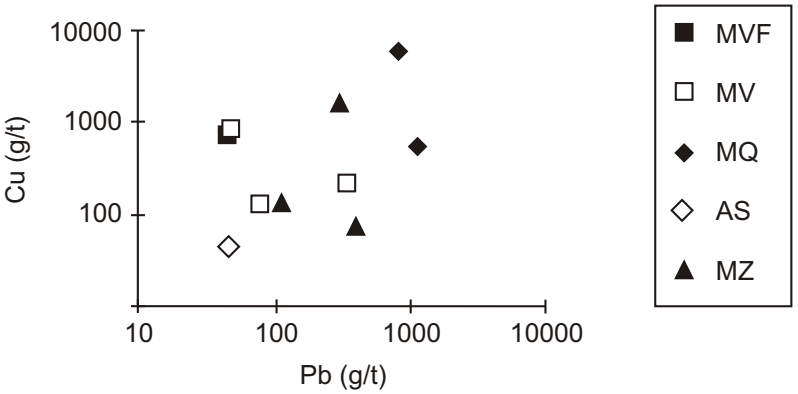

Figure 5.5

Pb vs Cu plot

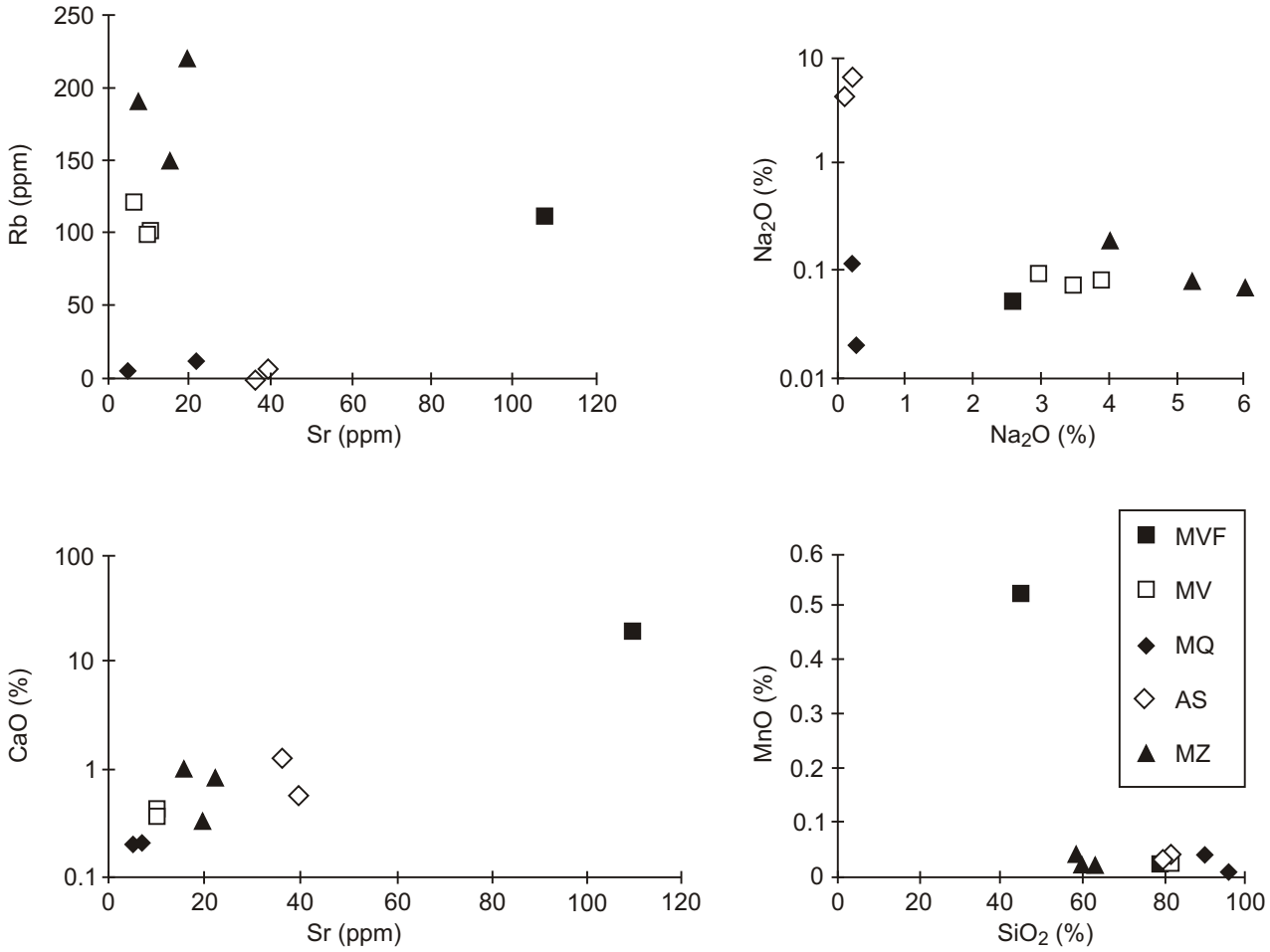

Figure 5.6

Graphs of Sr vs Rb, CaO vs Sr, Na_2O vs K_2O, and Mn vs SiO_2

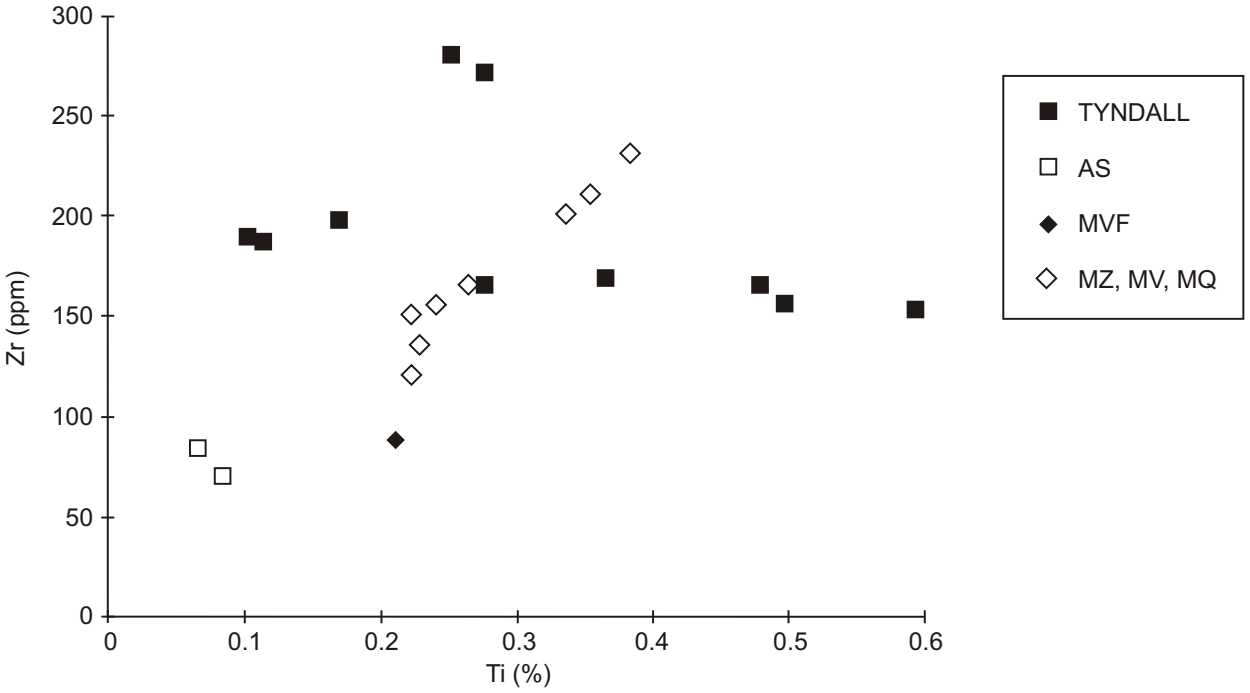

Figure 5.7

Graph of Zr vs Ti showing the Zr and Ti concentrations for some of the Tyndall Group rocks

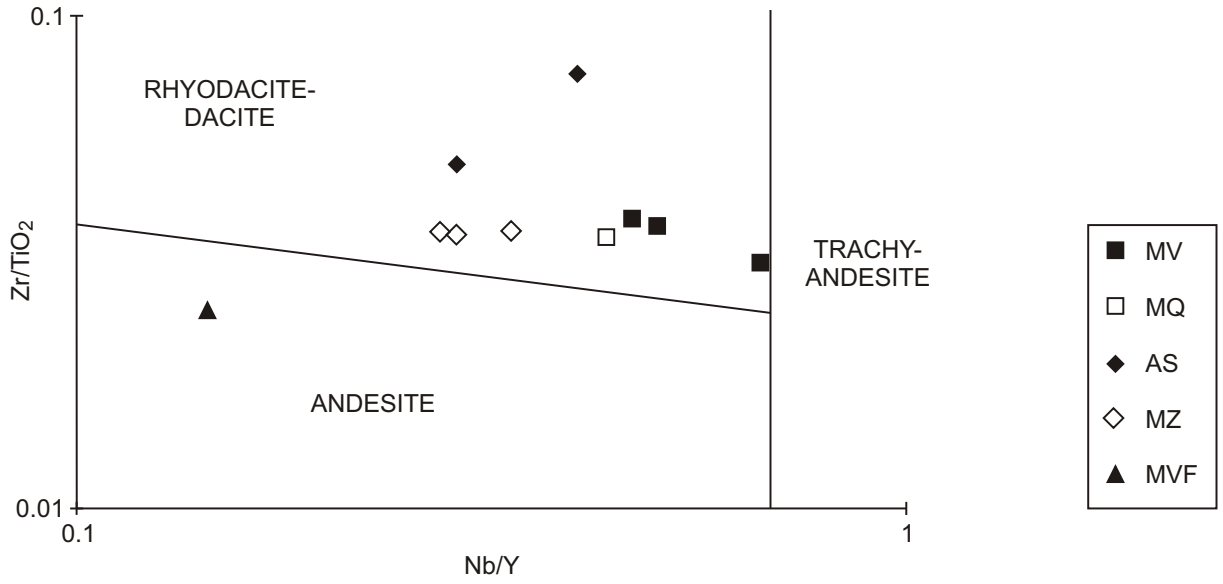

Figure 5.8

Plot of Zr / TiO2 vs Nb / Y for analysed rocks. Fields after Winchester and Floyd (1977)

CHAPTER 6

Ore Genesis

Salient features from our study which favour a Cambrian age for the mineralisation are:

1. The mineralisation is stratigraphically controlled, occurring in altered epiclastic rocks overlain by felsic lavas which are not significantly mineralised.
2. The mineralised zone shows some asymmetry, with massive pyrite lenses occurring near or at the top of the zone. Pyrite clasts however occur locally near the base of the alteration zone in DDH HP140, suggesting that there may have been a number of episodes of pyrite formation.
3. Pyrite in the MP displays framboidal, colloform and growth-zoned textures on a very fine scale. Such textures are typical of primitive to early diagenetic ores formed at or near the sea floor (e.g. Kuroko; Eldridge *et al.*, 1983: Hellyer; McArthur, 1986). Superimposed on these are extensive cementation textures related to brittle deformation, pyrite dissolution and reprecipitation during the Devonian.
4. The lateral transition from pyrite to carbonate-chlorite facies at the mineralised horizon is similar to that at Rosebery and Hercules. The fact that this transition occurs down dip below the 96 zone is difficult to reconcile with any mesothermal model.
5. Silicification of the MV and MQ alteration zones predates deformation, or even significant diagenetic compaction of the altered rocks as indicated by randomly orientated micas in the silicified zones.

Yeats (1989) inferred a high temperature origin for the deposit on the assumption that the Zn ratio (100Zn / (Zn + Pb)) could be applied. However our petrographic work shows that the method is inapplicable at Henty because of extensive evidence of sphalerite dissolution during deformation.

Stable and radiogenic isotope data have provided the following evidence for Cambrian age:–

1. The range of sulphur isotope values of 4 to 15‰ for the deposit is similar to that of Tasmanian VMS deposits, with the full range being displayed by the early pyrite types in the MP (framboidal, colloform and zoned). The data do not indicate any evidence for an additional input of sulphur during the Devonian.
2. Similarly, the Pb isotope evidence provided by CSIRO (Carr and Dean, 1990) is also consistent with lead introduction in the Cambrian with no additional Devonian input.
3. Carbon and oxygen isotope values of carbonates are similar to those of Cambrian hydrothermal carbonates. ^{13}C values are distinctly higher than those of Devonian carbonates and ^{18}O values are lower.
4. The ^{18}O values of both carbonates and quartz in the MQ are consistent with formation from a seawater-derived fluid (^{18}O = 0‰) at a temperature of about 200°C the 18O values of quartz in the MV, MZ and MQ (~12‰) are about 2‰ lighter than late gash veins and are consistent with different origins for the two types of quartz.
5. Sericitisation and pyrite formation appear to have preceded silicification. The geochemical characteristics of the MZ alteration are similar to those of footwall zones to VMS deposits in Tasmania:

   extreme depletion in Na, Sr

   enrichment in Rb, FeS_2, K

   variable Ca (related to carbonate content)

Features consistent with a Devonian mesothermal origin include:

1. Much of the gold in the MQ is associated with chalcopyrite, galena and tellurides in late fractures.
2. Gold was mobile during cleavage formation, as indicated by its occurrence in S_2 cleavages in fluorite-rich MV and with chalcopyrite-diseased sphalerite formed along cleavage fractures.
3. Fluids associated with the late quartz-gash gold-mobilisation event are typically mesothermal:

   T ~320°C (confirmed by limited chlorite geothermometry)

   P ~1 kilobar

   moderately saline (8.5 wt% NaCl equivalent)

   CO_2-rich — ~12 mole %

In general, the above suggests that **both** Cambrian volcanogenic and Devonian mesothermal processes may have contributed to the formation of the deposit, and the latter particularly to the 'nugget' effect in the deposit.

GENETIC MODELS

In considering the genesis of the deposit two models have been considered.

The first model assumed initial formation of exhalative massive pyrite and associated footwall quartz-pyrite-sericite (or precursor illite) alteration. Following further sedimentation and minor alteration, eruption of a massive lava provided a seal to the hydrothermal system. Subsequent fluids were forced to spread laterally beneath the cap and particularly permeable horizons were silicified selectively. During this second phase of alteration it was assumed that Na released from the main mineralised zone was responsible for the albitic alteration (AS) in the cap rock. Critical to this interpretation was the recognition of primary coherent quartz-feldspar phyric lavas with a similar grain size and proportion of phenocrysts at the same horizon as the AS alteration, which lacks recognisable primary groundmass textures.

Objections to this model include the possible lack of continuity of a capping lava, the difficulty of recognising why any particular horizon should be more permeable given the general uniformity of the mineralised rocks, and the means of explaining how quartz-albite-dolomite alteration should be proceeding at the same time, and in close proximity to, quartz-sericite-pyrite-calcite alteration.

The second, and favoured model (fig. 6.1) involves concurrent silicification and massive pyrite formation, followed by later sedimentation and weaker mineralisation and alteration events. A key component of this model is the kinetics of silica precipitation of a cooling solution.

Hydrothermal fluids in felsic rocks will maintain saturation with quartz until rapid cooling at or near the seafloor. The precipitation of silica is favoured by supersaturation induced by undercooling but is inhibited by declining rate constants for the precipitation reaction with decrease in temperature. These competing effects result in a maximum precipitation rate when the solution is cooled to between 25 and 50°C below the saturation temperature. With further cooling silica may remain metastably in solution (Rimstidt and Barnes, 1980).

This phenomenon is probably responsible for the transition from quartz-sericite-pyrite alteration, the "quartz schist", to quartz-poor chlorite or sericite rocks rich in disseminated pyrite immediately below massive pyrite in some volcanogenic massive sulphide deposits, for example, Rosebery (see Brathwaite, 1974, for description).

The nature of the footwall alteration zone to VMS deposits is strongly influenced by the mechanical behaviour of the rocks. Deposits in sequences dominated by massive volcanic rocks tend to have well-developed underlying stockwork ores (for example most Kuroko and Canadian Archaean deposits), whereas deposits overlying mixed volcanic sedimentary sequences or permeable pumiceous volcanics display more diffuse sheet-like alteration zones (Rosebery, most deposits in the Bathurst district, New Brunswick; Jambor, 1979; Green, 1983).

The petrographic evidence that silicification at the Henty deposit predated significant diagenetic compaction suggests that the sediments were probably water saturated and highly permeable during mineralisation. Such a situation would facilitate both rapid cooling of the hydrothermal fluid prior to discharge and horizontal, lateral flow of the solution. Thus the concordant MQ and MV alteration zones probably mark near isothermal surfaces in the footwall to a low temperature exhalative massive sulphide system. This mechanism explains the occurrence of the MQ alteration at a fairly consistent distance stratigraphically beneath the massive pyrite horizon.

Subsequent sedimentation was followed by a weaker alteration event resulting in formation of the upper "B" alteration zone, followed by the eruption of lavas, more sedimentation and formation of the quartz-albite (AS) alteration. The locus of hydrothermal venting appears to have remained broadly in the same place through time, as indicated by similar distributions of the MQ and AS alteration styles shown on the longitudinal projection (fig. 6.2). This is analogous to the situation in a number of volcanogenic deposits in which alteration exists in the rocks immediately overlying exhalative massive sulphide ore (e.g. Hellyer; McArthur 1986). The longitudinal projection also shows that both the MQ and AS alteration styles are absent in the gap between the 96 zone and the sill area. This may indicate that more than one vent area was responsible for the formation of the deposit, a situation similar to the northern and southern ore bodies at Rosebery.

Compaction of the sericitised volcanics and some fracturing of the MQ silicified rocks may have occurred prior to Devonian deformation. Locally the Tabberabberan deformation occurred in two main stages: initial folding and cleavage development and late dip-slip shearing. This latter event involved considerable remobilisation of material within the deposit and possibly the introduction of fluorite. In particular, gold was remobilised and some zinc may have been lost from the system. The MQ and AS alteration zones acted as competent blocks and were extensively fractured, with shearing being focussed in the surrounding sericitic rocks. Quartz, sulphides

tellurides and gold have precipitated in fractures in the MQ alteration, but the lack of significant mineralisation in the massive quartz-albite (AS) rocks implies this remobilisation event was probably only of local significance and did not involve the large-scale introduction of gold from depth. Although some zones of the orebody carry spectacular grades of gold (e.g. the MQ in the 96 zone with 160 000 tonnes of 91.2 g/t Au) the overall grades of known mineralisation are not inconsistent with those in other volcanogenic deposits. If the main alteration zone (MQ, MV and MZ) is considered as a whole there are some 5 million tonnes of material with an average grade of 3.8 g/t Au in the deposit (Carrasco *et al.*, 1991). Gold grades as high as those at Henty (15 to 100 g/t) occur in the core of the undeformed footwall siliceous pyrite-chalcopyrite ore of Nurukawa Kuroko deposit west of Lake Towada, Honshu (Yamada *et al.*, 1987).

Late stage low temperature quartz-carbonate veinlets at Henty contain relatively silver-rich electrum with traces of mercury. This, and the preceding discussion, suggests that mercury and zinc haloes might exist up dip of Henty-style deposits.

Figure 6.1

A. Formation of A mineralised zone involving deposition of massive pyrite with concomitant silicification in the footwall.

B. Continued deposition of epiclastic sediments precedes a hydrothermal event resulting in the formation of the upper B alteration zone. After more sedimentation and lava intrusion the quartz-albite (AS) alteration assemblage is formed.

C. Compaction with probably some fracturing to produce early barren veins.

D. Devonian deformation involving flattening during folding, subsequent thrusting, and hydrothermal remobilisation of gold into microfractures. Some fault repetition of lenses may have occurred at this stage.

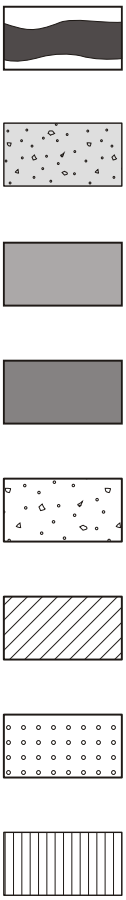

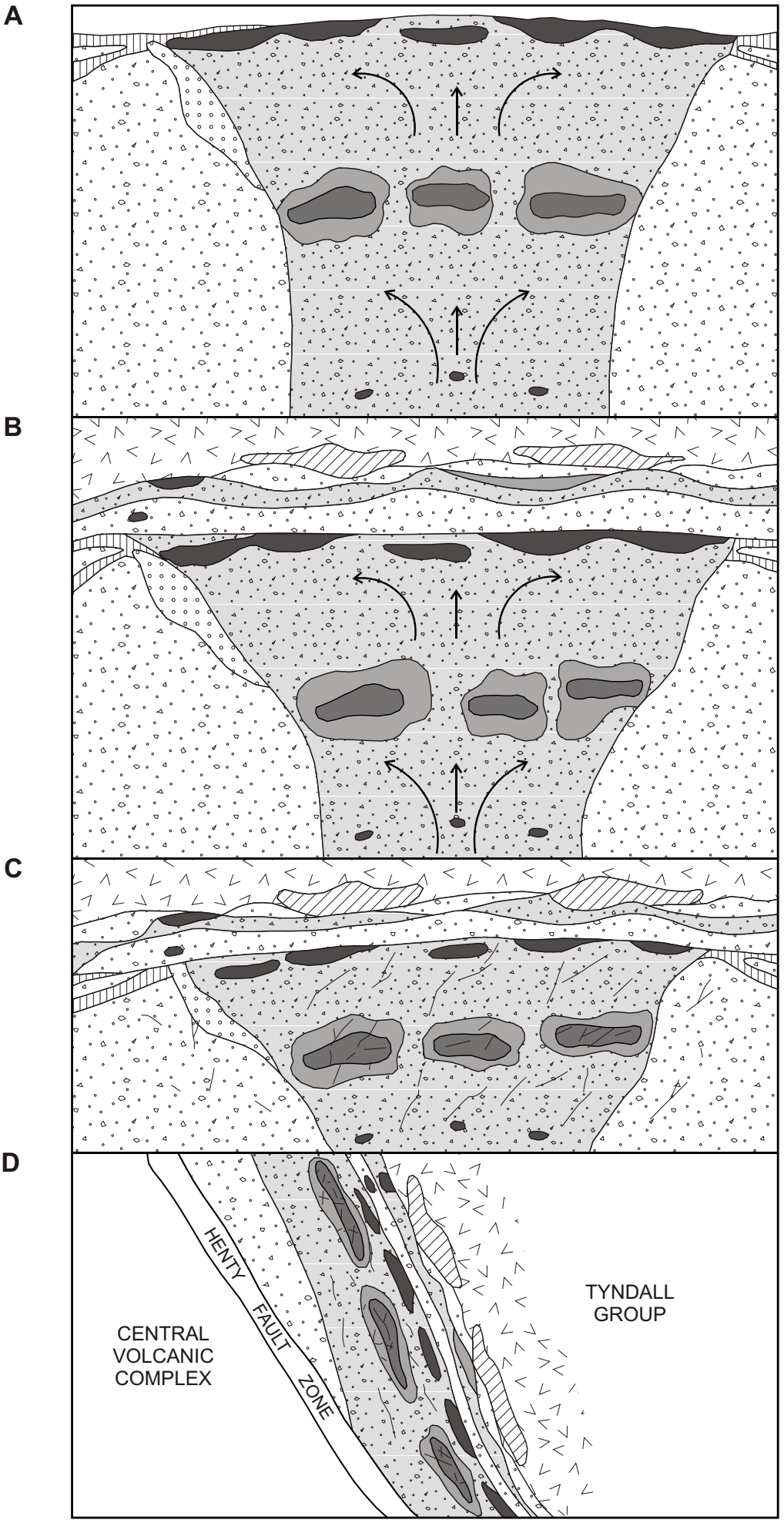
A
B
C
D
HENTY FAULT ZONE
CENTRAL VOLCANIC COMPLEX
TYNDALL GROUP

Figure 6.1

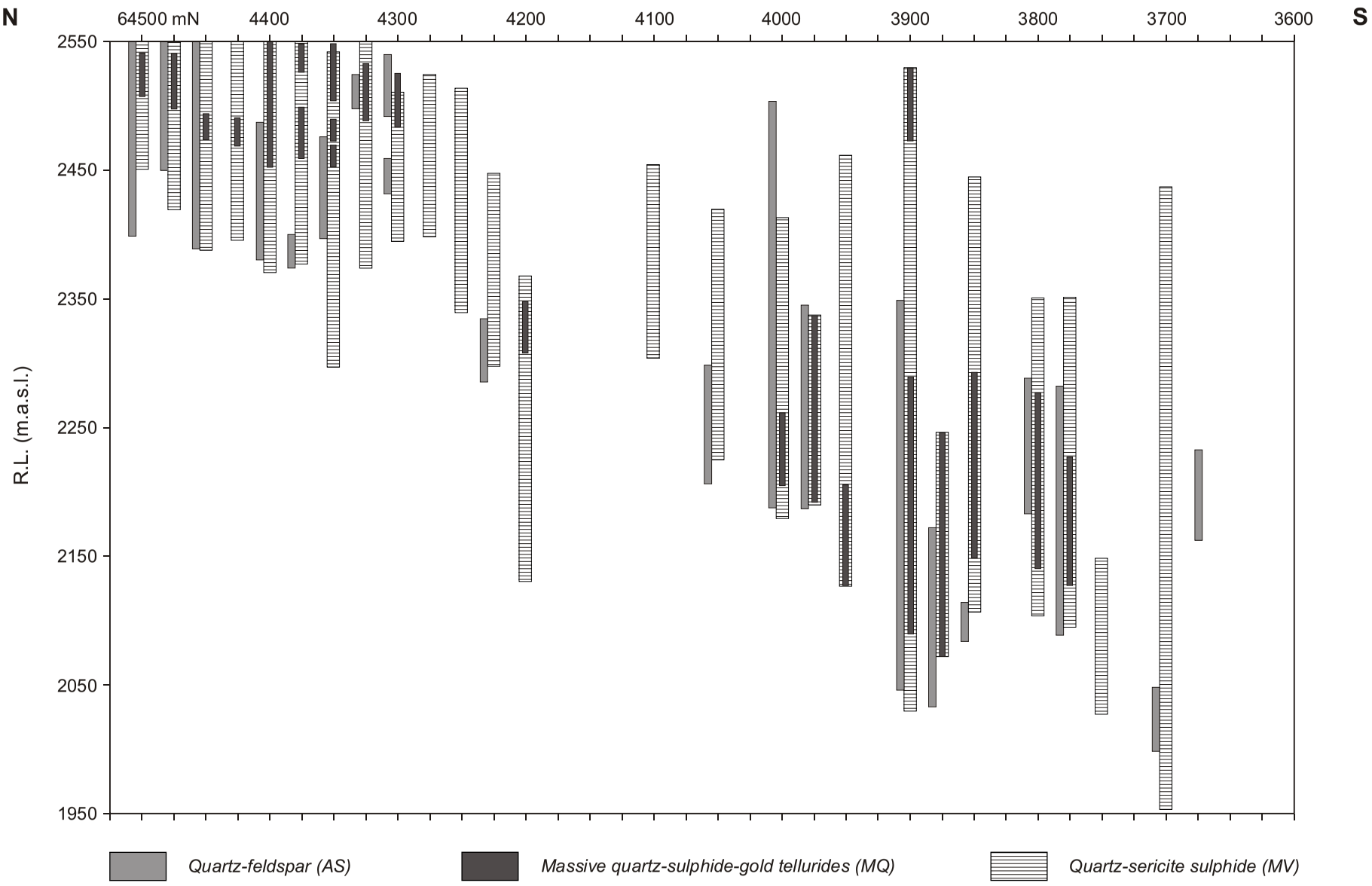

Figure 6.2
Longitudinal projection showing the relationship between the MQ mineralisation and the AS rocks, and the occurrence of a barren zone between the two mineralised zones

REFERENCES

ARNOLD, G. O. 1988. *The Henty Prospect. Geological appraisal.* RGC Exploration Pty Ltd. Report Cr 88/2/3. [TCR 88-2830].

ARNOLD, G. O. 1989. *Faulting in the Henty sill*. RGC Exploration Pty Ltd. (Memorandum 23/11/1989).

ATKINSON, B. K. 1975. Experimental deformation of polycrystalline pyrite : Effects of temperature, confining pressure, strain, rate, and porosity. *Economic Geology* 70:473.

BERRY, R. F. 1989. The history of movement on the Henty Fault Zone, western Tasmania. An analysis of fault striations. *Australian Journal of Science* 36:189–205.

BERRY, R. F. 1990. *Henty Prospect. A report to RGC Exploration Pty Ltd. Tasmania*. (unpublished).

BERRY, R. F.; CRAWFORD, A. J. 1988. The tectonic significance of Cambrian allocthonous mafic-ultramafic complexes in Tasmania. *Australian Journal of Earth Sciences* 36:189–205.

BOWERS, T. S.; HELGESON, H. C. 1983. Calculation of the thermodynamic and geochemical consequences of nonideal mixing in the system H_2O-CO_2-NaCl on phase relations in geologic systems : Equation of state for H_2O-CO_2-NaCL fluids at high pressures and temperatures. *Geochimica et Cosmochimica Acta*. 47:1247–1275.

BRALIA, A.; SABATINI, G.; TROJA, F. 1979. A revaluation of the Co/Ni ratio in pyrite as geochemical tool in ore genesis problems. *Mineraliun Deposita* 14:353–374.

BRATHWAITE, R. L. 1974. The geology and origin of the Rosebery ore deposit. *Economic Geology* 69:1086–1101.

BROOKS, C. 1962. *Geology of the Tullah area*. B.Sc. (Hons) thesis, University of Tasmania : Hobart.

BURRUSS, R. C. 1981. Hydrocarbon fluid inclusion in studies of sedimentary diagenesis. *Mineralogical Association of Canada Short Course Handbook* 6:148–156.

CARR, G. R.; DEAN, J. A. 1990. Report to RGC on the Pb isotope compositions of samples from the Henty Area, western Tasmania. *Report Division of Exploration Geoscience CSIRO Australia* SR 131.

CARRASCO, P.; FLEMING, M. J.; ROBERTS, R. H. 1990. *An estimate of the geological resources for the Henty Gold Project. West Coast, Tasmania.* RGC Exploration Pty Ltd. Report T/90/60 [TCR 91-3263].

CATHELINEAU, M.; NIEVA, D. 1985. A chlorite solid solution geothermometer; the Los Azufres (Mexico) geothermal system. *Contributions to Mineralogy and Petrology* 91:235–244.

CLARK, B. R.; PRICE, R. F.; KELLY, W. C. 1977. Effect of annealing on deformation textures in galena. *Contributions to Mineralogy and Petrology* 64:149–165.

CLARK, L. A. 1960. The Fe-As-S system phase relationships and applications. *Economic Geology* 55:1345–1381, 1631–1652.

CLAYPOOL, G. E.; HASKER, W. T.; KAPLAN, I. R.; SAKAI, H.; ZAK, I. 1980. The age curves of sulphur and oxygen isotopes in marine sulphate and their mutual interpretation. *Chemical Geology* 28:199–260.

CLAYTON, R. N.; O'NEIL, J. R.; MAYEDA, T. K. 1972. oxygen isotope exchange between quartz and water. *Journal Geophysical Research* 77:3057–3067.

COLLINS, P. L. F. 1979. Gas hydrates in CO_2-bearing fluid inclusions and the use of freezing data estimation of salinity. *Economic Geology* 74:1435–1444.

COLLINS, P. L. F. 1981. The geology and genesis of the Cleveland Tin deposit, western Tasmania : Fluid inclusion and stable isotope studies. *Economic Geology* 76:365–392.

COMPSTON, W.; WILLIAMS, I. S.; MEYER, C. 1984. U-Pb geochronology of zircons from Lunar breccia 73217 using a sensitive high mass-resolution ion microprobe, *in:* BOYNTON, W. V.; *et al.* (ed.). Proceedings of the fourteenth lunar and planetary science conference, Part 2. *Journal of Geophysical Research* 89 (suppl.):B525–B534..

CORBETT, K. D. 1975. Preliminary report on the geology of the Red Hills–Newtown Creek area West Coast Range, Tasmania. *Technical Reports Department of Mines Tasmania* 19:11–25.

CORBETT, K. D. 1981. Stratigraphy and mineralisation in the Mt Read Volcanics, western Tasmania. *Economic Geology* 76:209–230.

CORBETT, K. D.; KOMYSHAN, P. 1989. Geology of the Hellyer–Mt Charter area. *Geological Report Mt Read Volcanics Project Tasmania* 1.

CORBETT, K. D.; LEES, T. C. 1987. Stratigraphic and structural relationships and evidence for Cambrian deformation at the western margin of the Mt Read Volcanics, Tasmania. *Australian Journal of Earth Sciences* 34:45–67.

CORBETT, K. D.; MCNEILL, A. W. 1986. *Mt Read Volcanics Project 1:25 000 Series. Map 2. Geology of the Rosebery-Mt Black area*. Division of Mines and Mineral Resources, Tasmania.

CORBETT, K. D.; SOLOMON, M. 1989. Cambrian Mt Read Volcanics and associated mineral deposits, *in:* BURRETT, C. F.; MARTIN, E. L. (ed.). Geology and mineral resources of Tasmania. *Special Publication Geological Society of Australia* 15:84–153.

COWAN, D. 1985. *Petrographic/mineragraphic descriptions*. RGC Report CMS 85/3/18.

DURNEY, D. W. 1972. Solution-Transfer, an important geological deformation mechanism. *Nature* 235:315–317.

EDWARDS, A. B.; CARLOS, G. C. 1954. The selenium content of some Australian sulphide deposits. *Proceedings Australasian Institute of Mining and Metallurgy* 172:31–63.

ELDRIGE, C. S.; BARTON, P. B. Jr; OHMOTO, H. 1983. Mineral textures and their bearing on formation of the Kuroko ore bodies. *Economic Geology Monograph* 5:241–281.

ELDRIDGE, C. S.; COMPSTON, W.; WILLIAMS, I. S., WALSHE, J. L. 1987. In situ micro analysis for $^{34}S/^{32}S$ ratios using the 10 microprobe SHRIMP. *International Journal of Mass Spectrometry and Ion Processes* 76:65–83.

FINLOW-BATES, T.; STUMPFL, E. F. 1981. The behaviour of so-called immobile elements in hydrothermally altered rocks associated with volcanogenic submarine-exhalative ore deposits. *Mineralium Deposita* 16:319–328.

FLEET, M. E.; MACLEAN, P. J.; BARBIER, J. 1988. Oscillatory-zoned As-bearing pyrite from stratabound gold deposits. Evidence for primary mineralisation. *Abstracts Geological Society of Australia* 22.

FLEISHER, M. 1955. Minor elements in some sulphide minerals. *Economic Geology 50th Anniversary Volume* 970–1024.

GORBY, H. C. 1858. On the microscopic structure of crystals, indicating the origin of minerals and rocks. *Quarterly Journal Geological Society of London.* 14(1):453–500.

GRAF, J. L.; SKINNER, B. J. 1970. Strength and deformation of pyrite and pyrrhotite. *Economic Geology* 65:206–215.

GREEN, G. R. 1983. *The geological setting and formation of the Rosebery volcanic-hosted massive sulphide ore body, Tasmania.* Ph.D. thesis, University of Tasmania : Hobart.

GREEN, G. R. 1990. Palaeozoic geology and mineral deposits of Tasmania, *in:* HUGHES, F. E. (ed.). Geology of the mineral deposits of Australia and Papua New Guinea. *Monograph Serial Australasian Institute of Mining and Metallurgy* 14:1207–1223.

GREEN, G. R.; BAMFORD, A. L. 1986. *Mt Read Volcanics Project. 1:50 000 Metallic Mineral Deposits map series. Sheet 8014-IV. Tullah.* Division of Mines and Mineral Resources, Tasmania.

GREEN, G. R.; SOLOMON, M.; WALSHE, J. L. 1981. The formation of a volcanic-hosted massive sulphide ore deposit at Rosebery, Tasmania. *Economic Geology* 76:304–338.

HALL, G.; COTTLE, V. M.; ROSENHAIN, P. B.; MCGHIE, R. R. 1953. The lead zinc deposits of Read–Rosebery and Mount Farrell. *Publications 5th Empire Mining and Metallurgy Congress* 1:1145–1159.

HALL, G.; SOLOMON, M. 1962. Metallic mineral deposits, *in:* SPRY, A.; BANKS, M. R. (ed.). The geology of Tasmania. *Journal Geological Society of Australia* 9(2):285–309.

HIDDEN, W. E. 1882. A phenomenal find of fluid-bearing quartz crystals. New York. *Transactions Academy of Science* 1881–1882 (1):131–136.

HOLLISTER, L. S.; BURRUSS, R. C. 1976. Phase equilibria in fluid inclusions from the Khtada Lake metamorphic complex. *Geochimica et Cosmochimica Acta* 40:163–175.

HUSTON, D. L.; LARGE, R. R. 1987. Genetic and exploration significance of the zinc ratio (100 Zn/Zn + Pb) in massive sulphide systems. *Economic Geology* 82:1521–1539.

JACK, D. J. 1989. *Hellyer host rock alteration.* M.Sc. thesis, University of Tasmania : Hobart.

JAMBOR, J. L. 1979. Mineralogical evaluation of proximal-distal features in New Brunswick massive-sulfide deposits. *Canadian Mineralogist* 17:649–664.

JENSEN, M. L. 1967. Sulfur isotopes and mineral genesis, *in:* BARNES, H. L. (ed.). *Geochemistry of hydrothermal ore deposits.* 143–165. Halt, Rinehart, and Winston : NY and London.

KELLY, W. C.; CLARK, B. R. 1975. Sulphide deformation studies : III. Experimental deformation of chalcopyrite to 2000 bars and 500°C. *Economic Geology* 70:431–453.

KHIN ZAW; LARGE, R. R. 1990. ^{18}O and ^{13}C isotopic variation of hydrothermal carbonates from the Rosebery, Hercules and South Hercules deposits, Western Tasmania : Interplay of Cambrian vs. Devonian systems. *Abstracts Seventh International Conference on geochronology, cosmochronology and isotope geology.* Geological Society of Australia.

LARGE, R. R.; CRAWFORD, A. J.; ADRICHEM, S. 1986. *Primary and alteration chemistry of the Mt Read Volcanics.* AMIRA Project 84/P210 Report November, 1986. 38–45 (unpublished).

LEAMAN, D. E.; RICHARDSON, R. G. 1989. The granites of west and north-west Tasmania — a geophysical interpretation. *Bulletin Geological Survey Tasmania* 66.

LIGANY, Z.; JINGXIU, L.; HUANBO, Z.; ZENSBERG, C. 1989. Oxygen isotope fractionation in the quartz-water-salt system. *Economic Geology* 84:1643–1650.

LOFTUS-HILLS, G.; SOLOMON, M. 1967. Cobalt, nickel and selenium in sulphides as indicators of ore genesis. *Mineralium Deposita* 2:228–242.

MATSUHISA, Y.; GOLDSMITH, R.; CLAYTON, R. N. 1979. Oxygen isotope fractionation in the system quartz-albite-anorthite-water. *Geochimica et Cosmochimica Acta* 43:1131–1140.

MCARTHUR, G. 1986. The Hellyer massive sulphide deposit, *in:* LARGE, R. R. (ed.). *The Mt Read Volcanics and associated ore deposit*s. Geological Society of Australia, Tasmanian Division.

MCCLAY, K. R.; ELLIS, P. G. 1984. Deformation of pyrite. *Economic Geology* 79:400–403.

MCKIBBEN, J. P. 1972. *Annual report, Mt Tyndall EL 9/66.* The Consolidated Syndicate [TCR 72-882].

MERCER, W. 1976. Minor elements in metal deposits in sedimentary rocks. A400-403. Review of the recent literature, *in:* WOLF, K. H. (ed.). *Handbook of stratabound and stratiform ore deposits, Volume 2 : geochemical studies.* 1-27. Elsevier : Amsterdam.

MUEHLENBACHS, K. 1986. Alteration of the oceanic crust and the ^{18}O history of seawater *in:* VALLEY, J. W.; TAYLOR, H. P.; O'NEIL, J. R. (ed.). Stable isotopes in high temperature geological processes. *Reviews in Mineralogy* 16:425–444.

O'NEIL, J. R.; CLAYTON, R. N.; MAYEDA, T. K. 1969. Oxygen isotope fractionation in divalent metal carbonates. *Journal Chemistry and Physics* 51:5547–5558.

O'NEIL, J. R.; TAYLOR, H. P. 1969. Oxygen isotope equilibrium between muscovite and water. *Journal of Geophysical Research* 74:6012–6022.

OHMOTO, H. 1972. Systematics of sulfur and carbon isotopes in hydrothermal ore deposits. *Economic Geology* 67:551–579.

OHMOTO, H. 1986. Stable isotope geochemistry of ore deposits. In stable isotopes in high temperature geological processes. *Reviews in Mineralogy and Geochemistry* 16:445–486.

OHMOTO, H.; RYE, R. O. 1979. Isotopes of sulfur and carbon, *in:* BARNES, H. L. (ed.). *Geochemistry of hydrothermal ore deposits. 2nd edition.* 509–567. J. Wiley and Sons : New York.

PATERSON, M. S. 1973. Nonhydrostatic thermodynamics and its geologic applications. *Reviews of Geophysics and Space Physics* 11:255–389.

PATTERSON, D. J.; OHMOTO, H.; SOLOMON, M. 1981. Geologic setting and genesis of cassiterite-sulphide mineralisation at Renison Bell, western Tasmania. *Economic Geology* 76:393–438.

POTY, B.; STALDER, H. A.; WESBROD, A. M. 1974. Fluid inclusion studies in quartz from fissures of Western and Central Alps. *Schweis. Mineral. Petrogr. Mitt.* 54:717–752.

RANKIN, A. H.; GREENWAY, F. 1978. Macropscopic inclusions of fluid in British fluorites from the mineral collection of the British Museum (Natural History). *British Museum (Natural History) Bulletin of Geology* 30:295–325.

RIMSTIDT, J. D.; BARNES, H. L. 1980. The kinetics of silica-water reactions. *Geochimica et Cosmochimica Acta* 44:1683–1699.

ROBINSON, B. R.; KUSAKABE, M. 1975. Quantitative preparation of sulphur dioxide for $^{34}S/^{32}S$ analyses from sulphides by combustion with cuprous oxide. *Analytical Chemistry* 47:1179–1181.

ROEDDER, E. 1962. Studies of fluid inclusions I. Low temperature application of a dual-purpose freezing and heating stage. *Economic Geology* 57:1054–1061.

ROEDDER, E. 1963. Studies of fluid inclusions II: Freezing data and their interpretation. *Economic Geology* 58:167–211.

ROEDDER, E. 1965. Liquid CO_2 inclusions in olivine-bearing nodules and phenocrysts from basalts. *American Mineralogist* 50:1746–1782.

ROEDDER, E. 1984. Fluid inclusions. *Reviews in Mineralogy and Geochemistry* 12.

ROSCOE, W. E. 1975. Experimental deformation of natural chalcopyrite at temperatures up to 300°C over the strain rate range 10^{-2} to 10^{-6} sec^{-1}. *Economic Geology* 70:454–472.

RYE, R. O.; OHMOTO, H. 1974. Sulfur and carbon isotopes and ore genesis. A review. *Economic Geology* 69:826–842.

SALMON, B. C.; CLARK, B. R.; KELLY, W. C. 1974. Sulphide deformation studies : II. Experimental deformation of galena to 2000 bars and 400°C. *Economic Geology* 69:1–16.

SHEPPARD, S. M. F. 1986. Igneous rocks : III. Isotope case studies of magmatism in Africa, Eurasia and Oceanic Islands. In Stable isotopes in high temperature geological processes. *Reviews in Mineralogy and Geochemistry* 16:319–368.

SIMPSON, C.; SCHMIDT, S. M. 1983. An evaluation of criteria to deduce the sense of movement in sheared rocks. *Bulletin Geological Society of America* 94:1281–1288.

SOLOMON, M. 1981. An introduction to the geology and metallic ore deposits of Tasmania. *Economic Geology* 76:194–208.

SOLOMON, M.; EASTOE, J. C.; WALSHE, J. L.; GREEN, G. R. 1988. Mineral deposits and sulfur isotope abundances in the Mt Read Volcanics between Que River and Mt Darwin, Tasmania. *Economic Geology* 83:1307–1328.

SOLOMON, M.; RAFTER, T. A.; JENSEN, M. L. 1969. Isotope studies on the Rosebery, Mt Farrell and Mt Lyell ores, Tasmania. *Mineralium Deposita*. 4:172–199.

STANTON, R. L. 1972. *Ore petrology.* McGraw-Hill : New York.

SWANENBERG, H. E. C. 1980. *Fluid inclusions in high-grade metamorphic rocks from S.W. Norway.* Ph.D. Dissertation, University of Utrecht.

TAHERI, J. 1986. *The origin of mineralisation in South Heemskirk Granite, western Tasmania*. Ph.D. Thesis, University of Tasmania : Hobart.

TAHERI, J.; GREEN, G. R. 1990. The origin of gold-tin-copper mineralisation at the Lakeside deposit, western Tasmania. *Geological Report Mt Read Volcanics Project Tasmania* 5.

TAYLOR, H. P. Jr. 1979. Oxygen and hydrogen isotope relationships in hydrothermal mineral deposits, *in:* BARNES, H. H. (ed.). *Geochemistry of hydrothermal ore deposits, Volume 2.* 236–277. John Wiley and Sons : New York.

TAYLOR, H. P. Jr. 1974. The application of oxygen and hydrogen isotope studies to problems of hydrothermal alteration and ore deposition. *Economic Geology* 69:843–883.

UREY, H. C. 1947. The thermodynamic properties of isotopic substances *Journal Chemistry Society (London)* 562–581.

WALSHE, J. L.; SOLOMON, M. 1981. An investigation into the environment of formation of the volcanic-hosted Mt Lyell copper deposits using geology, mineralogy, stable isotopes and a six-component chlorite solid solution model. *Economic Geology* 76:246–284.

WELLS, K. 1974. *Annual report, Mt Tyndall EL 9/66, 1973–74*. The Consolidated Syndicate [TCR 74-1046].

WILLAN, R. C. R.; HALL, A. J. 1980. Sphalerite geothermometry and trace-elements studies on stratiform sulphide from McPhun's Cairn, Loch Fyne, Argyll, Scotland. *Transactions Institute of Mining and Metallurgy* 89 (B):31–40.

WILLIAMS, E. 1978. Tasman Fold Belt System in Tasmania. *Tectonophysics* 48:159–206.

WINCHESTER, J. A.; FLOYD, P. A. 1977. Geochemical discrimination of different magma series and their differentiation products using immobile elements. *Chemical Geology* 20:325–343.

YAMADA, R.; SUYAMA, T.; OGUSHI, N. 1987. Gold-bearing siliceous ore of the Nurukawa Kuroko deposit, Akita Prefecture Japan. *Mining Geology* 37:109–118.

YAMAMOTO, M. 1976. Relationship between Se/S and sulphur isotope ratios of hydrothermal sulphide minerals. *Mineralium Deposita* 11:197–209.

YEATS, C. J. 1989. *The geology and mineralisation of the Henty Gold Prospect, western Tasmania.* B.Sc. (Hons) thesis, University of Tasmania : Hobart.

ABBREVIATIONS USED IN APPENDICES

MP	massive pyrite	MA	moderate alteration	q	quartz
MZ	quartz-sericite-sulphide	QB	quartz-base metal	cpy	chalcopyrite
MV	quartz-sericite	MS	massive sulphide	gl	galena
MQ	massive quartz-sulphide-gold-telluride	AS	quartz-feldspar rock	sph	sphalerite
		CC	chlorite alteration	ser	sericite
SC	silica-carbonate alteration	MVF	quartz-sericite-fuchsite	chl	chlorite
LL	massive carbonate-hematite alteration			alt	alteration
				carb	carbonate

APPENDIX 1

Sample locations and rock types

Field No.	*RGC No.*	*DMMR No.*	*Rock type*
HP 7, 373 m	T17701	103745	MS
HP 51, 128.4 m	T17702	103784	late quartz vein
HP 51, 129.6 m	T17703	-	MQ (pyrite rich)
HP 51, 129.8 m	T17704	103785	late quartz in MQ
HP 47, 441.8 m	T17705	103781	MS
HP 47, 445.3 m	T17706	103782	LL
HP 47, 445.7 m	T17707	103783	LL
HP 17, 157.9 m	T17708	103749	MP
HP 17, 160 m	T17709	103750	AS
HP 20, 144.4 m	T17710	103754	MP
HP 53, 165.6 m	T17711	103787	QB
HP 53, 167.4 m	T17712	103788	MZ-QB
HP 55, 163.8 m	T17713	103789	MV-QB
HP 55, 165.5 m	T17714	103791	MP
HP 55, 165.8 m	T17715	103790	MZ
HP 24, 117.7 m	T17716	103761	MQ–late quartz vein
HP 24, 117.8 m	T17717	103755	MQ–late quartz vein
HP 24, 117.9 m	T17718	103756	MQ
HP 24, 118.5 m	T17719	103757	late quartz vein
HP 24, 120.8 m	T17720	103758	QB
HP 24, 122.6 m	T17721	103759	MA
HP 24, 124.9 m	T17722	103760	MZ
HP 24, 125.4 m	T17723	103762	MP
HP 28, 326.3 m	T17724	103765	MS
HP 28, 328.7 m	T17725	103766	QB
HP 28, 329.2 m	T17726	103767	MV-QB
HP 19, 280.4 m	T17727	103751	MQ
HP 19, 282.7 m	T17728	103752	MQ with pyrite veins
HP 19, 284.8 m	T17729	103754	MQ
HP 32, 164.1 m	T17730	103769	MA-MZ
HP 32, 166.0 m	T17731	103770	MZ
HP 32, 168.8 m	T17732	103771	MV-MQ
HP 28, 100.6 m	T17733	103763	MZ
HP 28, 112.2 m	T17734	103764	MQ
HP 12, 556.3 m	T17735	103747	QB
HP 12, 557.6 m	T17736	103748	QB
HP 9, 131.8 m	T17737	103746	QB
HP 31, 334.5 m	T17738	103768	MP
HP 4, 250.1 m	T17739	103736	q-py-cpy in MZ
HP 4, 258.7 m	T17740	103737	q-py-cpy in MZ
HP 4, 260.7 m	T17741	103738	MP

Field No.	*RGC No.*	*DMMR No.*	*Rock type*
HP 4, 263.2 m	T17742	103739	MA
HP 4, 266.0 m	T17743	103740	altered epiclastic rocks
HP 44, 111.0 m	T17744	103780	LL
HP 42, 603.8 m	T17745	103772	MZ-QB
HP 42, 605.6 m	T17746	103773	QB-MQ
HP 42, 606.1 m	T17747	103774	MQ
HP 42, 607.0 m	T17748	103775	MV-QB
HP 42, 611.1 m	T17749	103776	MZ
HP 42, 611.3 m	T17750	103777	MZ
HP 42, 612.7 m	T17751	103778	MZ
HP 42, 694.0 m	T17752	103779	MA
HP 57, 669.4 m	T17753	103792	QB
HP 57, 675.3 m	T17754	103793	MZ (pyrite rich)
HP 57, 679.0 m	T17755	103794	LL
HP 57, 680.8 m	T17756	103795	LL
HP 6, 310.6 m	T17757	103741	AS
HP 6, 310.8 m	T17758	103742	AS
HP 6, 314.6 m	T17759	103743	AS
HP 6, 318.1 m	T17760	103744	AS
HP 4, 259.6 m	T20118	103907	MZ
HP 4, 256.7 m	T20119	103904	QB
HP 4A, 234.1 m	T20120	103906	QB
HP 9, 128.5 m	T20121	103905	MQ (sulphide rich)
HP 12A, 550.8 m	T20122	103909	MQ
HP 17, 158.5 m	T20123	103903	MP
HP 25, 217.4 m	T20124	103902	QB-MP
HP 28, 321.6 m	T20125	-	MV
HP 28, 322.1 m	T20126	103908	QB
HP 42, 638.0 m	T20127	103901	MZ-QB
HP 96A, 598.6 m	T20130	-	MV-QB
HP 96A, 563.45 m	T20131	-	MQ
HP 96A, 565.6 m	T20132	104904	MQ-pyrite veins
HP 96A, 572.8 m	T20133	-	MZ
HP 96A, 573.45 m	T20134	104901	MV
HP 96A, 573.8 m	T20135	104916	MV + QB
HP 96A, 582.0 m	T20136	104917	MV
HP 96A, 583.5 m	T20137	104905	MV
HP 96A, 588.65 m	T20138	104932	QB
HP 96A, 590.65 m	T20139	104926	banded pyrite-carb.-q
HP 129D, 612,85 m	T20140	104906	MQ
HP 129D, 614.7 m	T20141	-	MV
HP 129D, 615.3 m	T20142	-	MQ
HP 129D, 622.15 m	T20143	104902	MV-fluorite
HP 129D, 628.15 m	T20144	104925	MZ
HP 129D, 630.1 m	T20145	104931	MV
HP 129D, 636.1 m	T20146	104934	MS (banded)-Q
HP 129D, 638.0 m	T20147	104930	MP-QB
HP 129D, 640.15 m	T20148	104929	MP-carb.
HP 129D, 641.5 m	T20149	104928	MP
HP 129D, 643.35 m	T20150	104927	quartz-phyric lava
HP 129D, 646.2 m	T20151	104949	shale/siltstone with pyrite lenses
HP 129D, 650.5 m	T20152	104903	quartz-carbonate vein
N. end of sill	T20153	104912	MV-fluorite
HP 49A, 910.9 m	T20296	-	chlorite alteration
HP 49A, 912.3 m	T20297	103954	chlorite alteration
HP 90, 723.9 m	T20298	-	chlorite alteration
HP 90, 725.5 m	T20299	103958	chlorite alteration
HP 57, 659.3 m	T20300	-	chlorite alteration
HP 57, 661.0 m	T21825	103955	chlorite alteration
HP 49, 959.5 m	T21826	-	chlorite alteration

Field No.	*RGC No.*	*DMMR No.*	*Rock type*
HP 49, 965.2 m	T21827	-	chlorite alteration
HP 49, 966.2 m	T21828	103957	chlorite alteration
SF 33C	-	104908	AS
NF 13-14W	-	104948	SC
NF 7-8W	-	104911	MQ
HP 49, 976.7 m	T21829	103956	chlorite alteration
NF 37-38W	T21830	103921	MV + fluorite.
NF 32-33W	T21831	103922	MVF
NF 20-21E	T21832	103923	MQ
NF 16-17W	T21833	103924	SC
NF 6-7W	T21834	103925	SC
NF 38W	T21835	103926A	MV
SF 33 Centre	T21836	103926	MQ-MP
SF 32-33W	T21837	103927	MQ-quartz vein
SF 32-33W	T21838	103928	MQ
NF 37-38E	T21839	103929	MZ
NF 19-20E	T21840	103930	MQ
NF 19-20W	-	103931	SC
NF 19-20E	T21842	103932	MA
NF 19E	T21843	103933	quartz gash
NF 13E	T21844	103934	MQ + quartz gash
NF 12-13E	T21845	103935	MQ + quartz gash
NF 38E	T21846	103936	MZ
SF 32-33W	T21847	103937	quartz gash
NF 38 Centre	T21848	103938	MQ
NF 37-38 Centre	T21849	103939	MQ + MV
NF 36-37B	T21850	103940	MQ
NF 34-35B	T21851	103941	MQ
NF 30-31E	T21852	103942	QB
NF 30-31E	T21853	103943	MV
NF 25-26W	T21854	103944	MQ + quartz gash
NF 23-24W	T21855	103945	MQ + quartz gash
NF 35-36E	T21856	103946	MA
NF 12-13E	T21857	103946A	MQ
NF 20-21E	T21858	103947	MQ + quartz gash
SF 20-21B	T21859	103949	MQ
SF 19-20E	T21860	103950	MP
SF 2-3B	T21861	103951	MQ
SF 15-16E	T21862	103953	MP
NF 36W	T21864	103961	MV
NF 34-35E	T21865	103962	MZ
NF 38E	T21866	103963	MZ
NF 30-31W	T21867	103964	SC
NF 32-33E	T21868	103965	MQ
NF 19-20E	T21869	103966	MQ
NF 35-36W	T21870	103967	MV
NF 7-8W	T21871	103968	MA
SF 1-2E	T21872	103968A	MA
NF 35-36W	T21873	103969	MV
NF 29-30E	T21874	103970	MV
NF 37-38W	T21875	103971	MV + fluorite
NF 35-36E	T21876	103972	MA
NF 16-17E	T21877	103973	MA
SF 33 Centre	T21878	103974	MQ
NF 27-28E	T21879	103975	MZ
SF 22-23W	T21880	103976	SC
SF 16-17B	T21881	103977	MQ
SF 9-10E	T21882	103978	MZ
SF 3-4B	T21883	103979	MQ
NF 23-24E	T21884	103980	MZ

Field No.	*RGC No.*	*DMMR No.*	*Rock type*
NF 7-8W	T21885	103981	SC
SF 21-22E	T21886	103982	MZ
SF 20-21E	T21887	103983	MZ
NF 33E	T21888	-	MZ
NF 16-17W	-	3032	SC
NF 34-35	-	3033	MZ-MA
NF 12-13W	-	3034	MV + fuchsite
NF 30-31	-	3037	MV
NF 12-13W	T21889	-	MA
HP 140, 557.30 m	T22001	3039	MQ
HP 140, 558.20 m	T22002	3040	MQ
HP 140, 563.10 m	T22003	3041	AS
HP 140, 564.4 m	T22004	3042	MV
HP 140, 533.4 m	T22005	3043	AS
HP 140, 562.80 m	T22006	3044	AS
HP 136B, 747.5 m	T22008	3046	AS
HP 129D, 620.90 m	T22009	104944	MV + fluorite
HP 129D, 621.5 m	T22010	104943	MV + fluorite
HP 129D, 673.6 m	T22011	3047	AS
HP 138A, 685.8 m	T22012	104946	AS
HP 138A, 687.9 m	T22013	104945	epiclastics with pyrite and base metal lenses
HP 49A,906.3	T22014	3048	AS
HP 49A, 955.9 m	T22015	3049	AS
HP 17, 157.9	T8820	-	MP
HP 17, 157.8	T8819	-	MP
NF 24W	-	104915	MQ
NF 30-31E	-	-	MQ
SF 32-33W	-	104909	AS
SF 33B	-	104910	AS
NF 33-34W	-	104933	MZ
	16778	Rep. CMS, 85/3/18	semi-massive py-q-ser (banded)

APPENDIX 2

Chlorite composition and geothermometry

Sample 103954 (light green chlorite)

Chemical composition					
SiO_2	23.86	23.36	23.36	22.76	23.21
Al_2O_3	20.63	19.89	19.91	20.08	20.16
FeO	29.24	27.60	29.04	29.18	28.81
MnO	0.35	0.36	0.23	0.23	0.39
MgO	12.48	12.19	12.04	12.52	12.67
No. of ions					
Si	2.62	2.65	2.63	2.56	2.59
Al^{IV}	1.38	1.35	1.36	1.44	1.41
Al^{VI}	1.29	1.30	1.27	1.22	1.24
Fe	2.70	2.61	2.72	2.75	2.69
Mn	0.03	0.03	0.03	0.02	0.04
MgO	2.04	2.06	2.01	2.10	2.10
Fe/Fe + Mg	0.57	0.56	0.57	0.57	0.56
*Geothermometry data**					
log fO_2 (1 Kbar)	-	-29.4	-28.8	-	-
log fO_2 (ht-mt)	-	-0.6	-0.9	-	-
T°C	-	321	329	-	-
T°C C & N**	310	304	306	323	317

Sample No. 103956 (dark green chlorite)

SiO_2	24.53	25.09	25.96	23.59	24.94	27.12
Al_2O_3	19.66	24.00	20.01	19.15	19.15	20.71
FeO	23.55	23.43	23.62	23.44	22.54	21.62
MnO	0.21	0.20	0.23	0.31	0.28	0.21
MgO	16.92	17.17	17.17	16.47	15.91	16.11
Fe/Fe + Mg	0.44	0.43	0.44	0.44	0.44	0.43
No of ions						
Si	2.66	2.67	2.73	2.63	2.75	2.83
Al^{IV}	1.34	1.32	1.26	1.37	1.24	1.16
Al^{VI}	1.17	1.22	1.22	1.18	1.24	1.39
Fe	2.13	2.09	2.08	2.19	2.08	1.89
Mn	0.02	0.02	0.02	0.03	0.02	0.02
Mg	2.73	2.73	2.7	2.74	2.61	2.50
*Geothermometry data**						
log fO_2 (1 kbar)	-	-	-30.7	-41.6	-32.1	-36.3
log fO_2 (ht-mt)	-	-	-0.07	-5.23	-0.64	-1.77
T°C	-	-	303	189	285	238
T°C C & N	302	298	285	308	281	264

* Walshe, 1986

** Cathelineau and Nieva, 1985

APPENDIX 3

Gold analyses

Sample No.	*Ag wt%*	*Au wt%*	*Hg wt%*	*Fineness*	*Ag atom %*	*Au atom %*	*Hg atom%*
103773 (T17746)	8.33	91.67	0	916.7	14.23	85.77	0
	4.87	95.13	0	951.30	8.55	91.45	0
	7.88	92.12	0	921.20	13.51	86.49	0
	8.54	91.45	0	914.59	14.57	85.43	0
	8.37	91.62	0	916.29	14.3	85.7	0
	8.38	91.61	0	916.19	14.32	85.68	0
	3.44	96.55	0	965.60	6.11	93.89	0
	3.07	96.92	0	969.30	5.47	94.53	0
	3.26	97.05	0	967.50	5.78	94.22	0
	3.36	96.63	0	966.40	5.97	94.03	0
	4.71	95.28	0	952.90	8.29	91.71	0
	4.82	95.18	0	951.80	8.46	91.54	0
	4.68	95.32	0	953.20	8.23	91.77	0
	4.65	95.35	0	953.50	8.18	91.82	0
	7.99	92	0	920.09	13.69	86.31	0
	4.22	95.59	0	957.72	7.76	92.24	0
	7.92	92.08	0	920.80	15.57	86.43	0
	8.38	91.62	0	916.20	14.32	85.68	0
	3.21	96.89	0	967.93	5.71	94.29	0
	3.54	96.46	0	964.60	6.28	93.72	0
103752 (T17728)	18.66	81.95	0.39	814.53	29.52	70.15	0.33
	18.75	80.71	0.54	811.48	29.65	69.89	0.46
	18.75	80.9	0.33	811.84	29.64	70.36	0.28
	19.91	80.28	0.56	801.28	31.04	68.47	0.49
	18.97	80.49	0.53	809.27	29.96	69.59	0.45
	18.39	81.33	0.28	815.58	29.15	70.61	0.24
103775 (T17748)	33.76	66.03	0.21	661.70	48.2	51.64	0.16
	33.05	42.51	0.33	562.59	58.49	41.2	0.32
	17.44	48.56	0.00	735.74	39.61	60.39	0
	23.93	75.98	0.00	760.45	36.52	63.48	0
T17748,	52.36	43.10	1.96	451.50	67.99	30.65	1.37
in late carb. vein	45.70	50.49	1.04	524.90	61.83	37.41	0.75
	22.45	80.00	0.00	780.87	33.88	66.12	0
	24.03	77.77	0.00	763.93	36.07	63.93	0
	46.81	49.39	0.83	513.41	63	36.4	0.6
	21.94	78.12	0.00	780.73		66.1	0
	22.31	77.04	0.00	775.44	34.59	65.41	0
T8820	25.39	74.50	0.23	745.82	38.29	61.52	0.19
	21.71	77.65	0.06	781.46	33.78	66.16	0.05
	25.03	73.76	0.08	746.63	38.23	61.71	0.06
	22.40	75.29	0.06	770.72	35.18	64.77	0.05
	21.50	77.86	0.06	783.62	33.46	66.5	0.05
T8819	4.50	95.50	0	955.00	7.87	92.13	0
103784	7.24	93.68	0	928.22	12.37	87.63	0
	7.45	93.65	0	926.31	12.68	87.32	0
	7.33	94.40	0	927.92	7.5	96.55	0
	7.03	94.86	0	931.00	7.19	97.02	0
	7.20	95.59	0	929.99	12.09	87.91	0
	8.47	92.23	0	915.91	14.35	85.65	0

Sample No.	*Ag wt%*	*Au wt%*	*Hg wt%*	*Fineness*	*Ag atom %*	*Au atom %*	*Hg atom%*
103946A (T21857)	7.5	92.5	0	925.00	12.91	87.09	0
	7.8	92	0	921.84	13.47	86.53	0
	7.3	92.7	0	927.00	12.46	87.52	0
	7.61	92.39	0	923.90	13.09	86.91	0
	13.8	86.2	0	862.00	22.68	77.32	0
	7.59	92.41	0	924.10	13.08	86.92	0
103966 (T21869)	7.69	92.31	0	923.10	13.41	86.59	0
	7.78	92.22	0	922.20	13.38	86.62	0
	9.05	90.95	0	909.50	15.49	84.51	0
	9.28	90.72	0	907.20	15.76	84.24	0
	6.67	93.33	0	933.30	11.58	88.42	0
	9.97	90.03	0	900.30	16.98	83.02	0
	7.23	92.77	0	927.70	12.46	87.54	0
103935 (T21845)	10.88	89.12	0	891.20	18.23	81.77	0
	10.31	89.69	0	896.90	17.34	82.66	0
	14.22	85.78	0	857.80	23.24	76.76	0
	12.56	87.44	0	874.40	20.91	79.09	0
	10.78	89.22	0	892.20	18.07	81.93	0
	13.56	86.41	0	864.36	22.31	77.69	0
103934 (T21844)	15.97	84.02	0	840.28	25.77	74.23	0
	19.1	81.9	0	810.89	30.03	69.98	0
	8.1	92.63	0	919.59	13.84	86.16	0
	12.5	87.5	0	875.00	20.69	87.5	0
	13.6	86.94	0	864.73	21.52	78.48	0
	14.2	91.8	0	866.04	13.9	86.1	0
	10.16	89.8	0	898.36	17.12	82.88	0
	8.4	91.6	0	916.00	14.38	85.62	0
	0.23	99.7	0	997.70	0.43	99.57	0
	12.55	87.45	0	874.50	20.81	79.19	0
103977 (T21881)	9.1	90.9	0	909.00	15.62	84.38	0
	8.9	91.9	0	911.71	15.25	84.75	0
	13.4	86.61	0	866.01	22.02	77.98	0
	10.4	89.5	0	895.90	17.6	82.4	0
	9.97	90.03	0	900.30	17.09	82.81	0
103905 (T20121)	22.75	77.17	0	772.32	34.97	64.96	0

APPENDIX 4

Pyrite analyses

Sample no.	*S wt%*	*Fe wt%*	*Co ppm*	*Ni ppm*	*As ppm*	*Se ppm*	*Co/Ni*	*Co/Se*	*S*10000/Se*
103765	52.05	47.6	<60	<60	670	70	?	?	7435.71
	51.74	48	<60	<60	<38	<44	?	?	-
	52.1	47.87	60	90	<38	100	0.67	0.60	5210.00
103939	51.47	47.75	<60	240	6900	<44	<1	?	12867.50
	52.05	47.89	<60	30	<38	<44	<1	?	-
	51.91	47.98	<60	260	<38	<44	<1	?	17303.33
	52.18	48.14	<60	50	<38	<44	<1	?	-
104928	51.87	47.69	680	220	700	820	3.09	0.83	632.56
	51.2	48.1	430	90	620	520	4.78	0.83	984.62
	51.89	47.76	190	70	2870	180	2.71	1.06	2882.78
	50.43	49.49	180	50	<38	110	3.60	1.64	4584.55
	51.72	47.64	1140	200	3120	870	5.70	1.31	594.48
103935	52.12	47.74	390	70	680	320	5.57	1.22	1628.75
	51.97	47.91	190	50	420	610	3.80	0.31	851.97

* Detection limits for Co, Ni, Se, As are 60, 60, 38 and 44 ppm respectively

APPENDIX 5

Fluid inclusion data

Sample No.	*Inclusion Type*	*Tm°C*		*Th °C*		*Th H_2O (L)*	*Tm ice*
		°C	*Clathrate*	*CO_2 (L)*	*CO_2 + H_2O (L)*	*°C*	*°C*
103784	C	-	-	29	306		
		-	4.8	28.9	306		
		-56.8	-	28.2	-		
		-56.1	-	-	304		
		-	-	28.9	309		
		-56.8	-	-	308		
		-	4.1	27.1	314		
		-	4.8	28.8	-		
		-56.3	4.9	-	319		
103927		-	4.6	-	318		
		-	-	28.8	302		
		-	-	27.6	306.5		
		-	-	28.5	310		
		-56.5	-	26.8	312		
		-	-	27.5	-		
		-56.1	4.2	27	-		
		-57.7	-	-	303		
		-	-	27.8	307.1		
103933		-	-	-	325		
		-56.6	-	29.7	310.4		
103784		-56.2	-	28.1	-		
		-57.1	4.1	28.2	-		
	B	-	-	-	285		
		-	-	-	289		
		-	-	-	283		
		-	-	-	290.7		
		-	-	-	270.6		
103927		-	-	-	292.7		
		-	-	-	290.1		
		-	-	-	270.8		
		-	-	-	325.3		
		-	-	-	315.8		
		-	-	-	285		
		-	-	-	285		
		-	-	-	331.7		
		-	-	-	297.1		
		-	-	-	294		
103933		-	-	-	327.3		
		-	-	-	315		
		-	-	-	248		
		-	-	-	246.3		
103927		-	-	-	244		
		-	-	-	266.4		
103784	A					147.4	
						143	
						195	
						197.9	
						192.3	

Sample No.	*Inclusion Type*	*Tm°C* °C	*Clathrate*	*Th °C* CO_2 (L)	$CO_2 + H_2O$ (L)	*Th* H_2O (L) °C	*Tm ice* °C
103784						200.1	
						110.2	
103757	A					112.5	
						171	-2.7
						177.4	-2.9
						181.1	-2.5
						181	-3.1
						185.2	-3.4
						189.3	
						192	
103921						186.5	
						131	
						126.8	
						129.9	
						133.1	-3.5
						110.5	
						138.3	-1.5
						130	
						129.8	
						131.7	-2.5
						110.6	
						140.7	
						131.4	
						139.7	
						130.7	
						132.4	

APPENDIX 6

Geochemical data

Cat. No.	*Detect. limit*	*3034*	*3037*	*104933*	*103967*	*103927*	*104915*	*104909*	*104910*	*103973*	*103983*	*103963*
RGC No.		-	-	-	T21870	T21837	-	-	-	T21866	T21877	T21887
RGC classn.		MV+FU	MV	MV	MV	MQ	MQ	AS	AS	MZ	MZ	MZ
SiO_2		45.59	80.02	81.96	80.98	90.52	96.83	79.61	81.96	63.50	60.19	58.81
TiO_2		0.35	0.44	0.37	0.40	0.59	0.37	0.14	0.11	0.56	0.64	0.38
Al_2O_3		8.06	10.81	8.45	11.61	0.91	0.61	11.44	8.20	15.35	16.98	11.38
Fe_2O_3		0.36	0.26	0.87	0.38	0.06	0.00	0.26	0.62	1.30	0.83	1.47
MnO		0.52	0.02	0.02	0.01	0.04	0.01	0.03	0.04	0.02	0.02	0.04
MgO		1.35	0.52	0.69	0.65	0.35	0.12	0.29	0.53	1.13	1.34	0.90
CaO		19.30	0.36	0.43	0.21	0.82	0.20	0.55	1.24	0.20	0.35	1.00
Na_2O		0.05	0.07	0.09	0.08	0.02	0.11	6.43	4.47	0.08	0.07	0.14
K_2O		2.62	3.50	2.96	3.94	0.28	0.21	0.19	0.09	5.28	5.99	4.02
P_2O_5		0.07	0.03	0.03	0.03	0.02	0.01	0.01	0.02	0.04	0.05	0.07
FeO		1.94	0.13	0.12	0.06	0.64	0.38	0.26	0.52	0.32	0.64	0.64
FeS_2		0.94	0.76	2.06	1.03	3.12	1.12	0.49	0.24	9.53	9.88	19.23
$H_2O + CO_2$		18.19	3.34	1.56	1.79	0.83	0.45	0.89	1.82	2.25	2.63	1.86
Total	**-**	**98.89**	**99.79**	**99.52**	**100.4**	**97.8**	**99.53**	**100.19**	**99.64**	**99.55**	**99.55**	**98.98**
Ce	28	47	53	54	57	69	37	32	260	110	115	69
Th	10	21	22	19	21	39	16	27	19	29	23	23
Sr	5	110	10	10	6	22	5	39	36	7	19	15
Ba	23	125	150	165	130	29	<23	77	70	270	440	250
Rb	5	100	99	100	120	12	6	8	<5	190	220	150
Y	5	42	16	9	15	23	12	21	20	33	28	15
Zr	5	88	165	120	155	210	150	70	84	200	230	135
Nb	5	6	8	6	7	10	7	6	8	9	8	5
Mo	5	<5	<5	10	7	14	12	<5	6	5	6	22
Sn	9	300?	300?	11	23	190?	15	15	9	23	11	22
Pb	10	43	49	340	79	830	1100	1	46	380	110	300
As	20	<20	<20	<20	<20	<20	<20	<20	<20	<20	21	130
Bi	5	<5	<5	5	<5	44	5	<5	<5	10	6	12
Ga	5	8	5	10	6	<5	8	6	<5	17	19	14
Zn	5	105	21	26	19	96	195	9	21	98	23	110
W	10	71	24	<10	13	<10	<10	10	<10	<10	<10	11
Cu	5	700	780	200	120	5700	530	33	44	72	130	1650
Ni	5	50	7	19	8	11	12	6	10	11	10	14
Co	8	10	<8	<8	<8	<8	<8	<8	<8	10	12	26

APPENDIX 7

XRD analyses

(a) Semi-quantitative analyses of MA (separates), AS and MQ:

Sample No.	*Description*	*Quartz (%)*	*Feldspar (%)*	*Mica (%)*	*Dolomite (%)*	*Calcite (%)*	*Pyrite (%)*
SF 32-33W	pink massive (from MA)	45	55	-	-	-	-
NF 30-31W	pink massive	65	20	15	-	-	-
NF 16-17E	pink massive	55	20	15	5	5	-
T17709	AS	55	45	2	-	-	-
T17760	AS	40	60	2	-	-	-
SF 32-33 W	AS	45	55	-	-	-	-
SF 33 C	AS	50	45	2	2	-	2
T22005	AS	45	45	-	2	-	2
T22007	AS	55	45	-	-	-	2
T22006	AS	45	45	5	5	-	-
T22008	AS	45	55	-	-	-	2
T22011	AS	45	55	-	-	-	2
T22015	AS	45	55	-	-	-	-
T17757	AS	70	20	10	2	-	-
T17758	AS	80	10	7	-	-	-
T17759	AS	50	45	5	-	-	-
T22001	MQ	80	-	-	-	20	2
T22002	MQ	90	-	2	-	5	2
T22003	MQ	80	-	-	-	20	-
T17747	MQ	90	-	-	-	10	-
NF 20-21E	MQ	95	-	-	-	2	-
NF 32-33 W	MQ	95	-	-	5	2	-
SF 3-4B	MQ	95	-	-	2	-	2
NF 7-8W	MQ	95	-	-	5	-	-
T20137	MQ	95	-	5	-	-	-

(b) SC, MZ, MV AND CHLORITISED ROCKS

The purpose of these analyses was to investigate the possibility of the occurrence of some sheet silicates such as pyrophyllite which are common in epithermal gold deposits. No such minerals were detected.

CHLORITISED ROCKS:

Sample no.	*Mineral constituents*
T20297	quartz, feldspar, chlorite, calcite, mica
T21825	quartz, feldspar, chlorite, mica
T21828	quartz, mica, chlorite, feldspar, calcite
T21829	quartz, feldspar, chlorite, dolomite, calcite, mica
T20299	chlorite, feldspar, mica, quartz

MA, MZ, MV ROCKS:

Sample no.	*Rock type (%)*	*Quartz (%)*	*Mica (%)*	*Pyrite (%)*	*Dolomite (%)*	*Calcite (%)*
T21846	-	50	45	5	-	-
NF 7-8W	SC	60	15	2	10	15
NF 30-31E	MV	85	15	-	-	-
SF20-21E	MZ	60	30	5	5	-
SF21-22E	MZ	50	40	10	2	-